Characteristic-Curve Finite Element Schemes for the Navier-Stokes Equations

A Dissertation Submitted to the Graduate School of Mathematics
of the Kyushu University in Partial Fulfillment of the Requirements
for the Degree of Doctor of Philosophy
(Mathematics)

Hirofumi NOTSU

Acknowledgments

First and foremost, I would like to express my sincere gratitude to Professor Masahisa Tabata, Kyushu University who gave me the chance to study in this research field for five years, and guided me toward the completion of this thesis. He also provided me with good computational environment and opportunity to talk at many conferences. Without his great encouragement with fruitful suggestions and stimulating discussions, this work could not have been possible.

Next I wish to express my sincere thanks to Professor Mitsuhiro T. Nakao, Kyushu University for his fruitful comments and warm encouragement.

I also wish to express my sincere thanks to Professor Masato Kimura, Kyushu University who had been my supervisor when I was a student at Hiroshima University, and introduced me into this research field with his insightful instruction. My early interest in this field was fostered in the period. His continuous support and discussions often helped me.

I am grateful to my parents and sister for their continuous encouragement and endless support.

Finally I wish to express my deepest gratitude to my wife for her understanding, continuous encouragement and endless support, and to my son and daughter for their warm smiles that cheer me up.

Contents

List of Tables

List of Figures

Chapter 1

Introduction

The purpose of this thesis is to present two characteristic-curve finite element schemes for the incompressible Navier-Stokes equations and to show two- and three-dimensional numerical results in order to see the advantages of the schemes.

In devising the numerical schemes for the Navier-Stokes equations, a key issue is how to approximate the nonlinear convection term. It is well known that the conventional Galerkin method causes severe oscillating results for high Reynolds number problems. To deal with this phenomenon, many kinds of approximations have been developed based on ideas such as upwinding, balancing tensor diffusivity, streamline diffusion, least square, characteristic-curve and so on. (See Baba and Tabata [1], Boukir et al. [3], Brooks and Hughes [5], Douglas Jr. and Russell [10], Franca and Frey [11], Franca and Stenberg [12], Fujima et al. [14], Gresho et al. [15], Hansbo and Johnson [18], Hughes et al. [19, 20], Hughes and Tezduyar [21], Johnson [22], Le Beau et al. [23], Kondo et al. [26], Pironneau [33, 34], Pironneau et al. [35], Süli [38], Tabata [39], Tabata and Fujima [42], Tezduyar [47] and references therein.)

We focus on characteristic-curve method. The method is based on an approximation of the material derivative along the trajectory of the fluid particle, and is natural from the physical point of view. From this the method seems to be considered as one of the upwind type methods. Moreover, the matrix for the system of linear equations is symmetric and identical, which enables us to use symmetric linear solvers. Characteristic-curve finite element schemes for the Navier-Stokes equations of first order in time have been developed and analyzed in Pironneau [33, 34] and Süli [38]. A scheme of second order in time has been presented and analyzed in Boukir et al. [3]. They use two-step method and approximate the material derivative by the values of two previous steps along the trajectory. These characteristic-curve finite element schemes impose the inf-sup condition [4, 7, 17] for the finite elements to be used.

One of the characteristic-curve schemes to be presented in this thesis is of second order in time and of single-step. The scheme has been proposed in the author and Tabata [32]. The material derivative is approximated in the Crank-Nicolson way along the trajectory. The original idea of the approximation has been developed in Rui and Tabata [36] for the convection-diffusion equations, which is extended to the Navier-Stokes equations in this thesis. As is pointed out in [36], in the Crank-Nicolson approximation on the trajectory, an additional correction term is indispensable to realize a second order accuracy. After supplying a correction term for the Navier-Stokes equations, the scheme is proved to be of second order in time. In the case of the Navier-Stokes equations the velocity is unknown and the obtained scheme becomes nonlinear. For the solution we present an internal iteration procedure which consists of solving a series of Stokes type equations. The scheme has such advantages that it is of second order in time and that every matrix to be treated is symmetric and identical. We present the numerical results in 2D to recognize the second order accuracy in time.

The other scheme does not impose the inf-sup condition and employs P1/P1 element, i.e., velocity and pressure are both approximated by the piecewise linear elements in triangles (2D) or tetrahedra (3D), which requires small memory to compute and leads to easy three-dimensional computation. The scheme keeps symmetry of the matrix for the system of linear equations. Since P1/P1 element does not satisfy the inf-sup condition, a pressure-stabilized method in Brezzi and

Douglas Jr. [6] is used. The scheme is an implicit and mixed one, and has such advantages that the matrix is symmetric and identical and that it is useful for large scale computation. We call the scheme a pressure-stabilized characteristic-curve finite element scheme, which has been developed in the author and Tabata [31] and applied to cavity flow problems in the author [30]. The numerical results in 2D and 3D are presented, and the problems consist of test problems and cavity flow problems. Test problems are set to see the convergence rate of the scheme to the exact solution. Applicability of the scheme for practical problems is checked by cavity flow problems, whose Reynolds number is up to 5,000 in 2D and 1,000 in 3D.

In the cavity flow problems we set discontinuous, C^0 and C^1 continuous Dirichlet boundary conditions. The classical cavity flow problem, whose Dirichlet boundary condition is given by a discontinuous function on the boundary, is well known as a benchmark one for incompressible fluid flows. Many authors solve the problem, such as Cruchaga and Oñate [9], Ghia et al. [16], Kondo et al. [26], Nallasamy and Prasad [29], Tabata and Fujima [42] in 2D, Fujima et al. [14], Iwatsu et al. [24], Jiang et al. [25], Ku et al. [27] in 3D, and so on. We compute the problem in 2D too. We have some doubt on solving the classical cavity flow problem, because the problem has no weak solution. Therefore, we also compute two other cavity flow problems in 2D and 3D, which are regularized by C^0 and C^1 continuous functions to be used for the Dirichlet boundary condition.

The contents of this thesis are as follows. In Chapter 2 the Navier-Stokes problem is set. The characteristic-curve method is introduced in Chapter 3. In Chapter 4, we consider numerical integration for characteristic-curve finite element schemes. Chapter 5 is devoted to a single-step characteristic-curve finite element scheme of second order in time. In Chapter 6, we review two stabilized methods for the stationary Stokes equations. In Chapter 7 a pressure-stabilized characteristic-curve finite element scheme is studied. In the last chapter we give conclusions of the thesis.

Chapter 2

The Navier-Stokes equations

In this chapter we set the Navier-Stokes problem and review a scheme. After preparing function spaces and notations in Section 2.1, the Navier-Stokes problem is set in Section 2.2. In Section 2.3 we review a scheme based on the conventional Galerkin method.

2.1 Preliminaries

In this section we introduce function spaces and notations to be used in this thesis.

Fundamentals of functional analysis

Let $\mathbb{N}$ and $\mathbb{R}$ be the sets of positive integers and real numbers, respectively, and $\mathbb{N}_0 \equiv \mathbb{N} \cup \{0\}$. For any normed space X, the norm is denoted by $\|\cdot\|_X$, and for any inner product space X, $(\cdot,\cdot)_X$ means the inner product. Let X and Y be real normed spaces. A mapping $A: X \to Y$ is a linear operator provided

$$A(c_1x_1 + c_2x_2) = c_1Ax_1 + c_2Ax_2, \quad \forall x_1,\ x_2 \in X,\ \forall c_1,\ c_2 \in \mathbb{R}.$$

When $Y = \mathbb{R}$, A is called a linear functional. A linear operator $A: X \to Y$ is continuous if there exists a constant C such that

$$\|Ax\|_Y \le C\|x\|_X, \quad \forall x \in X.$$

Let $\mathscr{L}(X,Y)$ be the set of continuous linear operators from X to Y. If Y is a Banach space, the set $\mathscr{L}(X,Y)$ is a Banach space with the norm

$$\|A\|_{\mathscr{L}(X,Y)} \equiv \sup_{\substack{x\in X,\\ x\neq 0}} \frac{\|Ax\|_Y}{\|x\|_X}.$$

We denote by $X' \equiv \mathscr{L}(X,\mathbb{R})$ the dual space of X and by $\langle\cdot,\cdot\rangle$ the dual pairing between X and X'.

We say that a mapping $b(\cdot,\cdot):\ X\times Y \to \mathbb{R}$ is a bilinear form provided

$$\begin{cases} b(c_1x_1+c_2x_2,\ y) = c_1b(x_1,y)+c_2b(x_2,y), & \forall x_1,x_2\in X,\ \forall y\in Y,\ \forall c_1,c_2\in\mathbb{R}, \\ b(x,\ c_1y_1+c_2y_2) = c_1b(x,y_1)+c_2b(x,y_2), & \forall x\in X,\ \forall y_1,y_2\in Y,\ \forall c_1,c_2\in\mathbb{R}. \end{cases}$$

A bilinear form $b(\cdot,\cdot)$ on $X\times Y$ is said to be continuous if there exists a constant C such that

$$|b(x,y)| \le C\|x\|_X\|y\|_Y, \quad \forall (x,y)\in X\times Y.$$

Let Z be a real normed space. A continuous trilinear form on $X\times Y\times Z$ is defined similarly.

Sobolev spaces

For $d=2$ or 3, let Ω be a bounded domain in $\mathbb{R}^d$ with a piecewise smooth boundary $\Gamma\equiv\partial\Omega$, and $n=(n_1,\cdots,n_d)^T$ be a unit outward normal to Γ (see Figure 2.1), where the superscript T means to transpose. For a real number p $(1\le p\le+\infty)$, let $L^p(\Omega)$ be the space of p-th power summable functions on Ω,

$$L^p(\Omega) \equiv \Big\{\phi:\ \Omega\to\mathbb{R};\ \phi \text{ is Lebesgue measurable},\ \|\phi\|_{L^p(\Omega)} < +\infty\Big\},$$

where

$$\|\phi\|_{L^p(\Omega)} \equiv \begin{cases} \left\{\displaystyle\int_\Omega |\phi(x)|^p\,dx\right\}^{1/p} & (1\le p<+\infty), \\ \text{ess.sup}\big\{|\phi(x)|;\ x\in\Omega\big\} & (p=+\infty), \end{cases}$$

and for real-valued and Lebesgue measurable function f,

$$\text{ess.sup}\big\{f(x);\ x\in\Omega\big\} \equiv \inf\Big\{\mu\in\mathbb{R};\ \text{meas}\{x\in\Omega;\ f(x)>\mu\}=0\Big\}.$$

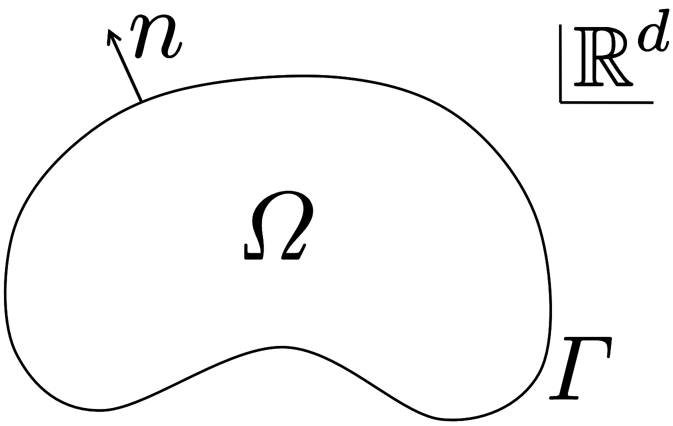

Figure 2.1: The domain Ω and its boundary Γ.

We set the space of test functions on Ω,

$$\mathscr{D}(\Omega) \equiv C_0^\infty(\Omega) \equiv \{\phi \in C^\infty(\Omega);\ \text{supp}[\phi] \text{ is compact in } \Omega\},$$

where supp$[\phi]$ is the support of ϕ,

$$\text{supp}[\phi] \equiv \overline{\{x \in \Omega;\ \phi(x) \neq 0\}}.$$

Let $L^1_{\text{loc}}(\Omega)$ be the space of locally summable functions,

$$L^1_{\text{loc}}(\Omega) \equiv \left\{\phi :\ \Omega \to \mathbb{R};\ \phi \in L^1(K),\ \forall K :\ \text{compact in } \Omega\right\}.$$

We call a vector of the form $\alpha = (\alpha_1, \cdots, \alpha_d) \in \mathbb{N}_0^d$ a multi-index of order

$$|\alpha| \equiv \sum_{i=1}^d \alpha_i,$$

and D^α means a differential operator,

$$D^\alpha \equiv \prod_{i=1}^d \left(\frac{\partial}{\partial x_i}\right)^{\alpha_i}.$$

Definition 2.1. *A mapping $T :\ \mathscr{D}(\Omega) \to \mathbb{R}$ is called a distribution if T satisfies the following two properties,*

- *Linearity*

$$\langle T,\ c_1\varphi_1 + c_2\varphi_2\rangle = c_1\langle T, \varphi_1\rangle + c_2\langle T, \varphi_2\rangle, \quad \forall\varphi_1,\ \varphi_2 \in \mathscr{D}(\Omega),\ \forall c_1,\ c_2 \in \mathbb{R},$$

- *Continuity*
  For any sequence $\{\varphi_j\}_{j=1}^{\infty} \subset \mathscr{D}(\Omega)$*, which satisfies*

$$\cdot\ \exists K \subset \Omega :\ \textit{compact set} \quad \textit{s.t.} \quad \forall j,\ \ \mathrm{supp}[\varphi_j] \subset K,$$
$$\cdot\ \forall\alpha :\ \textit{multi-index}, \quad \max_{x\in K} |D^{\alpha}\varphi_j(x)| \to 0\ (j \to \infty),$$

  it holds that

$$\langle T, \varphi_j\rangle \to 0\ (j \to \infty).$$

We denote the set of distributions by $\mathscr{D}'(\Omega)$*.* □

Lemma 2.1. *Suppose that* $f \in L^1_{\mathrm{loc}}(\Omega)$ *and that* $\alpha \in \mathbb{N}_0^d$ *is any multi-index. Then there exists a distribution* $D^{\alpha} f \in \mathscr{D}'(\Omega)$ *defined by*

$$\langle D^{\alpha} f, \varphi\rangle \equiv (-1)^{|\alpha|} \int_{\Omega} f(x) D^{\alpha}\varphi(x)\ dx, \quad \forall\varphi \in \mathscr{D}(\Omega).$$

$D^{\alpha} f$ *is called a derivative of* f *in the sense of distribution.* □

If functions $f,\ g \in L^1_{\mathrm{loc}}(\Omega)$ satisfy

$$\langle D^{\alpha} f, \varphi\rangle = \int_{\Omega} g(x)\varphi(x)\ dx, \quad \forall\varphi \in \mathscr{D}(\Omega),$$

then, we write $D^{\alpha} f = g$.

For a real number p $(1 \le p \le +\infty)$ and an integer $k \in \mathbb{N}_0$, we define the Sobolev space $W^{k,p}(\Omega)$ by

$$W^{k,p}(\Omega) \equiv \Big\{\phi :\ \Omega \to \mathbb{R};\ D^{\alpha}\phi \in L^p(\Omega),\ |\alpha| \le k\Big\},$$

with the norm,

$$\|\phi\|_{W^{k,p}(\Omega)} \equiv \begin{cases} \left\{\displaystyle\sum_{j=0}^{k} |\phi|^p_{W^{j,p}(\Omega)}\right\}^{1/p} & (1 \le p < +\infty), \\ \max\Big\{|\phi|_{W^{j,\infty}(\Omega)};\ 0 \le j \le k\Big\} & (p = +\infty), \end{cases}$$

where $|\phi|_{W^{j,p}(\Omega)}$ is a seminorm,

$$|\phi|_{W^{j,p}(\Omega)} \equiv \begin{cases} \left\{ \displaystyle\sum_{|\alpha|=j} \|D^\alpha \phi\|^p_{L^p(\Omega)} \right\}^{1/p} & (1 \le p < +\infty), \\ \max\left\{ \|D^\alpha \phi\|_{L^\infty(\Omega)};\ |\alpha| = j \right\} & (p = +\infty). \end{cases}$$

If $p = 2$, we usually write

$$H^k(\Omega) \equiv W^{k,2}(\Omega),$$

for $k = 0,\ 1,\ 2,\ \cdots$. Note that $H^0(\Omega) = L^2(\Omega)$. $H^k(\Omega)$ is a Hilbert space with the inner product,

$$(f,g)_{H^k(\Omega)} \equiv \sum_{|\alpha|\le k} \int_\Omega D^\alpha f\, D^\alpha g\, dx.$$

We introduce another Hilbert space $L^2_0(\Omega)$ defined by

$$L^2_0(\Omega) \equiv \left\{ \phi \in L^2(\Omega);\ \int_\Omega \phi\, dx = 0 \right\}.$$

Let $g : \Gamma \times (0,\ T) \to \mathbb{R}^d$ be a function. Throughout the thesis, we use the following notations,

$$\begin{aligned} X &\equiv H^1(\Omega)^d, \quad M \equiv L^2(\Omega), \\ V(g(t)) &\equiv \left\{ v \in X;\ v = g(\cdot,t) \text{ on } \Gamma \right\}, \\ V &\equiv V(0)\ (= H^1_0(\Omega)^d), \\ Q &\equiv L^2_0(\Omega). \end{aligned}$$

The partial derivative $\partial\phi/\partial x_i$ of a function ϕ is denoted by $\phi_{,i}$ and the Einstein convention $a_i b_i$ is used in place of $\sum_{i=1}^d a_i b_i$. We define a differential operator ∇ by

$$\nabla \equiv \left(\frac{\partial}{\partial x_1},\ \cdots,\ \frac{\partial}{\partial x_d} \right)^T.$$

Let $p\,(1 \le p \le \infty)$ be a real number. The gradient of $f \in W^{1,p}(\Omega)$ is written as

$$\nabla f = \left(\frac{\partial f}{\partial x_1},\ \cdots,\ \frac{\partial f}{\partial x_d} \right)^T = \left(f_{,1},\ \cdots,\ f_{,d} \right)^T \in L^p(\Omega)^d,$$

Let X and Y be sets, e.g., $X = Y = \mathbb{R}$. For vectors $a \in X^d$ and $b \in Y^d$, $a \cdot b$ represents

$$a \cdot b \equiv a_i b_i = \sum_{i=1}^{d} a_i b_i.$$

By the above notations, for a function $v \in W^{1,p}(\Omega)^d$, we have

$$\nabla \cdot v = v_{i,i} = \sum_{i=1}^{d} \frac{\partial v_i}{\partial x_i} \in L^p(\Omega),$$

which is the divergence of v.

Trace operator

Let $L^p(\Gamma)$ be the space of p-th power summable functions on Γ. From the smoothness of Γ, there exists a trace operator $\gamma \in \mathscr{L}(W^{1,p}(\Omega), L^p(\Omega))$ [4, 8, 40]. For $v \in W^{1,p}(\Omega)$, γv is simply denoted by v, if there is no confusion. We define the function space $H_0^1(\Omega)$ by

$$H_0^1(\Omega) \equiv \left\{\phi \in H^1(\Omega);\ \gamma v = 0\right\}.$$

The following formula of integration by parts is often used in this thesis.

Theorem 2.1 (Gauss-Green)**.** *Let $f \in W^{1,p}(\Omega)$ and $g \in W^{1,q}(\Omega)$, where $1/p + 1/q = 1$ and $1 \leq p \leq +\infty$. Then it holds that, for $i = 1, \cdots, d$,*

$$\int_\Omega f_{,i}\, g\, dx = -\int_\Omega f g_{,i}\, dx + \int_\Gamma f g n_i\, ds. \tag{2.1}$$

□

Notations

We introduce additional useful notations. For $i,\ j \in \mathbb{N}$, let δ_{ij} be Kronecker's delta defined by

$$\delta_{ij} \equiv \begin{cases} 1 & (i = j) \\ 0 & (\text{otherwise}) \end{cases}.$$

Ω and d are often omitted from subscript of norms, e.g., $\|\cdot\|_{H^1(\Omega)^d}$ is denoted by $\|\cdot\|_{H^1}$. When $X = L^2(\Omega),\ L^2(\Omega)^d$ or $L^2(\Omega)^{d\times d}$, we often omit the subscript X from the notations $(\cdot,\cdot)_X$ and $\|\cdot\|_X$.

Let Δt be a time increment and T be a positive constant. We use two types of time subdivisions. Since the one is used only in Chapter 5, there should be no confusion. Let $n \in \mathbb{N}_0$. In this thesis except Chapter 5, we use definitions,

$$t^n \equiv n\Delta t, \quad N_T \equiv [T/\Delta t]. \tag{2.2}$$

In only Chapter 5, we employ other definitions,

$$t^n \equiv \begin{cases} \Delta t_0 + (n-1)\Delta t & (n \geq 1) \\ 0 & (n = 0) \end{cases}, \quad N_T \equiv [(T - \Delta t_0)/\Delta t] + 1, \tag{2.3}$$

where Δt_0 is another time increment used only in the first step of the computation. For a function ϕ on $\Omega \times (0,T)$ or $\Gamma \times (0,T)$ and an integer n $(0 \leq n \leq N_T)$, ϕ^n means $\phi^n \equiv \phi(\cdot, t^n)$. For a given sequence $\{\phi^n\}_{n=1}^{N_T}$ in a normed space X, we define

$$\|\phi\|_{l^\infty(X)} \equiv \max\big\{\|\phi^n\|_X;\ n = 1,\cdots,N_T\big\},$$
$$\|\phi\|_{l^2(X)} \equiv \left\{\sum_{n=1}^{N_T}(t^n - t^{n-1})\|\phi^n\|_X^2\right\}^{1/2}.$$

Let $\mathscr{T}_h \equiv \{K\}$ be a triangulation of Ω and $N_e \equiv \sharp\mathscr{T}_h$ be the total number of elements, where the subscript h means representative length of the triangulation and K is closed. We define Ω_h by

$$\Omega_h \equiv \mathrm{int} \bigcup\{K;\ K \in \mathscr{T}_h\}$$

and $\Gamma_h \equiv \partial\Omega_h$. Generally Ω_h is different from Ω, and in the finite element method every integral over Ω is replaced by one over Ω_h. Therefore, we prepare the notation $(\cdot,\cdot)_h$ as $L^2(\Omega_h)$-inner product.

Let $l \in \mathbb{N}$. We set conforming finite element spaces,

$$\begin{aligned} X_{hl} &\equiv \big\{v_h \in C^0(\overline{\Omega}_h)^d;\ v_h|_K \in P_l(K)^d,\ \forall K \in \mathscr{T}_h\big\}, \\ M_{hl} &\equiv \big\{q_h \in C^0(\overline{\Omega}_h);\ q_h|_K \in P_l(K),\ \forall K \in \mathscr{T}_h\big\}, \end{aligned} \tag{2.4}$$

where $P_l(K)$ is the space of polynomials of degree l defined in $K \in \mathscr{T}_h$. We denote by the same notation Π_{hl} the interpolation operators from $C^0(\overline{\Omega})^d$ to X_{hl} and from $C^0(\overline{\Omega})$ to M_{hl}. For given finite element spaces X_h and M_h and a given vector valued function g on Γ we define,

$$\begin{gathered} V_h(g) \equiv \big\{ v_h \in X_h;\ v_h(P) = g(P),\ \forall P \in \Gamma_h \big\}, \\ V_h \equiv V_h(0), \quad Q_h \equiv\ M_h \cap L_0^2(\Omega_h), \end{gathered} \tag{2.5}$$

where P is any nodal point on Γ_h. The norms in V_h and Q_h are defined by $\|\cdot\|_{V_h} \equiv \|\cdot\|_{H^1}$ and $\|\cdot\|_{Q_h} \equiv \|\cdot\|_{L^2}$, respectively.

2.2 Statement of the problem

Let $d = 2$ or 3. We consider the nonstationary Navier-Stokes problem subject to the Dirichlet boundary condition; find $(u,\ p) : \Omega \times (0,T) \to \mathbb{R}^d \times \mathbb{R}$ such that

$$\left\{ \begin{aligned} \frac{\partial u}{\partial t} + (u \cdot \nabla)u - \nabla\big(2\nu D(u)\big) + \nabla p = f \quad & \text{in } \Omega \times (0,T), \\ \nabla \cdot u = 0 \quad & \text{in } \Omega \times (0,T), \\ u = g \quad & \text{on } \Gamma \times (0,T), \\ u = u^0 \quad & \text{in } \Omega,\ \text{at } t = 0, \end{aligned} \right. \tag{2.6}$$

where $u = (u_1,\ \cdots,\ u_d)^T$ is the velocity, p is the pressure, $f = (f_1,\ \cdots,\ f_d)^T$ is an external force, $g = (g_1,\ \cdots,\ g_d)^T$ is a boundary velocity, $u^0 = (u_1^0,\ \cdots,\ u_d^0)^T$ is an initial velocity, $\nu (> 0)$ is a viscosity, $D(u)$ is the strain-rate tensor defined by

$$D_{ij}(u) \equiv \frac{1}{2}(u_{i,j} + u_{j,i}) \quad (i, j = 1, \cdots, d),$$

and

$$\big[\nabla\big(2\nu D(u)\big)\big]_i \equiv 2\nu D_{ij,j}(u) \quad (i = 1, \cdots, d).$$

Throughout this thesis we deal with this problem.

In order to give a variational formulation for (2.6), we prepare the following. We define continuous bilinear forms a on $X \times X$, b on $X \times M$ and a trilinear form

a_1 on $X \times X \times X$ by

$$a(u,v) \equiv 2\nu\big(D(u),\ D(v)\big), \tag{2.7a}$$

$$b(v,q) \equiv -(\nabla \cdot v,\ q), \tag{2.7b}$$

and

$$a_1(w,u,v) \equiv \frac{1}{2}\left\{\Big((w\cdot\nabla)u,\ v\Big) - \Big((w\cdot\nabla)v,\ u\Big)\right\}, \tag{2.7c}$$

respectively. For functions $u \in X$ which satisfies $\nabla \cdot u = 0$ and $v \in V$, it holds the identity,

$$a_1(u,u,v) = \Big((u\cdot\nabla)u,\ v\Big).$$

A variational formulation for (2.6) is to find $\{(u,p)(t) \in V(g(t)) \times Q;\ t \in (0,T)\}$ such that, for any $t \in (0,T)$,

$$\begin{cases} \Big(\dfrac{\partial u}{\partial t}(t), v\Big) + a_1(u(t), u(t), v) \\ \qquad\qquad + a(u(t),v) + b(v, p(t)) = (f(t), v), \quad \forall v \in V, \\ \qquad\qquad\qquad\qquad b(u(t),q) = 0 \qquad\qquad \forall q \in Q, \end{cases} \tag{2.8}$$

and the initial condition

$$u(0) = u^0. \tag{2.9}$$

By the material derivation defined by

$$\frac{D}{Dt} \equiv \frac{\partial}{\partial t} + (u\cdot\nabla),$$

the variational formulation (2.8) is equivalent to the equations,

$$\begin{cases} \Big(\dfrac{Du}{Dt}(t), v\Big) + a(u(t),v) + b(v,p(t)) = (f(t),v), \quad \forall v \in V, \\ \qquad\qquad\qquad\qquad b(u(t),q) = 0, \qquad\qquad \forall q \in Q. \end{cases} \tag{2.10}$$

2.3 A finite element scheme based on the conventional Galerkin method

In this section we review a scheme for (2.6), which is analyzed in Tabata and Tagami [46]. For the sake of simplicity, we assume $\Omega = \Omega_h$ throughout the section. We choose a typical element P2/P1, which implies that $X_h \equiv X_{h2}$ and $M_h \equiv M_{h1}$. Then, the bilinear form b satisfies the uniform inf-sup condition [4, 7, 17] on $V_h \times Q_h$, i.e., there exists a positive constant β^* such that, for any h,

$$\inf_{q_h \in Q_h} \sup_{v_h \in V_h} \frac{b(v_h, q_h)}{\|v_h\|_{V_h} \|q_h\|_{Q_h}} \geq \beta^*. \tag{2.11}$$

For a given sequence $\{u^n\}_{n=0}^{N_T}$, we define the backward difference quotient of u at time step n by

$$\bar{D}_{\Delta t} u^n \equiv \frac{u^n - u^{n-1}}{\Delta t}.$$

We now write the scheme discretized by the semi-implicit backward Euler method in time and by the finite element method in space; find $\{(u_h^n, p_h^n) \in V_h(g^n) \times Q_h;\ n = 1, \cdots, N_T\}$ such that, for $n = 1, \cdots, N_T$,

$$\begin{cases} \big(\bar{D}_{\Delta t} u_h^n, v_h\big) + a_1(u_h^{n-1}, u_h^n, v_h) & \\ \qquad\qquad + a(u_h^n, v_h) + b(v_h, p_h^n) = (f^n, v_h), & \forall v_h \in V_h, \\ \qquad\qquad\qquad\qquad b(u_h^n, q_h) = 0, & \forall q_h \in Q_h, \end{cases} \tag{2.12}$$

where $u_h^0 \in V_h(g^0)$ is a function approximating u^0.

Let (u_h, p_h) be a solution of (2.12). For the sufficiently smooth solution (u, p) of (2.6), the scheme (2.12) has the following convergence property. There exists a positive constant C, independent of h and Δt, such that

$$\|u - u_h\|_{l^2(H^1)} + \|p - p_h\|_{l^2(L^2)} \leq C(\Delta t + h^2). \tag{2.13}$$

The proof has been done in Tabata and Tagami [46].

We consider the scheme (2.12) on computational and mathematical sides. The matrix appearing in the scheme is nonsymmetric and is not invariant at each time step, because of a_1 corresponding to the nonlinear convection term $(u \cdot \nabla)u$. Consequently, we need a nonsymmetric linear solver. From the mathematical aspect, this scheme is reliable by the convergence property (2.13). In constructing the numerical scheme, such error analysis is one of goals. However, since the conventional Galerkin method is employed in the scheme, we need to use small h and Δt for high Reynolds number problems ($0 < \nu \ll 1$). This point is the problem of the scheme.

Chapter 3

The characteristic-curve method

This chapter is devoted to the study of the characteristic-curve method. The idea of the characteristic-curve method is to consider the trajectory of the fluid particle and discretize the material derivative term along the trajectory.

In Section 3.1, first and second order approximations of the material derivative are introduced. The first order approximation is employed for the scheme to be presented in Chapter 7, and the second order approximation using a single step method is used for the scheme to be proposed in Chapter 5. In Section 3.2, characteristic-curve finite element schemes using the first and second order approximations are reviewed. The first order scheme has been proposed and analyzed in Pironneau [33, 34] and Süli [38]. The second order scheme using a multi step method has been presented and analyzed in Boukir et al. [3].

3.1 Discretization of the material derivative

In this section we give first and second order approximations of the material derivative.

3.1.1 First order approximation

We introduce the characteristic-curve method of first order in time. For a velocity $w : \Omega \to \mathbb{R}^d$, we define $X_1(w, \Delta t) : \ \Omega \to \mathbb{R}^d$ by

$$X_1(w, \Delta t)(x) \equiv x - w(x)\Delta t.$$

We use the symbol $\circ$ to designate the composition of functions, e.g., for a function ϕ defined in Ω

$$\big(\phi \circ X_1(w, \Delta t)\big)(x) \equiv \phi(X_1(w, \Delta t)(x)).$$

Let $u : \Omega \times (0,T) \to \mathbb{R}^d$ be a smooth function and $X(\cdot;x) : (0,T) \to \mathbb{R}^d$ be a solution of the ordinary differential equation,

$$\begin{cases} X'(t) = u(X,t) \quad \text{in } (t^{n-1}, t^n), \\ X(t^n) = x, \end{cases} \tag{3.1}$$

for a point $x \in \Omega$ and an integer n $(1 \le n \le N_T)$ (see Figure 3.1). Then, for a smooth function $\phi : \ \Omega \times (0,T) \to \mathbb{R}$, it holds that

$$\frac{D\phi}{Dt}(X(t),t) = \frac{d}{dt}\phi(X(t),t) \quad \text{in } (t^{n-1}, t^n). \tag{3.2}$$

The material derivative of ϕ at $t = t^n$ is approximated as follows;

$$\begin{aligned} \frac{D\phi}{Dt}(x,t) &= \frac{d}{dt}\phi(X(t),t) \\ &= \frac{\phi^n(X(t^n)) - \phi^{n-1}(X(t^{n-1}))}{\Delta t} + O(\Delta t) \\ &= \frac{\phi^n - \phi^{n-1} \circ X_1(u^{n-1}, \Delta t)}{\Delta t}(x) + O(\Delta t), \end{aligned} \tag{3.3}$$

where we have used the relation,

$$X(t^{n-1};x) = X_1(u^{n-1}, \Delta t)(x) + O(\Delta t^2).$$

For the Navier-Stokes equations, substituting u_i $(i = 1, \cdots, d)$ into ϕ in (3.3), we get the approximation of the material derivative of u at $t = t^n$,

$$\frac{Du}{Dt}(x,t) = \frac{u^n - u^{n-1} \circ X_1(u^{n-1}, \Delta t)}{\Delta t}(x) + O(\Delta t). \tag{3.4}$$

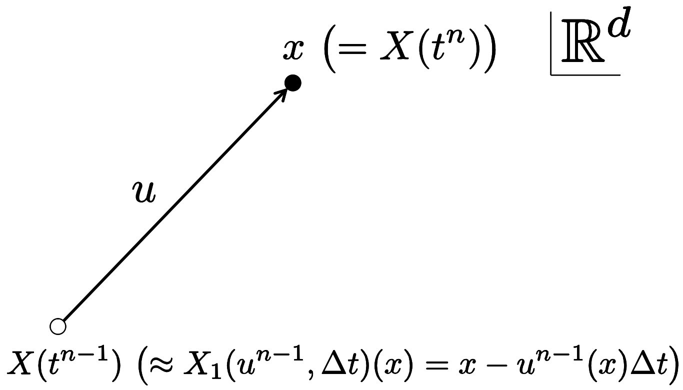

Figure 3.1: Trajectory of a fluid particle whose position is x at $t = t^n$.

Let us consider a scheme using the equality (3.4), and assume that u^n is an unknown function and u^{n-1} is a known function. The nonlinearity of the Navier-Stokes equations is in the composite function $u^{n-1} \circ X_1(u^{n-1}, \Delta t)$. Since u^{n-1} is a known function, the scheme is linear and symmetric.

3.1.2 Second order approximation

For velocities $u,\ w : \Omega \to \mathbb{R}^d$, we define $X_2(u,w,\Delta t)$ and $\bar{X}_1(u,w,\Delta t) :\ \Omega \to \mathbb{R}^d$ by

$$
\begin{aligned}
X_2(u,w,\Delta t)(x) &\equiv x - \big\{u(x) + w(x - w(x)\Delta t)\big\}\frac{\Delta t}{2}, \\
\bar{X}_1(u,w,\Delta t)(x) &\equiv x - \big\{2u(x) - w(x)\big\}\Delta t,
\end{aligned}
$$

respectively, where X_2 is based on the Heun method.

Single step method

First, we explain a second order approximation of $D\phi/Dt$ by a single step method. The evaluation point is $(X(t^{n-1/2}), t^{n-1/2})$, which is different from the point in the case of the first order approximation, $(X(t^n),t^n)$. From (3.2), we have

$$\frac{D\phi}{Dt}(X(t^{n-1/2}),t^{n-1/2}) = \frac{\phi^n(X(t^n)) - \phi^{n-1}(X(t^{n-1}))}{\Delta t} + O(\Delta t^2)$$
$$= \frac{\phi^n(x) - \phi^{n-1} \circ X_2(u^n,u^{n-1},\Delta t)(x)}{\Delta t} + O(\Delta t^2), \quad (3.5)$$

where the last equality is derived by the identity, see (5.11) later,

$$X(t^{n-1};x) = X_2(u^n,u^{n-1},\Delta t)(x) + O(\Delta t^3).$$

In the case of the Navier-Stokes equations, we obtain the approximation of the material derivative of u,

$$\frac{Du}{Dt}(X(t^{n-1/2}),t^{n-1/2}) = \frac{u^n - u^{n-1} \circ X_2(u^n,u^{n-1},\Delta t)}{\Delta t}(x) + O(\Delta t^2). \quad (3.6)$$

Details are discussed in Section 5.2.

Let us consider a scheme using the equality (3.6), and assume that u^n is an unknown function and u^{n-1} is a known function. This second order approximation uses u^n and u^{n-1}, and the scheme is nonlinear because of u^n in X_2. For this problem, we give an internal iteration procedure in Chapter 5, which keeps symmetry of the matrix appearing the procedure.

Multi (two) step method

Next, we introduce a second order approximation by a multi (two) step method which is employed in Boukir et al. [3]. The second order approximation of the material derivative of ϕ using the multi (two) step method is given by

$$\frac{D\phi}{Dt}(X(t^n),t^n)$$
$$= \frac{3\phi^n - 4\phi^{n-1} \circ \bar{X}_1(u^{n-1},u^{n-2},\Delta t) + \phi^{n-2} \circ \bar{X}_1(u^{n-1},u^{n-2},2\Delta t)}{2\Delta t}(x) + O(\Delta t^2). \quad (3.7)$$

We give the proof of (3.7). Since it holds that

$$f'(t) = \frac{3f(t) - 4f(t-\Delta t) + f(t-2\Delta t)}{2\Delta t} + O(\Delta t^2)$$

for a smooth function f, we have

$$\begin{aligned}\frac{D\phi}{Dt}(X(t^n),t^n) &= \frac{d}{dt}\phi(X(t),t)\Big|_{t=t^n} \\ &= \frac{3\phi^n(X(t^n)) - 4\phi^{n-1}(X(t^{n-1})) + \phi^{n-2}(X(t^{n-2}))}{2\Delta t} + O(\Delta t^2).\end{aligned} \tag{3.8}$$

From the Taylor expansion of X,

$$X(t-\Delta t) = X(t) - \Delta t X'(t) + \frac{\Delta t^2}{2}X''(t) + O(\Delta t^3),$$

we get

$$\begin{aligned}&\phi^{n-1}(X(t^{n-1})) = \phi^{n-1}(X(t^n - \Delta t)) \\ &= \phi^{n-1}\big(X(t^n) - \Delta t X'(t^n) + \frac{\Delta t^2}{2}X''(t^n) + O(\Delta t^3)\big) \\ &= \phi^{n-1}\big(X(t^n) - \Delta t X'(t^n)\big) + \frac{\Delta t^2}{2}X''(t^n)\cdot\nabla\phi^{n-1}\big(X(t^n)\big) + O(\Delta t^3) \\ &= \phi^{n-1}\circ\bar{X}_1(u^{n-1},u^{n-2},\Delta t)(x) + \frac{\Delta t^2}{2}X''(t^n)\cdot\nabla\phi^{n-1}\big(X(t^n)\big) + O(\Delta t^3),\end{aligned} \tag{3.9}$$

where for the last equality we have used the relation,

$$X'(t^n;x) = u^n(x) = 2u^{n-1}(x) - u^{n-2}(x) + O(\Delta t^2)$$

Similarly it holds that

$$\begin{aligned}&\phi^{n-2}(X(t^{n-2})) \\ &\quad = \phi^{n-2}\circ\bar{X}_1(u^{n-1},u^{n-2},2\Delta t)(x) + 2\Delta t^2 X''(t^n)\cdot\nabla\phi^{n-2}\big(X(t^n)\big) + O(\Delta t^3) \\ &\quad = \phi^{n-2}\circ\bar{X}_1(u^{n-1},u^{n-2},2\Delta t)(x) + 2\Delta t^2 X''(t^n)\cdot\nabla\phi^{n-1}\big(X(t^n)\big) + O(\Delta t^3).\end{aligned} \tag{3.10}$$

Combining (3.9) and (3.10) with (3.8) leads to (3.7), because the coefficient of $X''(t^n)\cdot\nabla\phi^{n-1}\big(X(t^n)\big)$ vanishes.

In the case of the Navier-Stokes equations, we get the approximation of the material derivative of u,

$$\frac{Du}{Dt}(X(t^n),t^n) =$$

$$\frac{3u^n - 4u^{n-1} \circ \bar{X}_1(u^{n-1}, u^{n-2}, \Delta t) + u^{n-2} \circ \bar{X}_1(u^{n-1}, u^{n-2}, 2\Delta t)}{2\Delta t}(x) + O(\Delta t^2). \tag{3.11}$$

Now, we consider a scheme using the equality (3.11). The second order approximation needs u^{n-2} in addition to u^n and u^{n-1} which imposes $n \geq 2$, and the scheme is linear and symmetric.

3.2 Finite element schemes based on the characteristic-curve method

In this section we review two schemes for (2.6), which are proposed and analyzed in Pironneau [33, 34], Süli [38] and Boukir et al. [3]. For the sake of simplicity, we assume $\Omega = \Omega_h$ and a boundary velocity $g = 0$ throughout the section. We choose a typical element P2/P1, i.e., $X_h \equiv X_{h2}$ and $M_h \equiv M_{h1}$. The bilinear form b satisfies the uniform inf-sup condition (2.11) on $V_h \times Q_h$.

3.2.1 First order scheme

For $u, w \in H^1(\Omega)^d$ we define a linear form $\mathscr{M}_{h1}(u, w; \Delta t)$,

$$\langle \mathscr{M}_{h1}(u, w; \Delta t),\ v_h \rangle \equiv \left(\frac{u - w \circ X_1(w, \Delta t)}{\Delta t},\ v_h \right).$$

We show the scheme discretized by the backward Euler method using the first order characteristic-curve method in time and by the finite element method in space; find $\{(u_h^n, p_h^n)\}_{n=1}^{N_T} \subset V_h \times Q_h$ such that, for $n = 1, \cdots, N_T$,

$$\begin{cases} \langle \mathscr{M}_{h1}(u_h^n, u_h^{n-1}; \Delta t),\ v_h \rangle + a(u_h^n, v_h) + b(v_h, p_h^n) = (f^n, v_h), & \forall v_h \in V_h, \\ \hfill b(u_h^n, q_h) = 0, & \forall q_h \in Q_h, \end{cases} \tag{3.12}$$

where u_h^0 is a function approximating u^0.

Let (u_h, p_h) be a solution of (3.12) and (u, p) be the sufficiently smooth solution of (2.6). The scheme (3.12) has a convergence property, as follows. Suppose

$\sigma > (d-1)/2$ and $\Delta t = O(h^\sigma)$. Then, there exists a positive constant C, independent of h and Δt, such that, for sufficiently small h and Δt,

$$\|u - u_h\|_{l^\infty(H^1)} + \|p - p_h\|_{l^2(L^2)} \le C(\Delta t + h^2). \tag{3.13}$$

For the proof, see Süli [38].

The scheme is of first order in time, and we can see the accuracy in (3.13). The matrix appearing in the scheme (3.12) is symmetric and identical by the first order characteristic-curve method. Therefore, we can use symmetric linear solvers, which makes the computational time short. By using the characteristic-curve method, the scheme is an upwind type one, and works for high Reynolds number problems. On the other hand, it is difficult to integrate the term including the composite function, $u_h^{n-1} \circ X_1(u_h^{n-1}, \Delta t)$, for the computation.

3.2.2 Second order scheme

For u, w, $\zeta \in H^1(\Omega)^d$ we define a linear form $\bar{\mathscr{M}}_{h2}(u, w, \zeta, \Delta t)$,

$$\langle \bar{\mathscr{M}}_{h2}(u, w, \zeta; \Delta t),\ v_h \rangle \equiv \Big(\frac{3u - 4w \circ \bar{X}_1(w, \zeta, \Delta t) + \zeta \circ \bar{X}_1(w, \zeta, 2\Delta t)}{2\Delta t},\ v_h \Big).$$

Let (u, p) be the smooth solution of (2.6) and we assume that $u_h^1 \in V_h$ approximating u^1 is given. The scheme discretized by the backward Euler method using the second order characteristic-curve method in time and by the finite element method in space is to find $\{(u_h^n, p_h^n)\}_{n=2}^{N_T} \subset V_h \times Q_h$ such that, for $n = 2, \cdots, N_T$,

$$\begin{cases} \langle \bar{\mathscr{M}}_{h2}(u_h^n, u_h^{n-1}, u_h^{n-2}; \Delta t),\ v_h \rangle + a(u_h^n, v_h) + b(v_h, p_h^n) = (f^n, v_h), & \forall v_h \in V_h, \\ b(u_h^n, q_h) = 0, & \forall q_h \in Q_h. \end{cases} \tag{3.14}$$

The scheme (3.14) has a convergence property,

$$\|u - u_h\|_{l^\infty(H^1)} + \|p - p_h\|_{l^2(L^2)} \le C(\Delta t + h^2). \tag{3.15}$$

under some assumptions including the condition

$$\Delta t \le C h^{d/6}.$$

In addition to the property of the scheme (3.12), the scheme (3.14) is of second order in time. The hypothesis that u_h^1 is given is supposed. Therefore, we need to find u_h^1 of a second order approximation to u^1 by another scheme.

Chapter 4

Numerical integration for characteristic-curve finite element schemes

In computation by characteristic-curve finite element schemes, it is not so easy to integrate composite functions on triangular elements. In this chapter we show a numerical integration procedure to compute the integrals. In Section 4.1, numerical integration formulas of degree two and five are introduced. In Section 4.2, we give our numerical integration procedure which includes an efficient element-search algorithm.

4.1 Numerical integration formulas

Let $K \in \mathscr{T}_h$ be a fixed triangular element. In this section we refer to Stroud [37] and introduce numerical integration formulas of degree two and five on K in $\mathbb{R}^2$ and $\mathbb{R}^3$.

In order to introduce the formulas, we prepare the barycentric coordinates. Let $\{P_i\}_{i=1}^{d+1}$ be the nodal points of the element K and $(x_1^i, \cdots, x_d^i)^T$ be the coordinates of P_i. For $x \in \mathbb{R}^d$, we define the barycentric coordinates $(\lambda_1(x), \cdots, \lambda_{d+1}(x))^T \in \mathbb{R}^{d+1}$ by

$$\lambda_i(x) \equiv \frac{1}{\triangle} \det \begin{array}{c} \begin{array}{ccccc} & & \underset{\smile}{i} & & \end{array} \\ \begin{bmatrix} 1 & \cdots & 1 & \cdots & 1 \\ x_1^1 & \cdots & x_1 & \cdots & x_1^{d+1} \\ \vdots & & \vdots & & \vdots \\ x_d^1 & \cdots & x_d & \cdots & x_d^{d+1} \end{bmatrix} \end{array},$$

where $\triangle \in \mathbb{R}$ is defined by

$$\triangle \equiv \det \begin{bmatrix} 1 & \cdots & 1 \\ x_1^1 & \cdots & x_1^{d+1} \\ \vdots & & \vdots \\ x_d^1 & \cdots & x_d^{d+1} \end{bmatrix} > 0.$$

Figure 4.1 shows the two-dimensional barycentric coordinates. λ_i $(i = 1, \cdots, d+1)$ is a linear function and barycentric coordinates satisfy the following properties,

$$\lambda_i(P_j) = \delta_{ij}, \qquad \sum_{i=1}^{d+1} \lambda_i(x) = 1.$$

If $x \notin K$, there is $i_* \in \{1, \cdots, d+1\}$ such that $\lambda_{i_*}(x) < 0$ (see Figure 4.1 again).

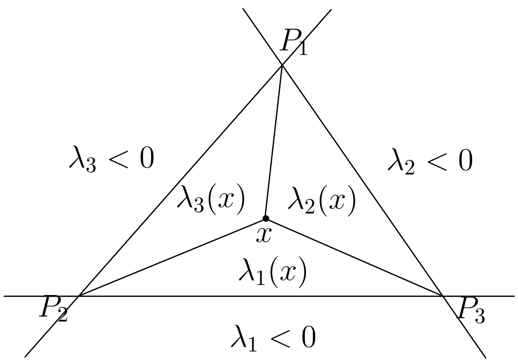

Figure 4.1: The barycentric coordinates in $\mathbb{R}^2$.

In the following, for $\beta_1,\cdots,\beta_{d+1}\in\mathbb{R}$, we use the notation $(\beta_1,\cdots,\beta_d;\beta_{d+1})$, which is the set defined by

$$\begin{aligned}&(\beta_1,\cdots,\beta_d;\beta_{d+1})\\&\qquad\equiv\left\{(\gamma_1,\cdots,\gamma_{d+1});\ (\gamma_1,\cdots,\gamma_{d+1})\text{ is a permutation of }(\beta_1,\cdots,\beta_{d+1})\right\}.\end{aligned}$$

If all the $\beta_i,\ i=1,\cdots,d+1$, are distinct, then, $\sharp(\beta_1,\cdots,\beta_d;\beta_{d+1})=(d+1)!$. For example, the set $(p,p,p;q)$ consists of the four elements, (p,p,p,q), (p,p,q,p), (p,q,p,q) and (q,p,p,p).

Let $f\in C^0(K)$ be a function. We set

$$I[f,K]\equiv\int_K f\,dx. \tag{4.1}$$

The numerical approximation of $I[f,K]$ is often done by the formula of the type

$$I[f,K]\approx I_h[f,K]\equiv\sum_{i=1}^{N}f\big(a_i\big)w_i,$$

Here a_i, $i=1,\cdots,N$, are points in $K\in\mathscr{T}_h$, and $w_i\in\mathbb{R}$, $i=1,\cdots,N$, are called weights. For the error term of the formula $E_h[f,K]\equiv I[f,K]-I_h[f,K]$, we define $\deg(E_h)$ by

$$\deg(E_h)\equiv\sup\{k\in\mathbb{N}_0;\ E_h[p,K]=0,\ \forall p\in P_k(K)\}.$$

When $\deg(E_h)=l$, we say that $I_h[f,K]$ is a numerical integration formula of degree l.

For $l=2$ and 5, we use a numerical integration formula of degree l,

$$I_h[f,K;l]\equiv\operatorname{meas}(K)\sum_{i=1}^{N_d^{(l)}}f\big(a_i^{(l)}\big)\omega_i^{(l)} \tag{4.2}$$

as $I_h[f,K]$, where the notations are defined as follows.

(i) $l=2$ (see Figure 4.2 (left)) :

$N_d^{(2)}\equiv d+1,\quad p\equiv\frac{d+2-\sqrt{d+2}}{(d+1)(d+2)},\quad q\equiv\frac{d+2+d\sqrt{d+2}}{(d+1)(d+2)},$

$\omega_i^{(2)} \equiv \frac{1}{d+1}\ (i = 1, \cdots, d+1)$,

for each i, $a_i^{(2)}$ corresponds to the following barycenter coordinates,

$a_i^{(2)}:\ (\lambda_1, \cdots, \lambda_{d+1}) \in (p, \cdots, p; q) \quad (i = 1, \cdots, d+1)$.

(ii) $l = 5,\ d = 2$ (see Figure 4.2 (right)) :

$N_2^{(5)} \equiv 7, \quad t \equiv \frac{1}{3}, \quad p \equiv \frac{6-\sqrt{15}}{21},\ q \equiv \frac{9+2\sqrt{15}}{21}, \quad r \equiv \frac{6+\sqrt{15}}{21},\ s \equiv \frac{9-2\sqrt{15}}{21}$,

$$\omega_i^{(5)} \equiv \begin{cases} \frac{9}{40} & (i = 1) \\ \frac{155-\sqrt{15}}{1200} & (i = 2,\,3,\,4) \\ \frac{155+\sqrt{15}}{1200} & (i = 5,\,6,\,7) \end{cases},$$

for each i, $a_i^{(5)}$ corresponds to the following barycenter coordinates,

$$a_i^{(5)}: \begin{cases} (\lambda_1, \lambda_2, \lambda_3) \in (t, t; t) & (i = 1) \\ (\lambda_1, \lambda_2, \lambda_3) \in (p, p; q) & (i = 2,\,3,\,4) \\ (\lambda_1, \lambda_2, \lambda_3) \in (r, r; s) & (i = 5,\,6,\,7) \end{cases}.$$

(iii) $l = 5,\ d = 3$:

$N_3^{(5)} \equiv 15$,

$t \equiv \frac{1}{4}, \quad p_1 \equiv \frac{7-\sqrt{15}}{34},\ q_1 \equiv \frac{13+3\sqrt{15}}{34}, \quad p_2 \equiv \frac{7+\sqrt{15}}{34},\ q_2 \equiv \frac{13-3\sqrt{15}}{34}$,

$r \equiv \frac{10-2\sqrt{15}}{40},\ s \equiv \frac{10+2\sqrt{15}}{40}$,

$$\omega_i^{(5)} \equiv \begin{cases} \frac{16}{135} & (i = 1) \\ \frac{2665+14\sqrt{15}}{37800} & (i = 2, \cdots, 5) \\ \frac{2665-14\sqrt{15}}{37800} & (i = 6, \cdots, 9) \\ \frac{20}{378} & (i = 10, \cdots, 15) \end{cases},$$

for each i, $a_i^{(5)}$ corresponds to the following barycenter coordinates,

$$a_i^{(5)}: \begin{cases} (\lambda_1, \cdots, \lambda_{d+1}) \in (t, t, t; t) & (i = 1) \\ (\lambda_1, \cdots, \lambda_{d+1}) \in (p_1, p_1, p_1; q_1) & (i = 2, \cdots, 5) \\ (\lambda_1, \cdots, \lambda_{d+1}) \in (p_2, p_2, p_2; q_2) & (i = 6, \cdots, 9) \\ (\lambda_1, \cdots, \lambda_{d+1}) \in (r, r, s; s) & (i = 10, \cdots, 15) \end{cases}.$$

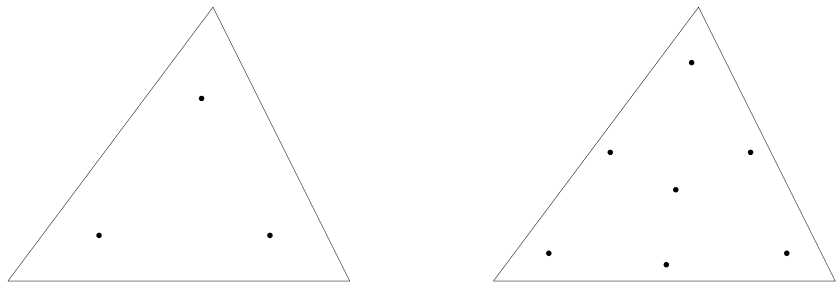

Figure 4.2: The points used for the numerical integration formulas of degree two (left) and five (right) in $\mathbb{R}^2$.

4.2 Element-search algorithms

In characteristic-curve finite element schemes, we have to compute integrals of composite functions such as,

$$\int_K u_h^{n-1} \circ X_1(u_h^{n-1}, \Delta t) \cdot v_h \, dx$$

on triangular elements K. We set $f \equiv u_h^{n-1} \circ X_1(u_h^{n-1}, \Delta t) \cdot v_h$ and the above integral is equal to $I[f, K]$, which is approximated by $I_h[f, K; l]$ for $l = 2$, 5, i.e.,

$$I[f,K] \approx I_h[f,K;l] = \mathrm{meas}(K) \sum_{i=1}^{N_d^{(l)}} f\big(a_i^{(l)}\big)\, \omega_i^{(l)}.$$

Then, we need the value,

$$f(a_i^{(l)}) = \Big(u_h^{n-1} \circ X_1(u_h^{n-1}, \Delta t) \cdot v_h\Big)\big(a_i^{(l)}\big) = u_h^{n-1} \circ X_1(u_h^{n-1}, \Delta t)\big(a_i^{(l)}\big) \cdot v_h\big(a_i^{(l)}\big),$$

for $i = 1, \cdots, N_d^{(l)}$. Generally, the point $X_1(u_h^{n-1}, \Delta t)(a_i^{(l)})$ is not in K, although $a_i^{(l)}$ is always in K. Therefore, we set the following problem (see Figure 4.3).

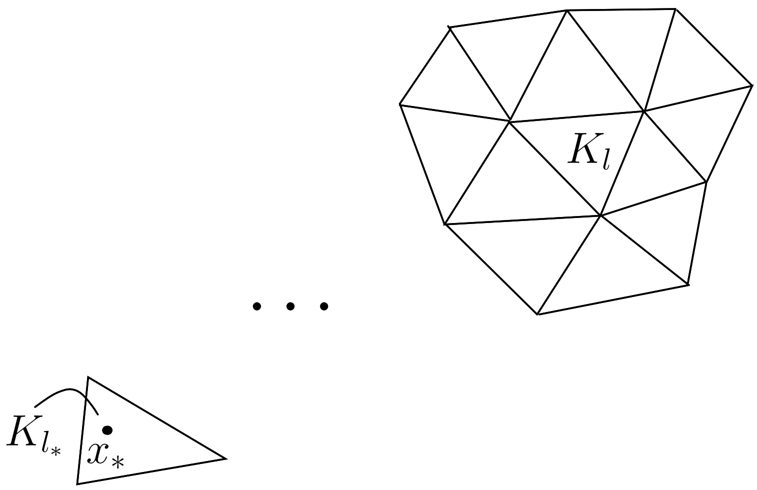

Figure 4.3: The point x_* and the element K_{l_*} in Problem 4.1.

Problem 4.1. *Let* $\mathscr{T}_h = \{K_l\}_{l=1}^{N_e}$ *and* $x_* \in \overline{\Omega}_h$ *be given. Find* $l_* \in \{1, \cdots, N_e\}$ *such that* $x_* \in K_{l_*}$.

For any integer $l \in \{1, \cdots, N_e\}$, let $(\lambda_1^{(l)}, \cdots, \lambda_{d+1}^{(l)})^T$ be the barycentric coordinates for the element K_l. It holds that $x_* \in K_l$, if and only if,

$$\lambda_i^{(l)} \geq 0, \quad \forall i \in \{1, \cdots, d+1\}. \tag{C_l}$$

For any $l \in \{1, \cdots, N_e\}$, let $\{m_i^{(l)}\}_{i=1}^{d+1} \subset \{1, \cdots, N_e\} \cup \{-1\}$ be the neighbor element numbers for the element K_l (see Figure 4.4). We note that

(i) $\forall i \in \{1, \cdots, d+1\},\ \forall x \in K_{m_i^{(l)}}, \quad \lambda_i^{(l)}(x) \leq 0,$

(ii) if $m_i^{(l)} = -1$, then, $K_l \cap \Gamma_h = \{x \in K_l;\ \lambda_i^{(l)}(x) = 0\} \neq \emptyset$.

Let us introduce the following simple element-search algorithm. It may be easy to code, but it takes a lot of computational time.

Algorithm 4.1 (Simple algorithm)**.**

```
01:   for n =1,...,Ne, begin
```

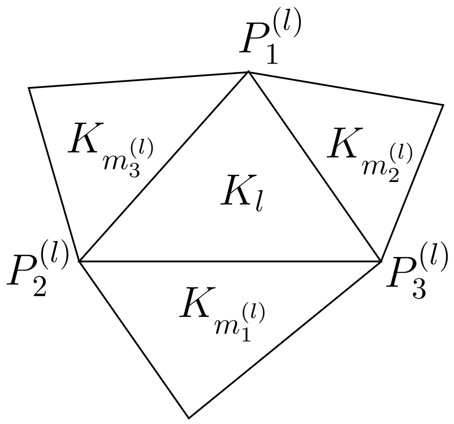

Figure 4.4: Correspondence between an element K_l and elements $K_{m_i^{(l)}}\,(i = 1,\,2,\,3)$ in $\mathbb{R}^2$.

    `if` (C_n) `is satisfied, set` $l_* \equiv n$ `and break`

`end`

`return` l_*.

Our element-search algorithm for Problem 4.1 is an efficient one, which is illustrated by Figure 4.5. For our algorithm, we need the data $\{m_i^{(l)}\}_{i=1}^{d+1}$ for all $l \in \{1,\cdots,N_e\}$. The algorithm is as follows.

Algorithm 4.2 (Efficient algorithm)**.**

$l_0 \in$ `{1,...,Ne}: initial guess, given`

`while(1), begin`

    `if` (C_{l_0}) `is satisfied, set` $l_* \equiv l_0$ `and break`

    `for` i `=1,...,d+1, begin`

        `if( (` $\lambda_i^{(l_0)}$`<0) and (` $m_i^{(l_0)} \neq$ `-1) ), set` $l_1 \equiv m_i^{(l_0)}$ `and break`

    `end`

    `set` $l_0 \equiv l_1$

`end`

`return` l_*.

Remark 4.1. *(i) When we compute $I_h[f,K_m;l]$, for the first numerical integration* *point, it may be the best choice to set the initial guess $l_0 = m$ in Algorithm 4.2.*

(ii) If Ω_h is nonconvex, we should pay attention to the initial guess l_0 in the algorithm.

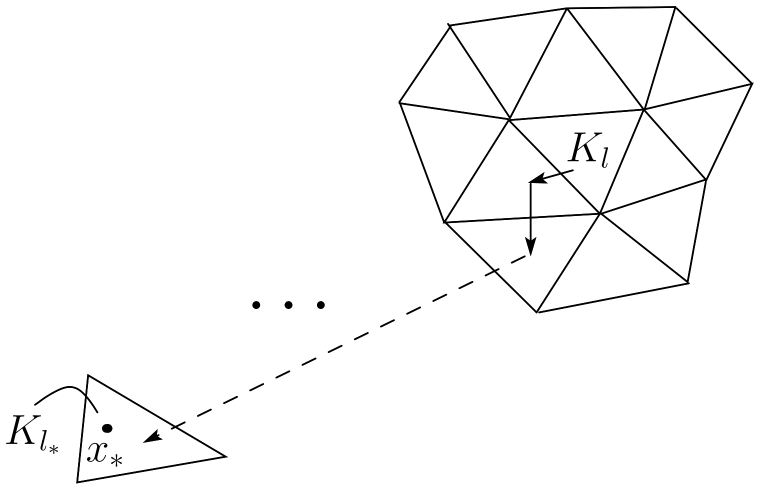

Figure 4.5: An element-search order by Algorithm 4.2 in $\mathbb{R}^2$.

Chapter 5

A single-step characteristic-curve finite element scheme of second order in time

This chapter deals with a single-step characteristic-curve finite element scheme of second order in time, which has been developed by the author and Tabata [32]. Throughout this chapter we set $g = 0$ in the Navier-Stokes problem (2.6). The scheme is given in the first section. In Section 5.2 the consistency of the scheme, second order accuracy, is proved. Numerical results for a test problem are given in Section 5.3. The importance of the additional correction term is shown in the results. Contents of this chapter have been reported in the author and Tabata [32].

Only in this chapter, we use the definitions of time subdivisions (2.3).

5.1 The finite element scheme

In this section we present a characteristic-curve finite element scheme for the Navier-Stokes equations. It is of single step and second order in time.

In order to present our scheme for (2.6) we prepare the following. We choose a typical element P2/P1, i.e., $X_h \equiv X_{h2}$ and $M_h \equiv M_{h1}$. For $u,\ w,\ \zeta \in H_0^1(\Omega_h)^d$, $p,\ q \in H^1(\Omega_h)$, $r \in L^2(\Omega_h)$ and $f,\ g \in L^2(\Omega_h)^d$, we define linear forms $\mathscr{A}_{h1}$ (u,w,r), $\mathscr{A}_{h2}(u,\zeta,w,p,q)$, $\mathscr{F}_{h1}f$ and $\mathscr{F}_{h2}(f,g,w)$ on V_h and $\mathscr{B}_h u$ on Q_h by

$$
\begin{aligned}
\mathscr{A}_{h1}(u,w,r) &\equiv \mathscr{M}_{h1}(u,w\,;\Delta t_0) + \mathscr{D}_{h1}u + \mathscr{P}_{h1}r,\\
\mathscr{A}_{h2}(u,\zeta,w,p,q) &\equiv \mathscr{M}_{h2}(u,\zeta,w\,;\Delta t) + \mathscr{D}_{h2}(u,w) + \mathscr{P}_{h2}(w,p,q),\\
\Big\langle \mathscr{B}_h u, q_h \Big\rangle &\equiv -\Big(\nabla\cdot u, q_h\Big)_h, \quad \Big\langle \mathscr{F}_{h1}f, v_h\Big\rangle \equiv \Big(f, v_h\Big)_h,\\
\Big\langle \mathscr{F}_{h2}(f,g,w), v_h \Big\rangle &\equiv \frac{1}{2}\Big(f + g\circ X_1(w,\Delta t), v_h\Big)_h,
\end{aligned}
$$

where

$$
\begin{aligned}
\left(\Big\langle \mathscr{M}_{h1}(u,w\,;\Delta t_0), v_h\Big\rangle = \Big(\frac{u - w\circ X_1(w,\Delta t_0)}{\Delta t_0},\ v_h\Big)_h,\right)\\
\Big\langle \mathscr{M}_{h2}(u,\zeta,w\,;\Delta t), v_h\Big\rangle \equiv \Big(\frac{u - w\circ X_2(\zeta,w,\Delta t)}{\Delta t},\ v_h\Big)_h,\\
\Big\langle \mathscr{D}_{h1}u, v_h\Big\rangle \equiv 2\nu\Big(D(u), D(v_h)\Big)_h, \quad \Big\langle \mathscr{P}_{h1}r, v_h\Big\rangle \equiv -\Big(\nabla\cdot v_h,\ r\Big)_h,\\
\Big\langle \mathscr{D}_{h2}(u,w), v_h\Big\rangle \equiv \nu\Big(D(u) + D(w)\circ X_1(w,\Delta t),\ D(v_h)\Big)_h\\
+ \nu\Delta t\Big(D_{ij}(w)w_{k,j},\ v_{hi,k}\Big)_h,\\
\Big\langle \mathscr{P}_{h2}(w,p,q), v_h\Big\rangle \equiv \frac{1}{2}\Big(\nabla p + \nabla q\circ X_1(w,\Delta t),\ v_h\Big)_h.
\end{aligned}
$$

For $\{u^n\}_{n=0}^{N_T} \subset H_0^1(\Omega_h)^d$, $\{p^n\}_{n=1}^{N_T} \subset H^1(\Omega_h)$ and $\{f^n\}_{n=1}^{N_T} \subset L^2(\Omega_h)^d$, linear forms $\mathscr{A}_h^n(u,p)$ and $\mathscr{F}_h^n(f,u)$ on V_h are defined by

$$
\mathscr{A}_h^n(u,p) \equiv \begin{cases} \mathscr{A}_{h2}(u^n,u^n,u^{n-1},p^n,p^{n-1}) & (n\ge 2),\\ \mathscr{A}_{h1}(u^1,u^0,p^1) & (n=1),\end{cases}
$$

$$
\mathscr{F}_h^n(f,u) \equiv \begin{cases} \mathscr{F}_{h2}(f^n,f^{n-1},u^{n-1}) & (n\ge 2),\\ \mathscr{F}_{h1}f^1 & (n=1).\end{cases}
$$

In order to unify the notation we put $\mathscr{B}_h^n u \equiv \mathscr{B}_h u^n$. For a given continuous function f we set $f_h^n \equiv \Pi_{h2} f(t^n)$ in this chapter.

We now present the scheme for (2.6); find $\{(u_h^n,\ p_h^n)\}_{n=1}^{N_T} \subset V_h \times Q_h$ such that, for $n = 1, \cdots, N_T$,

$$\begin{cases} \mathscr{A}_h^n(u_h, p_h) = \mathscr{F}_h^n(f_h, u_h) & \text{in } V_h', \\ \mathscr{B}_h^n u_h = 0 & \text{in } Q_h', \end{cases} \tag{S1}$$

where $u_h^0 \equiv \Pi_{h2} u^0$. For $n \geq 2$ this is equivalent to the equations,

$$\begin{cases} \Big(\dfrac{u_h^n - u_h^{n-1} \circ X_2(u_h^n, u_h^{n-1}, \Delta t)}{\Delta t},\ v_h\Big)_h \\ \quad + \nu\Big(D(u_h^n) + D(u_h^{n-1}) \circ X_1(u_h^{n-1}, \Delta t),\ D(v_h)\Big)_h + \nu\Delta t\Big(D_{ij}(u_h^{n-1})u_{hk,j}^{n-1},\ v_{hi,k}\Big)_h \\ \quad + \dfrac{1}{2}\Big(\nabla p_h^n + \nabla p_h^{n-1} \circ X_1(u_h^{n-1}, \Delta t),\ v_h\Big)_h \\ \quad = \dfrac{1}{2}\Big(f_h^n + f_h^{n-1} \circ X_1(u_h^{n-1}, \Delta t),\ v_h\Big)_h, \qquad \forall v_h \in V_h, \\ \Big(\nabla \cdot u_h^n,\ q_h\Big)_h = 0, \qquad \forall q_h \in Q_h. \end{cases}$$

In the next section the scheme is shown to be of second order in Δt for $n \geq 2$, and of first order in Δt_0 for $n = 1$. By taking $\Delta t_0 = O(\Delta t^2)$, the whole scheme becomes of second order in time increment Δt.

Remark 5.1. *(i) For $v_h \in V_h$ and $q_h \in Q_h$ it holds that*

$$\Big\langle \mathscr{P}_{h1} q_h, v_h \Big\rangle = \Big\langle \mathscr{B}_h v_h, q_h \Big\rangle,$$

i.e., $\mathscr{P}_{h1} = \mathscr{B}_h'$ on Q_h, though $\mathscr{P}_{h1}$ is defined on $L^2(\Omega_h)$.
(ii) In $\mathscr{A}_h^n$ $(n \geq 2)$, we need u^{n-1} and p^{n-1} to get u^n and p^n. If $\mathscr{A}_{h2}$ were used when $n = 1$, we would need p^0, which is not given as the initial condition in the Navier-Stokes equations. This is the reason why we use $\mathscr{A}_{h1}$ at $n = 1$. In the case of the convection-diffusion equation, such fact does not occur.

Since the scheme is nonlinear in u_h^n for $n \geq 2$, we prepare an *internal iteration procedure*. Let $\{(w_h^k, r_h^k)\}_{k=1}^{\infty} \subset V_h \times Q_h$ be the solution of

$$\begin{cases} \mathscr{A}_{h2}(w_h^k, w_h^{k-1}, u_h^{n-1}, r_h^k, p_h^{n-1}) = \mathscr{F}_{h2}(f_h^n, f_h^{n-1}, u_h^{n-1}) & \text{in } V_h', \\ \mathscr{B}_h w_h^k = 0 & \text{in } Q_h', \end{cases} \tag{5.1}$$

where $w_h^0 \equiv u_h^{n-1}$. (u_h^n, p_h^n) is obtained as the limit of the sequence $\{(w_h^k, r_h^k)\}_{k=1}^{\infty}$. In the real computation if the convergence criterion,

$$\frac{\|w_h^k - w_h^{k-1}\|_{H^1(\Omega_h)^d} + \|r_h^k - r_h^{k-1}\|_{L^2(\Omega_h)}}{\|w_h^k\|_{H^1(\Omega_h)^d} + \|r_h^k\|_{L^2(\Omega_h)}} < \varepsilon_I \tag{5.2}$$

is satisfied for some k, we set $(u_h^n, p_h^n) \equiv (w_h^k, r_h^k)$. Here ε_I is a sufficiently small positive constant. We note that (5.1) is a linear problem in w_h^k and r_h^k whose matrix is symmetric.

Remark 5.2. *One can choose other finite element spaces $V_h \times Q_h$ satisfying the inf-sup condition* (2.11) *and $Q_h \subset H^1(\Omega_h)$.*

Remark 5.3. *Scheme* (S1) *requires that Q_h is a subset of $H^1(\Omega_h)$, because the pressure term is written in a strong form. Using a weak form for the pressure, which requires only $Q_h \subset L^2(\Omega_h)$, we can derive a scheme,*

$$\begin{cases} \tilde{\mathscr{A}}_h^n(u_h, p_h) = \mathscr{F}_h^n(f_h, u_h) & \text{in } V_h', \\ \qquad \mathscr{B}_h^n u_h = 0 & \text{in } Q_h', \end{cases} \tag{5.3}$$

where $u_h^0 \equiv \Pi_{h2} u^0$,

$$\begin{aligned} &\tilde{\mathscr{A}}_h^n(u, p) \\ &\equiv \begin{cases} \mathscr{M}_{h2}(u^n, u^n, u^{n-1}; \Delta t) + \mathscr{D}_{h2}(u^n, u^{n-1}) + \tilde{\mathscr{P}}_{h2}(u^{n-1}, p^n, p^{n-1}) & (n \geq 2), \\ \mathscr{M}_{h1}(u^1, u^0; \Delta t_0) + \mathscr{D}_{h1} u^1 + \mathscr{P}_{h1} p^1 & (n = 1), \end{cases} \\ &\Big\langle \tilde{\mathscr{P}}_{h2}(w, p, q), v_h \Big\rangle \equiv -\frac{1}{2}\Big(\nabla \cdot v_h,\ p + q \circ X_1(w, \Delta t)\Big)_h - \frac{\Delta t}{2}\Big(q w_{i,j},\ v_{hj,i}\Big)_h. \end{aligned} \tag{5.4}$$

The last term of (5.4) *is a correction term for second order accuracy in Δt. This scheme is proved to be of second order in Δt in a similar way to scheme* (S1) *by using the analysis in the next section. Numerical experiments, however, show that scheme* (5.3) *is not so stable. In fact, we could not get solutions for $\nu \leq 10^{-2}$ in Example 5.1 of Section 5.3 because of oscillation. Hence we do not use this scheme. To make a stable scheme in a weak form of the pressure is an open problem.*

5.2 Consistency of the scheme

In this section we assume $\Omega_h = \Omega$ for the sake of simplicity. For an integer n $(2 \le n \le N_T)$, we set

$$t^{n-1/2} \equiv \frac{1}{2}(t^n + t^{n-1}).$$

For a function ψ on $\Omega \times (0,T)$ and $m \in \mathbb{N} \cup \{\mathbb{N} - 1/2\} \cup \{0\}$ $(m \le N_T)$, ψ^m means

$$\psi^m \equiv \psi(\cdot, t^m).$$

Proposition 5.1 (consistency)**.** *Let $n \ge 2$. Suppose that f is a sufficiently smooth function, (u,p) is the sufficiently smooth solution of (2.6) and that $X_1(u^{n-1}, \Delta t)(\Omega)$, $X_2(u^n, u^{n-1}, \Delta t)(\Omega)$, $X_1(u^0, \Delta t_0)(\Omega) \subset \Omega$. Then for any $v_h \in V_h$ it holds that*

$$\Big\langle \mathscr{A}_{h2}(u^n, u^n, u^{n-1}, p^n, p^{n-1}) - \mathscr{F}_{h2}(f^n, f^{n-1}, u^{n-1}),\ v_h \Big\rangle = O(\Delta t^2)\|v_h\|, \quad \text{(5.5a)}$$

$$\Big\langle \mathscr{A}_{h1}(u^1, u^0, p^1) - \mathscr{F}_{h1} f^1,\ v_h \Big\rangle = O(\Delta t_0)\|v_h\|. \quad \text{(5.5b)}$$

□

We prepare some lemmas for the proof. The first one is trivial, but it is often used.

Lemma 5.1. *For a smooth function f it holds that*

$$\frac{1}{2}\Big(f(t) + f(t - \Delta t)\Big) = f(t - \frac{\Delta t}{2}) + O(\Delta t^2), \quad \text{(5.6a)}$$

$$\frac{f(t) - f(t - \Delta t)}{\Delta t} = f'(t - \frac{\Delta t}{2}) + O(\Delta t^2). \quad \text{(5.6b)}$$

□

Let $u : \Omega \times (0,T) \to \mathbb{R}^d$ be a smooth function. For a point $x \in \Omega$, let $X(\,\cdot\,; x) : (0,T) \to \mathbb{R}^d$ be the solution of the ordinary differential equation (3.1). We note that the material derivative of a function $f : \Omega \times (0,T) \to \mathbb{R}$ is written as

$$\frac{Df}{Dt}\big(X(t), t\big) = \frac{d}{dt} f\big(X(t), t\big). \quad \text{(5.7)}$$

Setting

$$Y_1(u,\Delta t)(x) \equiv \frac{x + X_1(u,\Delta t)(x)}{2},$$

we evaluate the equations at a point

$$P^{n-1/2}(x) \equiv \left(Y_1(u^{n-1},\Delta t)(x),\ t^{n-1/2}\right), \tag{5.8}$$

shown in Figure 5.1.

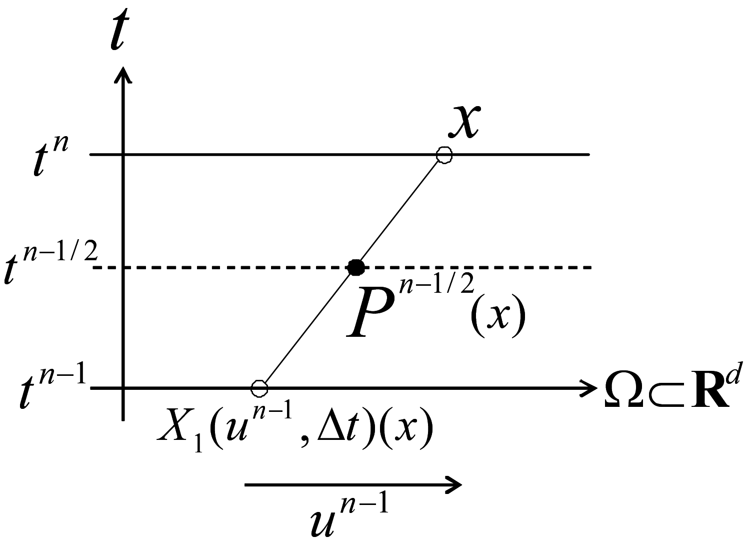

Figure 5.1: The evaluation point for the consistency

Using the approximation X_2 for $X(t^{n-1})$, we can construct a second order discretization of the material derivative as follows.

Lemma 5.2. *Let u be a sufficiently smooth function and* $X_2\,(u^n,u^{n-1},\Delta t)(\Omega) \subset \Omega$. *Then it holds that*

$$\frac{u^n(x) - u^{n-1} \circ X_2(u^n,u^{n-1},\Delta t)(x)}{\Delta t} = \frac{Du}{Dt}\left(P^{n-1/2}(x)\right) + O(\Delta t^2). \tag{5.9}$$

Proof. Let X be the solution of (3.1). Substituting u into f in (5.7) and using (5.6b), we have

$$\frac{Du}{Dt}(X(t^{n-1/2}),t^{n-1/2}) = \frac{u^n(X(t^n)) - u^{n-1}(X(t^{n-1}))}{\Delta t} + O(\Delta t^2). \tag{5.10}$$

Since the Heun method is of second order in time, we have

$$
\begin{aligned}
X(t^{n-1};x) &= x - \Big\{u^n(x) + u^{n-1}\big(x - u^n(x)\Delta t\big)\Big\}\frac{\Delta t}{2} + O(\Delta t^3) \\
&= x - \Big\{u^n(x) + u^{n-1}\big(x - u^{n-1}(x)\Delta t\big)\Big\}\frac{\Delta t}{2} + O(\Delta t^3) \\
&= X_2(u^n, u^{n-1}, \Delta t)(x) + O(\Delta t^3). \qquad (5.11)
\end{aligned}
$$

On the other hand, by (5.6a), it holds that

$$
X(t^{n-1/2};x) = Y_1(u^{n-1}, \Delta t)(x) + O(\Delta t^2). \qquad (5.12)
$$

Combining (5.11) and (5.12) with (5.10), we get (5.9). □

Lemma 5.3. *Suppose that* $u,\ f:\ \Omega\times(0,T)\to\mathbb{R}^d$ *and* $p:\ \Omega\times(0,T)\to\mathbb{R}$ *are sufficiently smooth functions and that* $X_1(u^{n-1},\Delta t)(\Omega)$ *and* $X_2(u^n,u^{n-1},\Delta t)(\Omega)\subset\Omega$. *Then for any* $x\in\Omega$ *it holds that*

$$
\begin{aligned}
&\frac{u^n - u^{n-1}\circ X_2(u^n,u^{n-1},\Delta t)}{\Delta t}(x) - \nu\Big\{\nabla D(u^n) + \nabla D(u^{n-1})\circ X_1(u^{n-1},\Delta t)\Big\}(x) \\
&\quad + \frac{1}{2}\Big\{\nabla p^n + \nabla p^{n-1}\circ X_1(u^{n-1},\Delta t)\Big\}(x) - \frac{1}{2}\Big\{f^n + f^{n-1}\circ X_1(u^{n-1},\Delta t)\Big\}(x) \\
&= \Big(\frac{Du}{Dt} - 2\nu\nabla D(u) + \nabla p - f\Big)\big(P^{n-1/2}(x)\big) + O(\Delta t^2), \qquad (5.13)
\end{aligned}
$$

where $P^{n-1/2}(x)$ *is a point defined by* (5.8).

Proof. Let $X(\cdot;x)$ be the solution of (3.1). Substituting $(-2\nu\nabla D(u)+\nabla p - f)(X(\cdot),\cdot)$ into f and t^n into t in (5.6a), using the relation

$$
X(t^{n-1};x) = X_1(u^{n-1},\Delta t)(x) + O(\Delta t^2),
$$

we have

$$
\begin{aligned}
&-\nu\Big\{\nabla D(u^n) + \nabla D(u^{n-1})\circ X_1(u^{n-1},\Delta t)\Big\}(x) + \frac{1}{2}\Big\{\nabla p^n + \nabla p^{n-1}\circ X_1(u^{n-1},\Delta t)\Big\}(x) \\
&\quad - \frac{1}{2}\Big\{f^n + f^{n-1}\circ X_1(u^{n-1},\Delta t)\Big\}(x) \\
&= \Big\{-2\nu\nabla D(u) + \nabla p - f\Big\}\Big(P^{n-1/2}(x)\Big) + O(\Delta t^2). \qquad (5.14)
\end{aligned}
$$

Combining (5.14) with Lemma 5.2, we get the result. □

Lemma 5.4. *Let $u : \Omega \to \mathbb{R}^d$ be a sufficiently smooth function satisfying $\nabla \cdot u = 0$ in Ω and $X_1(u, \Delta t)(\Omega) \subset \Omega$. Then for any $v_h \in V_h$ it holds that*

$$
\begin{aligned}
& -\Big(\nabla D(u) \circ X_1(u, \Delta t), v_h\Big) \\
& \quad = \Big(D(u) \circ X_1(u, \Delta t), D(v_h)\Big) + \Delta t \Big(D_{ij}(u) u_{k,j}, v_{hi,k}\Big) + O(\Delta t^2)\|v_h\|. \qquad (5.15)
\end{aligned}
$$

Proof. Since $\nabla \cdot u = 0$ in Ω, it holds that

$$
\begin{aligned}
& \Big(u_{i,j} \circ X_1(u, \Delta t), v_{hi,j}\Big) = -\Big(\big(u_{i,j} \circ X_1(u, \Delta t)\big)_{,j}, v_{hi}\Big) \\
& = -\Big(u_{i,jk} \circ X_1(u, \Delta t)(\delta_{kj} - u_{k,j}\Delta t), v_{hi}\Big) \\
& = -\Big(u_{i,jj} \circ X_1(u, \Delta t), v_{hi}\Big) + \Delta t \Big(u_{i,jk} \circ X_1(u, \Delta t) u_{k,j}, v_{hi}\Big) \\
& = -\Big(u_{i,jj} \circ X_1(u, \Delta t), v_{hi}\Big) + \Delta t \Big(u_{i,jk} u_{k,j}, v_{hi}\Big) + O(\Delta t^2)\|v_h\| \\
& = -\Big(u_{i,jj} \circ X_1(u, \Delta t), v_{hi}\Big) - \Delta t \Big(u_{i,j} u_{k,j}, v_{hi,k}\Big) + O(\Delta t^2)\|v_h\|.
\end{aligned}
$$

Similarly we have

$$
\begin{aligned}
& \Big(u_{i,j} \circ X_1(u, \Delta t), v_{hj,i}\Big) = -\Big(\big(u_{i,j} \circ X_1(u, \Delta t)\big)_{,i}, v_{hj}\Big) \\
& = -\Big(u_{i,ji} \circ X_1(u, \Delta t), v_{hj}\Big) - \Delta t \Big(u_{i,j} u_{k,i}, v_{hj,k}\Big) + O(\Delta t^2)\|v_h\| \\
& = -\Big(u_{j,ij} \circ X_1(u, \Delta t), v_{hi}\Big) - \Delta t \Big(u_{j,i} u_{k,j}, v_{hi,k}\Big) + O(\Delta t^2)\|v_h\|.
\end{aligned}
$$

Therefore, it holds that

$$
\begin{aligned}
\Big(D(u) \circ X_1(u, \Delta t), D(v_h)\Big) &= \frac{1}{2}\Big\{\Big(u_{i,j} \circ X_1(u, \Delta t), v_{hi,j}\Big) + \Big(u_{i,j} \circ X_1(u, \Delta t), v_{hj,i}\Big)\Big\} \\
&= -\Big(\nabla D(u) \circ X_1(u, \Delta t), v_h\Big) - \Delta t \Big(D_{ij}(u) u_{k,j}, v_{hi,k}\Big) \\
&\qquad + O(\Delta t^2)\|v_h\|,
\end{aligned}
$$

which completes the proof. □

Proof of Proposition 5.1. Substituting u^{n-1} into u in Lemma 5.4, we have

$$
-\nu\Big(\nabla D(u^{n-1}) \circ X_1(u^{n-1}, \Delta t), v_h\Big)
$$

$$= \nu \Big\{ \Big(D(u^{n-1}) \circ X_1(u^{n-1}, \Delta t), D(v_h) \Big) + \Delta t \Big(D_{ij}(u^{n-1}) u_{k,j}^{n-1}, v_{hi,k} \Big) \Big\} + O(\Delta t^2) \|v_h\|. \tag{5.16}$$

Obviously it holds that

$$-\nu \Big(\nabla D(u^n), v_h \Big) = \nu \Big(D(u^n), D(v_h) \Big). \tag{5.17}$$

Combining (5.16) and (5.17) with Lemma 5.3, we have

$$\begin{aligned} & \Big\langle \mathscr{A}_{h2}(u^n, u^n, u^{n-1}, p^n, p^{n-1}) - \mathscr{F}_h^n(f, u), v_h \Big\rangle \\ = & \Big(\big(\frac{Du}{Dt} - \nabla(2\nu D(u)) + \nabla p - f \big)^{n-1/2} \circ Y_1(u^{n-1}, \Delta t), v_h \Big) + O(\Delta t^2) \|v_h\|. \end{aligned}$$

Here we have used (5.6b) again. Since (u, p) is the solution of (2.6), we get (5.5a). The proof of (5.5b) is similar. □

5.3 Numerical results

In this section we show numerical results in $d = 2$ to observe the numerical convergence rate of the scheme. We use the CG method with ILU(0) preconditioner [2] for solving the system of linear equations. In the scheme we have to compute integrals of composite functions such as,

$$\int_K u_h^{n-1} \circ X_2(w^{k-1}, u_h^{n-1}, \Delta t) v_h \, dx$$

on triangular elements K. The integrand

$$u_h^{n-1} \circ X_2(w^{k-1}, u_h^{n-1}, \Delta t) v_h$$

is not smooth on K. It is known that rough numerical integration causes oscillation even in the case that the stability is theoretically proved for a scheme with exact integration, see Tabata [41] and Tabata and Fujima [44]. Hence, much attention should be paid to numerical integration of composite functions. Here, we use a numerical integration formula of degree five on each triangle described in Section 4.1.

Example 5.1. *In (2.6) we take* $\Omega = (0,1)^2$, $T = 1$, *and five values of* ν,

$$\nu = 1,\ 10^{-1},\ 10^{-2},\ 10^{-3},\ 10^{-4}.$$

The functions f *and* u^0 *are given so that the exact solution is*

$$\begin{pmatrix} u \\ p \end{pmatrix}(x,t) = \{1+\sin(\pi t)\}\begin{pmatrix} \sin^2(\pi x_1)\sin(2\pi x_2) \\ -\sin^2(\pi x_2)\sin(2\pi x_1) \\ \cos(\pi x_1)\cos(\pi x_2) \end{pmatrix}. \tag{5.18}$$

We used FreeFem++ [13] for mesh generation. Let N_Ω be the division number of each side of Ω and $h \equiv 1/N_\Omega$ be the representative length of each mesh. Figure 5.2 (left) shows a sample mesh $(N_\Omega = 8)$. We solve the problem by the scheme (S1). Since the convergence rate of the backward Euler scheme of the P2/P1 Galerkin approximation is $O(\Delta t + h^2)$ for the Navier-Stokes equations, e.g., (2.13), we choose $\Delta t = h$. Furthermore we set $\Delta t_0 = h^2$ and $\varepsilon_I = 10^{-5}$. We calculated $Err_{\mathrm{P2/P1}}$ defined by

$$Err_{\mathrm{P2/P1}} \equiv \frac{\|\Pi_{h2}u - u_h\|_{l^2(H^1(\Omega)^2)} + \|\Pi_{h1}p - p_h\|_{l^2(L^2(\Omega))}}{\|u_h\|_{l^2(H^1(\Omega)^2)} + \|p_h\|_{l^2(L^2(\Omega))}}.$$

Figure 5.2 (right) shows the graph of $Err_{\mathrm{P2/P1}}$ versus Δt in logarithmic scale for $N_\Omega = 8,\ 16,\ 32$ and 64, and the values of $Err_{\mathrm{P2/P1}}$ and the slopes are given in Table 5.1. We can observe a second order convergence in Δt. Figure 5.3 exhibits the graph of maximum internal iteration number versus Δt. It decreases as Δt becomes small and was equal to 3 or 4 for $\Delta t = 1/64$.

Now we examine the importance of the additional correction term

$$\nu\Delta t\Big(D_{ij}(u^{n-1})u^{n-1}_{k,j},\ v_{hi,k}\Big) \tag{5.19}$$

in the definition of $\mathscr{D}_{h2}$. We compare results obtained by schemes with and without this term as well as the first order scheme. Dropping the term from the scheme (S1), we get

$$\begin{cases} \hat{\mathscr{A}}^n_h(u_h, p_h) = \mathscr{F}^n_h(f_h, u_h) & \text{in } V_h', \\ \mathscr{B}^n_h u_h = 0 & \text{in } Q_h', \end{cases} \tag{5.20}$$

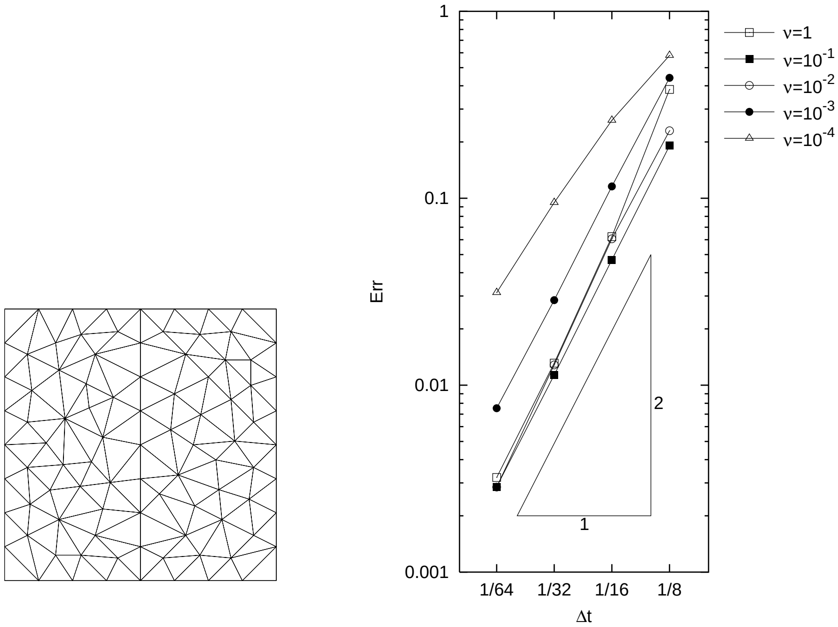

Figure 5.2: A sample mesh $(N_\Omega = 8)$ and the graph of $Err_{\mathrm{P2/P1}}$ versus Δt in logarithmic scale

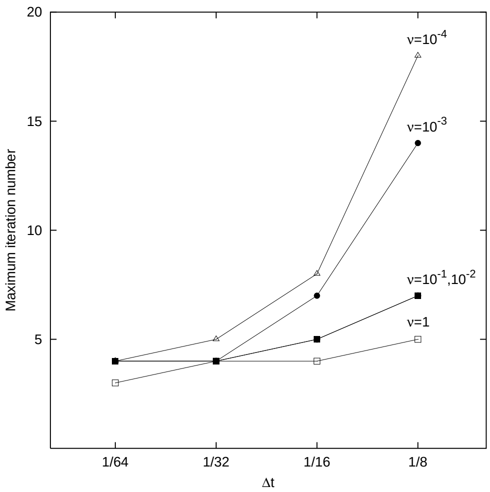

Figure 5.3: The graph of maximum iteration number versus Δt for each ν

where $u_h^0 \equiv \Pi_{h2} u^0$,

$$\hat{\mathscr{A}}_h^n(u,p) \equiv \begin{cases} \hat{\mathscr{A}}_{h2}(u^n, u^n, u^{n-1}, p^n, p^{n-1}) & (n \geq 2), \\ \mathscr{A}_{h1}(u^1, u^0, p^1) & (n = 1), \end{cases}$$

$$
\begin{aligned}
\hat{\mathscr{A}}_{h2}(u,\zeta,w,p,q) &\equiv \mathscr{M}_{h2}(u,\zeta,w\,;\Delta t) + \hat{\mathscr{D}}_{h2}(u,w) + \mathscr{P}_{h2}(w,p,q),\\
\left\langle \hat{\mathscr{D}}_{h2}(u,w), v_h \right\rangle &\equiv \nu\Big(D(u) + D(w)\circ X_1(w,\Delta t),\ D(v_h)\Big).
\end{aligned}
$$

The first order scheme is

$$
\begin{cases}
\mathscr{A}^n_{h1}(u_h,p_h) = \mathscr{F}^n_{h1} f_h & \text{in } V_h',\\
\mathscr{B}^n_h u_h = 0 & \text{in } Q_h',
\end{cases}
\tag{5.21}
$$

where $u_h^0 \equiv \Pi_{h2} u^0$,

$$
\begin{aligned}
\mathscr{A}^n_{h1}(u,p) &\equiv \begin{cases}
\mathscr{M}_{h1}(u^n,u^{n-1};\Delta t) + \mathscr{D}_{h1}u^n + \mathscr{P}_{h1}p^n & (n \ge 2),\\
\mathscr{M}_{h1}(u^1,u^0;\Delta t_0) + \mathscr{D}_{h1}u^1 + \mathscr{P}_{h1}p^1 & (n = 1).
\end{cases}\\
\mathscr{F}^n_{h1} f &\equiv \mathscr{F}_{h1} f^n.
\end{aligned}
$$

In the first order scheme we do not need to use a first step with a small time increment Δt_0. For the comparison with other schemes, however, we use the first step with Δt_0. We solve Example 5.1 under the same condition. The results obtained from the three schemes are shown in Figure 5.4 and Table 5.1. In the case of $\nu = 1$ the values of $Err_{\mathrm{P2/P1}}$ of the scheme (5.20) are worse than those of the scheme (5.21). In the case of $\nu = 10^{-1}$ the results of (5.20) is better than those of (5.21), but the slope of (5.20) is worse than that of the present scheme (S1). In the cases $\nu = 10^{-2}, 10^{-3}$ and 10^{-4} there is no clear difference between the results by (5.20) and (S1). These results are explained from the fact that the additional correction term (5.19) contains ν and is proportional to it. These results exhibit the necessity of the additional correction term for second order in Δt.

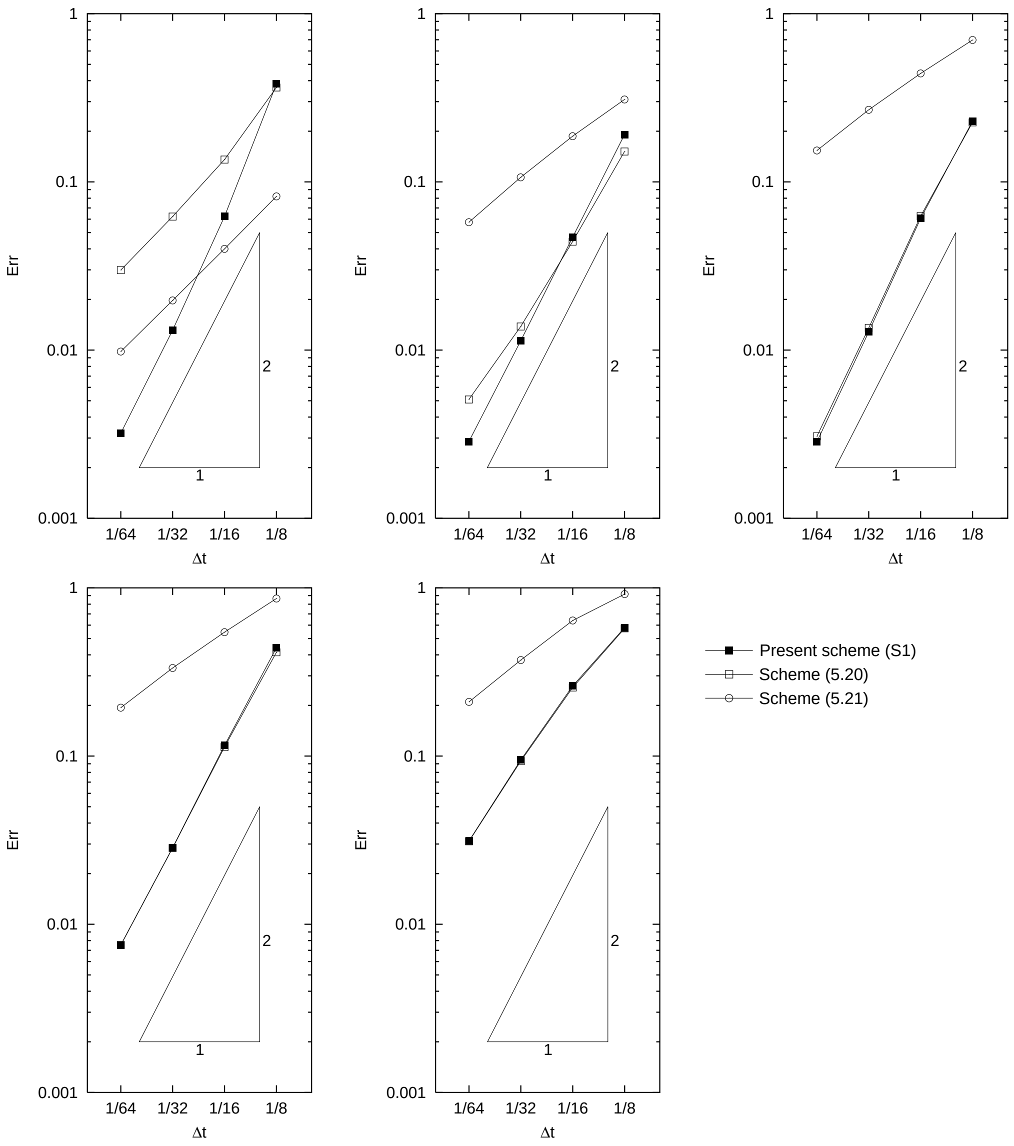

Figure 5.4: Comparison of convergence order: $\nu = 1$ (top left), 10^{-1} (top center), 10^{-2} (top right), 10^{-3} (bottom left) and 10^{-4} (bottom right)

Table 5.1: Values of $Err_{\mathrm{P2/P1}}$ and slopes of the graphs in Figures 5.2 and 5.4

	N_Ω	Present scheme (S1) $Err_{\mathrm{P2/P1}}$	slope	Scheme (5.20) $Err_{\mathrm{P2/P1}}$	slope	Scheme (5.21) $Err_{\mathrm{P2/P1}}$	slope
$\nu = 1:$	8	3.82×10^{-1}	—	3.64×10^{-1}	—	8.20×10^{-2}	—
	16	6.23×10^{-2}	2.62	1.36×10^{-1}	1.42	4.00×10^{-2}	1.04
	32	1.31×10^{-2}	2.25	6.22×10^{-2}	1.13	1.97×10^{-2}	1.02
	64	3.21×10^{-3}	2.03	2.99×10^{-2}	1.06	9.80×10^{-3}	1.01
$\nu = 10^{-1}:$	8	1.91×10^{-1}	—	1.51×10^{-1}	—	3.09×10^{-1}	—
	16	4.68×10^{-2}	2.03	4.41×10^{-2}	1.78	1.87×10^{-1}	0.73
	32	1.13×10^{-2}	2.05	1.38×10^{-2}	1.68	1.06×10^{-1}	0.81
	64	2.86×10^{-3}	1.99	5.08×10^{-3}	1.44	5.76×10^{-2}	0.89
$\nu = 10^{-2}:$	8	2.30×10^{-1}	—	2.26×10^{-1}	—	6.98×10^{-1}	—
	16	6.07×10^{-2}	1.92	6.26×10^{-2}	1.85	4.41×10^{-1}	0.66
	32	1.28×10^{-2}	2.24	1.35×10^{-2}	2.21	2.68×10^{-1}	0.72
	64	2.85×10^{-3}	2.17	3.07×10^{-3}	2.14	1.54×10^{-1}	0.80
$\nu = 10^{-3}:$	8	4.41×10^{-1}	—	4.14×10^{-1}	—	8.65×10^{-1}	—
	16	1.16×10^{-1}	1.93	1.13×10^{-1}	1.87	5.45×10^{-1}	0.67
	32	2.85×10^{-2}	2.02	2.84×10^{-2}	2.00	3.34×10^{-1}	0.71
	64	7.53×10^{-3}	1.92	7.53×10^{-3}	1.92	1.94×10^{-1}	0.78
$\nu = 10^{-4}:$	8	5.81×10^{-1}	—	5.75×10^{-1}	—	9.18×10^{-1}	—
	16	2.61×10^{-1}	1.15	2.56×10^{-1}	1.17	6.39×10^{-1}	0.52
	32	9.48×10^{-2}	1.46	9.35×10^{-2}	1.45	3.72×10^{-1}	0.78
	64	3.13×10^{-2}	1.60	3.11×10^{-2}	1.59	2.10×10^{-1}	0.83

Chapter 6

Stabilized finite element method for the Stokes equations

In this chapter we deal with the Stokes equations, and the stabilized finite element methods are reviewed. In Section 6.1, the Stokes equations and its variational formulation are given. In Section 6.2 we review two stabilized finite element methods. These are called the Galerkin least square stabilized method and the penalty stabilized method, respectively.

6.1 Statement of the problem

We consider the stationary Stokes problem subject to the Dirichlet boundary condition; find $(u,\ p) : \Omega \to \mathbb{R}^d \times \mathbb{R}$ such that

$$\begin{cases} -2\nabla D(u) + \nabla p = f & \text{in } \Omega, \\ \nabla \cdot u = 0 & \text{in } \Omega, \\ u = g & \text{on } \Gamma, \end{cases} \tag{6.1}$$

where u is the velocity, p is the pressure, f is an external force and g is a boundary velocity. We assume that the velocity u vanishes on the boundary Γ, i.e., $g = 0$, for the sake of simplicity. We note that the Stokes equations (6.1) with $g = 0$ are linear.

Let a continuous bilinear form $\tilde{a}$ on $X \times X$ be the form a defined in (2.7a) with $\nu = 1$. A variational formulation for (6.1) is to find $(u, p) \in V \times Q$ such that

$$\begin{cases} \tilde{a}(u,v) + b(v,p) = (f,v), & \forall v \in V, \\ \qquad\qquad b(u,q) = 0, & \forall q \in Q. \end{cases} \tag{6.2}$$

Obviously, (6.2) is equivalent to the equation,

$$\tilde{a}(u,v) + b(v,p) + b(u,q) = (f,v), \quad \forall (v,q) \in V \times Q. \tag{6.3}$$

6.2 Stabilized finite element schemes for the Stokes equations

We refer to Franca and Stenberg [12] for the Galerkin least square stabilized method and Brezzi and Douglas Jr. [6] for the penalty stabilized method. For convenience, in this section we assume $\Omega = \Omega_h$.

6.2.1 Galerkin least square stabilization

Let δ be a positive constant, h_K be the diameter of element $K \in \mathscr{T}_h$ and $(\cdot,\cdot)_K \equiv (\cdot,\cdot)_{L^2(K)^d}$. We define a bilinear form $\mathscr{C}_h^{\mathrm{GLS}}$ on $(X \times M)^2$ by

$$\mathscr{C}_h^{\mathrm{GLS}}\big((u,p),(v,q)\big) \equiv -\delta \sum_{K \in \mathscr{T}_h} h_K^2 \big(-2\nabla D(u) + \nabla p,\ -2\nabla D(v) + \nabla q\big)_K,$$

and bilinear forms B_h^{GLS} on $(X \times M)^2$ and F_h^{GLS} on $X \times M$ by

$$B_h^{\mathrm{GLS}}\big((u,p),(v,q)\big) \equiv \tilde{a}(u,v) + b(v,p) + b(u,q) + \mathscr{C}_h^{\mathrm{GLS}}\big((u,p),(v,q)\big), \tag{6.4}$$

$$F_h^{\mathrm{GLS}}(v,q) \equiv (f,v) - \delta \sum_{K \in \mathscr{T}_h} h_K^2 \big(f,\ -2\nabla D(v) + \nabla q\big)_K, \tag{6.5}$$

respectively.

Let $V_h \subset V$ and $Q_h \subset Q$ be any conforming finite element spaces, i.e., for any fixed numbers $k,\ l \in \mathbb{N}$, $X_h \equiv X_{hk}$ and $M_h \equiv M_{hl}$. The scheme by the Galerkin least square stabilized method is to find $(u_h, p_h) \in V_h \times Q_h$ such that

$$B_h^{\mathrm{GLS}}\big((u_h, p_h),(v_h,q_h)\big) = F_h^{\mathrm{GLS}}(v_h,q_h), \quad \forall (v_h,q_h) \in V_h \times Q_h. \tag{6.6}$$

Let C_I be a fixed constant satisfying the inverse inequality,

$$C_I \sum_{K\in\mathscr{T}_h} h_K^2 \|\nabla D(v_h)\|^2_{L^2(K)^d} \le \|D(v_h)\|^2, \quad \forall v_h \in V_h.$$

For any fixed δ $(0 < \delta \le C_I)$, the sufficiently smooth solution (u,p) of (6.1) and the solution (u_h, p_h) of (6.6), the scheme has the following convergence property. There exits a constant $C > 0$ such that

$$\|u-u_h\|_{H^1} + \|p-p_h\| \le C(h^k + h^{l+1}). \tag{6.7}$$

For the proof, see Franca and Stenberg [12].

The scheme with P1/P1 element

Let us consider a special element P1/P1, i.e., $X_h \equiv X_{h1}$ and $M_h \equiv M_{h1}$. The scheme (6.6) does not impose inf-sup condition (2.11), and we can choose a cheap element P1/P1. Then, $\nabla D(v_h)\big|_K = 0$ for any $K \in \mathscr{T}_h$ and $v_h \in V_h$. Therefore, we can take any $\delta > 0$ and it holds that, for $(u_h, p_h),\ (v_h, q_h) \in V_h \times Q_h$,

$$B_h^{\mathrm{GLS}}\big((u_h, p_h),(v_h,q_h)\big) = \tilde{a}(u_h,v_h) + b(v_h,p_h) + b(u_h,q_h) + \mathscr{C}_h(p_h,q_h), \tag{6.8}$$

$$F_h^{\mathrm{GLS}}(v_h,q_h) = (f,v_h) - \delta \sum_{K\in\mathscr{T}_h} h_K^2 (f,\ \nabla q_h)_K, \tag{6.9}$$

where $\mathscr{C}_h$ is a bilinear form on $M \times M$ defined by

$$\mathscr{C}_h(p,q) \equiv -\delta \sum_{K\in\mathscr{T}_h} h_K^2 (\nabla p,\ \nabla q)_K. \tag{6.10}$$

The error estimate (6.7) becomes

$$\|u-u_h\|_{H^1} + \|p-p_h\| \le Ch. \tag{6.11}$$

6.2.2 Penalty stabilization with P1/P1 element

We use a cheap element P1/P1, i.e., $X_h \equiv X_{h1}$ and $M_h \equiv M_{h1}$. We define a bilinear forms on $(X \times M)^2$ by

$$B_h^{\mathrm{Pnlty}}\big((u,p),(v,q)\big) \equiv \tilde{a}(u,v) + b(v,p) + b(u,q) + \mathscr{C}_h(p,q). \tag{6.12}$$

The scheme by the penalty stabilized method is to find $(u_h, p_h) \in V_h \times Q_h$ such that

$$B_h^{\mathrm{Pnlty}}\big((u_h,p_h),(v_h,q_h)\big) = (f, v_h), \quad \forall (v_h,q_h) \in V_h \times Q_h. \tag{6.13}$$

The equation (6.13) is equivalent to the equations,

$$\begin{cases} \tilde{a}(u_h,v_h) + b(v_h,p_h) = (f,v_h), & \forall v_h \in V_h, \\ b(u_h,q_h) + \mathscr{C}_h(p_h,q_h) = 0, & \forall q_h \in Q_h. \end{cases} \tag{6.14}$$

For any fixed $\delta > 0$, the sufficiently smooth solution (u,p) of (6.1) and the solution (u_h,p_h) of (6.13), the scheme has the following convergence property. There exits a constant $C > 0$ such that

$$\|u - u_h\|_{H^1} + \|p - p_h\| \leq Ch. \tag{6.15}$$

The proof has been given in Brezzi and Douglas Jr. [6].

Let us compare the scheme (6.13) with the scheme (6.6) using P1/P1 element. The convergence order of (6.13) is the same as one of (6.6), see (6.15) and (6.11). For P1/P1 element, it holds that, for $(u_h,p_h),(v_h,q_h) \in V_h \times Q_h$,

$$B_h^{\mathrm{GLS}}\big((u_h,p_h),(v_h,q_h)\big) = B_h^{\mathrm{Pnlty}}\big((u_h,p_h),(v_h,q_h)\big).$$

Therefore, the difference of the schemes (6.6) and (6.13) is that there is or is not the term,

$$-\delta \sum_{K \in \mathscr{T}_h} h_K^2 (f,\ \nabla q_h)_K$$

in the right hand sides. For P1/P1 element, the scheme (6.13) is simpler than the scheme (6.6).

Chapter 7

A pressure-stabilized characteristic-curve finite element scheme

This chapter is devoted to a study of a pressure-stabilized characteristic-curve finite element scheme. The scheme is a combined one with a penalty stabilization method introduced in Subsection 6.2.2 and the first order characteristic-curve method explained in Subsection 3.1.1. The scheme is presented in Section 7.1 and a proposition on the stability of the scheme is given in Section 7.2. In Section 7.3 numerical results are shown. There, test problems and cavity flow problems are solved in 2D and 3D. Contents of this chapter are described in the author and Tabata [31] and the author [30].

7.1 The finite element scheme

We employ a cheap element P1/P1, i.e., $X_h \equiv X_{h1}$ and $M_h \equiv M_{h1}$. We define bilinear forms a_h on $H^1(\Omega)^d \times H^1(\Omega)^d$ and b_h on $H^1(\Omega)^d \times L^2(\Omega)$ by

$$a_h(u,v) \equiv 2\nu\Big(D(u),\ D(v)\Big)_h,$$

$$b_h(v,q) \equiv -(\nabla \cdot v,\ q)_h,$$

respectively, For a given continuous function f, we set $f_h^n \equiv \Pi_{h1} f^n$ in this chapter.

We present the scheme for (2.6); find $\{(u_h^n,\ p_h^n) \in V_h(g^n) \times Q_h;\ n = 1, \cdots, N_T\}$ such that, for $n = 1, \cdots, N_T$,

$$\begin{cases} \langle \mathscr{M}_h(u_h^n, u_h^{n-1}; \Delta t), v_h \rangle + a_h(u_h^n, v_h) + b_h(v_h, p_h^n) = (f_h^n, v_h)_h, & \forall v_h \in V_h, \\ b_h(u_h^n, q_h) + \mathscr{C}_h(p_h^n, q_h) = 0, & \forall q_h \in Q_h, \end{cases} \tag{S2}$$

where $u_h^0 \equiv \Pi_{h1} u^0$.

7.2 Stability of the scheme

Setting a seminorm $|\cdot|_h$ of M_h, for $q_h \in M_h$,

$$|q_h|_h \equiv \left\{ \sum_{K \in \mathscr{T}_h} h_K^2 (\nabla q_h,\ \nabla q_h)_K \right\}^{1/2},$$

we define, for a given sequence $\{r_h^n\}_{n=1}^{N_T} \subset M_h$,

$$|r_h|'_{l^2(M_h)} \equiv \left\{ \Delta t \sum_{n=1}^{N_T} |r_h^n|_h^2 \right\}^{1/2}.$$

For a solution $\{(u_h^n,\ p_h^n)\}_{n=1}^{N_T}$ of (S2), we assume the following hypothesis.

Hypothesis 7.1. *There exists a positive constant c_1, independent of h and Δt, such that, for $n = 0, \cdots, N_T - 1$,*

$$\frac{1}{\Delta t} \| u_h^n - u_h^n \circ X_1(u_h^n, \Delta t) \| \le c_1 \| u_h^n \|. \tag{H}$$

Remark 7.1. *In the case of convection-diffusion equation whose unknown function is ϕ, an inequality corresponding to* (H) *is*

$$\frac{1}{\Delta t} \| \phi_h^n - \phi_h^n \circ X_1(u^n, \Delta t) \| \le c_1 \| \phi_h^n \|.$$

The inequality (H) *holds, if* $u \in C^0([0,T];\ W^{1,\infty}(\Omega)^d)$ *[36, Lemma 1], where* $C^0([0,T];\ W^{1,\infty}(\Omega)^d)$ *is the space of* $W^{1,\infty}(\Omega)^d$*-valued continuous functions in* $[0,T]$*. Since u is the unknown function in the case of the Navier-Stokes equations, we assume* (H) *and examine it numerically.*

The scheme (S2) is stable under the hypothesis (H).

Proposition 7.1. *Suppose that* $g = 0$ *and* $f \in C^0(\overline{\Omega} \times [0,T])^d$*. Let* $\delta(> 0)$ *and* $\Delta t_0(< 1/2)$ *be a fixed number. Assume that for any* $\Delta t \le \Delta t_0$*,* $X_1(u_h^n, \Delta t)(\Omega_h) \subset \Omega_h\, (\forall n,\ 0 \le n \le N_T - 1)$ *and the Hypothesis 7.1 hold. Then, there exists a positive constant C, independent of h and* Δt*, such that*

$$\|u_h\|_{l^\infty(L^2)} + \sqrt{\nu}\,\|D(u_h)\|_{l^2(L^2)} + \sqrt{\delta}|p_h|'_{l^2(M_h)} \le C\big(\|u_h^0\| + \|f_h\|_{l^2(L^2)}\big). \quad (7.1)$$

Proof. We fix any number $n\,(1 \le n \le N_T)$. Substituting $(u_h^n,\ -p_h^n) \in V_h \times Q_h$ into $(v_h,\ q_h)$ in (S2), summing the two equations, we have

$$\frac{1}{\Delta t}\big(u_h^n - u_h^{n-1} \circ X_1(u_h^{n-1}, \Delta t),\ u_h^n\big)_h + 2\nu\|D(u_h^n)\|^2 + \delta|p_h^n|_h^2 = (f_h^n,\ u_h^n)_h.$$

It holds that

$$\begin{aligned}&\frac{1}{\Delta t}\big(u_h^n - u_h^{n-1},\ u_h^n\big)_h + 2\nu\|D(u_h^n)\|^2 + \delta|p_h^n|_h^2\\ &\quad = (f_h^n,\ u_h^n)_h - \frac{1}{\Delta t}\big(u_h^{n-1} - u_h^{n-1} \circ X_1(u_h^{n-1}, \Delta t),\ u_h^n\big)_h.\end{aligned}$$

Using the inequalities, $(a^2 - b^2)/2 \le (a-b)a$ and $ab \le (a^2 + b^2)/2$, we obtain

$$\begin{aligned}&\bar{D}_{\Delta t}\Big(\frac{1}{2}\|u_h^n\|^2\Big) + 2\nu\|D(u_h^n)\|^2 + \delta|p_h^n|_h^2\\ &\quad \le \|u_h^n\|^2 + \frac{1}{2}\|f_h^n\|^2 + \frac{1}{2}\big(\frac{1}{\Delta t}\|u_h^{n-1} - u_h^{n-1} \circ X_1(u_h^{n-1}, \Delta t)\|\big)^2.\end{aligned}$$

From the Hypothesis 7.1, it holds that

$$\bar{D}_{\Delta t}\Big(\frac{1}{2}\|u_h^n\|^2\Big) + 2\nu\|D(u_h^n)\|^2 + \delta|p_h^n|_h^2 \le \|u_h^n\|^2 + \frac{c_1^2}{2}\|u_h^{n-1}\|^2 + \frac{1}{2}\|f_h^n\|^2. \quad (7.2)$$

Since the above inequality (7.2) holds for $n = 1, \cdots, N_T$, the discrete Gronwall's inequality [46] leads to the desired result (7.1). □

Remark 7.2. *Proposition 7.1 implies the solvability of the scheme* (S2)*, because the scheme is linear in* (u_h^n, p_h^n).

Now, we consider the stability and advantages of the scheme (S2). Generally, for time integration, the forward Euler method yields such advantages as symmetry of the matrix and an explicit scheme, and a disadvantage, strict choice of time increment, e.g., for a constant $C > 0$ a stability condition $\Delta t \le Ch^2$ is required, and the backward Euler method (or Crank-Nicolson method) has the opposite properties, i.e., the matrix is nonsymmetric because of the convection term, and stability condition is less severe. The scheme (S2) uses the backward Euler method, and we can take large Δt. In fact Proposition 7.1 on the stability holds, and neither a stability condition like $\Delta t \le Ch^2$ nor the CFL condition [34] is assumed in the proposition. Furthermore, the scheme has an advantage of the characteristic-curve method, i.e., the matrix is symmetric and identical, which enables us to use symmetric linear solvers. For the Navier-Stokes equations there are two types of stabilization. The one is a pressure-stabilization which is required when the inf-sup condition on V_h and Q_h is not satisfied. The other is a stabilization for the nonlinear convection term. It is well known that the conventional Galerkin method causes severe oscillating results for high Reynolds number problems. To deal with this phenomenon, many kinds of upwind type method have been proposed, such as SUPG, GLS, BTD, upwinding, characteristic-curve and so on (see Gresho et al. [15], Hughes et al. [19], Pironneau [34], Tabata and Fujima [42], Tezduyar [47] and references therein). As explained in Section 3.1, the characteristic-curve method is considered as an upwind type method, and we can expect the method to stabilize nonlinear convection term. The scheme (S2) is a combined finite element scheme with a pressure-stabilization method in Subsection 6.2.2 and the characteristic-curve method in Section 3.1. By the pressure-stabilization method, we can use P1/P1 element, and by the characteristic-curve method, the scheme works for high Reynolds number problems.

7.3 Numerical results

In this section we show two- and three-dimensional numerical results by the scheme (S2). We set two types of numerical example. The one is test problems to see the convergence rate to the exact solution, and the other is cavity flow problems to show the usefulness of the scheme. We use the CG and the CR methods [28] with the point Jacobi preconditioner [2] for solving the system of linear equations, which work for our symmetric matrix.

The two solutions using numerical integration formula of degree two and five in Section 4.1 are almost same for Examples 7.1 and 7.2 below. Therefore, in all the following computations we use the numerical integration formula of degree two.

For all examples the domain $\Omega \equiv (0,\ 1)^d\ (= \Omega_h)$ is an unit square. In 2D we used only FreeFEM++ [13] for mesh generation. In 3D the finite element subdivision of the domain is constructed by dividing the domain into a union of triangular prisms and further subdividing each triangular prism into three tedrahedra. In this process, a triangular mesh of the two-dimensional domain $\omega \equiv (0,1)^2$ by FreeFem++ is used.

We set $\delta = 0.2$ for two-dimensional problems and $\delta = 0.05$ for three-dimensional problems. In Example 7.1 with $\nu = 1$ and $N_\Omega = 32$ we have computed five cases $\delta = 0.01,\ 0.1,\ 0.2,\ 0.3$ and 1. The value $\delta = 0.2$ gave minimum value of error ($Err_{\mathrm{P1/P1}}$ defined in the following subsection) in the cases. Similarly, for Example 7.2 with $\nu = 1$ and $N_\Omega = 16$, the value $\delta = 0.05$ was the best in five cases $\delta = 0.01,\ 0.04,\ 0.05,\ 0.06$ and 0.1.

7.3.1 Test problems

In this subsection we set $\Delta t = h$ and use almost uniform meshes. Let (u, p) and (u_h, p_h) be the solutions of the problem (2.6) and the scheme (S2), respectively.

We define $Err_{\mathrm{P1/P1}}$ by

$$Err_{\mathrm{P1/P1}} \equiv \frac{\|\Pi_{h1}u - u_h\|_{l^2(H^1)} + \|\Pi_{h1}p - p_h\|_{l^2(L^2)}}{\|u_h\|_{l^2(H^1)} + \|p_h\|_{l^2(L^2)}},$$

which represents an error. To examine Hypothesis 7.1 numerically, we set

$$\Xi^n(h,\Delta t) \equiv \frac{\|u_h^n - u_h^n \circ X_1(u_h^n,\Delta t)\|}{\Delta t\|u_h^n\|}.$$

Example 7.1 (2D)**.** *In* (2.6) *we take* $T = 1$*, and five values of* ν*,*

$$\nu = 1,\ 10^{-1},\ 10^{-2},\ 10^{-3},\ 10^{-4}$$

The functions $f,\ g(=0)$ *and* u^0 *are given so that the exact solution is the same as* (5.18)*.*

We solve the problem for $N_\Omega = 8,\ 16,\ 32,\ 64$ and 128. Figure 7.1 (left) shows a sample mesh $(N_\Omega = 8)$. Figure 7.1 (right) shows the graph of $Err_{\mathrm{P1/P1}}$ versus Δt in logarithmic scale and the values of $Err_{\mathrm{P1/P1}}$ and the slopes are given in Table 7.1. We can observe almost first order convergence in $\Delta t\ (= h)$. In Figure 7.2 we plotted the values of $\Xi^n(h,\Delta t)$ for all steps $(t = n\Delta t)$. The inequality (H) holds for $c_1 = 7$.

Example 7.2 (3D)**.** *In* (2.6) *we take* $T = 1$*, and five values of* ν*,*

$$\nu = 1,\ 10^{-1},\ 10^{-2},\ 10^{-3},\ 10^{-4}$$

The functions $f,\ g$ *and* u^0 *are given so that the exact solution is*

$$\begin{pmatrix} u \\ p \end{pmatrix}(x,t) = \begin{pmatrix} \sin(x_1+2x_2+x_3+t) - \sin(x_1+x_2+2x_3+t) \\ -\sin(2x_1+x_2+x_3+t) + \sin(x_1+x_2+2x_3+t) \\ \sin(2x_1+x_2+x_3+t) - \sin(x_1+2x_2+x_3+t) \\ \sin(x_1+x_2+x_3+t) - 8\sin^3(1/2)\sin(t+3/2) \end{pmatrix}.$$

Table 7.1: The values of $Err_{\mathrm{P1/P1}}$ and slopes of the graphs in Figures 7.1 and 7.3

	Example 7.1 ($d=2$)			Example 7.2 ($d=3$)		
	N_Ω	$Err_{\mathrm{P1/P1}}$	slope	N_Ω	$Err_{\mathrm{P1/P1}}$	slope
$\nu = 1:$	8	1.99×10^{-1}	—	4	1.07×10^{-1}	—
	16	7.60×10^{-2}	1.39	8	4.45×10^{-2}	1.26
	32	3.00×10^{-2}	1.34	16	1.74×10^{-2}	1.35
	64	1.36×10^{-2}	1.14	32	6.20×10^{-3}	1.47
	128	6.32×10^{-3}	1.11	64	3.11×10^{-3}	1.00
$\nu = 10^{-1}:$	8	3.67×10^{-1}	—	4	8.30×10^{-2}	—
	16	2.04×10^{-1}	0.85	8	3.68×10^{-2}	1.17
	32	1.11×10^{-1}	0.88	16	1.70×10^{-2}	1.12
	64	5.91×10^{-2}	0.91	32	7.09×10^{-3}	1.26
	128	3.06×10^{-2}	0.95	64	3.74×10^{-3}	0.92
$\nu = 10^{-2}:$	8	7.14×10^{-1}	—	4	1.26×10^{-1}	—
	16	4.53×10^{-1}	0.66	8	7.77×10^{-2}	0.70
	32	2.72×10^{-1}	0.73	16	4.25×10^{-2}	0.87
	64	1.55×10^{-1}	0.81	32	2.12×10^{-2}	1.01
	128	8.42×10^{-2}	0.88	64	1.10×10^{-2}	0.94
$\nu = 10^{-3}:$	8	8.15×10^{-1}	—	4	1.73×10^{-1}	—
	16	5.45×10^{-1}	0.58	8	1.36×10^{-1}	0.34
	32	3.39×10^{-1}	0.69	16	8.57×10^{-2}	0.70
	64	1.96×10^{-1}	0.79	32	4.95×10^{-2}	0.79
	128	1.08×10^{-1}	0.87	64	2.77×10^{-2}	0.84
$\nu = 10^{-4}:$	8	8.28×10^{-1}	—	4	1.83×10^{-1}	—
	16	5.65×10^{-1}	0.55	8	1.57×10^{-1}	0.22
	32	3.59×10^{-1}	0.65	16	1.11×10^{-1}	0.51
	64	2.10×10^{-1}	0.77	32	7.65×10^{-2}	0.53
	128	1.15×10^{-1}	0.87	64	5.01×10^{-2}	0.61

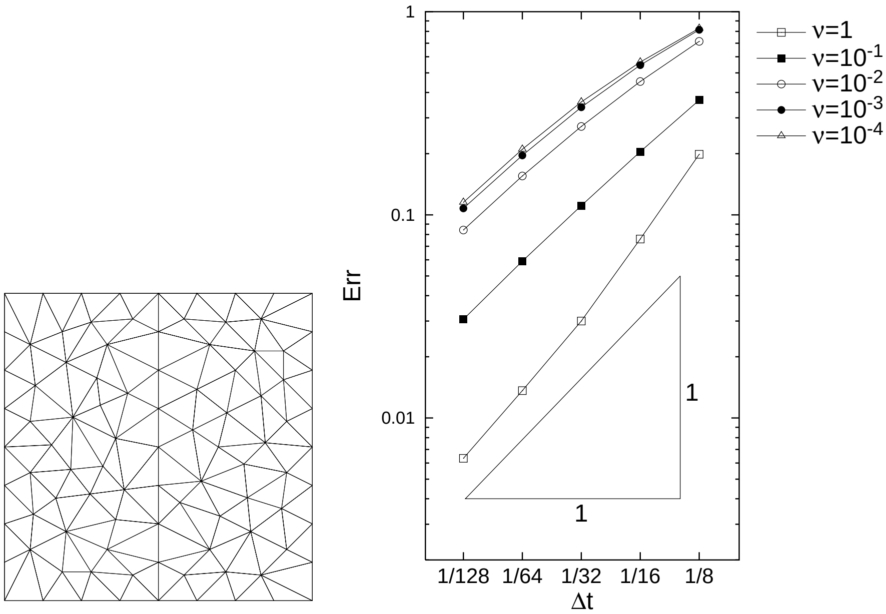

Figure 7.1: A sample mesh $(N_\Omega = 8)$ and the graph of $Err_{\mathrm{P1/P1}}$ versus Δt in logarithmic scale, Example 7.1.

We solve the problem for $N_\Omega = 4,\ 8,\ 16,\ 32$ and 64. In the case of $N_\Omega = 64$, the number of nodal points is $324,155$, the number of elements is $1,865,472$ and DOF (Degree Of Freedom) is $1,296,620$. Figure 7.3 (left) shows a sample mesh $(N_\Omega = 8)$. Figure 7.3 (right) exhibits the graph of $Err_{\mathrm{P1/P1}}$ versus Δt in logarithmic scale and the values of $Err_{\mathrm{P1/P1}}$ and the slopes are given in Table 7.1. We can observe, as in results of Example 7.1, almost first order convergence in $\Delta t\ (= h)$. In the cases of $\nu = 10^{-3}$ and 10^{-4} the values of the slope increase as Δt tends to small value, and we can expect the values to be 1 as Δt tends to 0. In Figure 7.4 we plotted the values of $\Xi^n(h, \Delta t)$ for all steps $(t = n\Delta t)$. The inequality (H) holds for $c_1 = 1.5$.

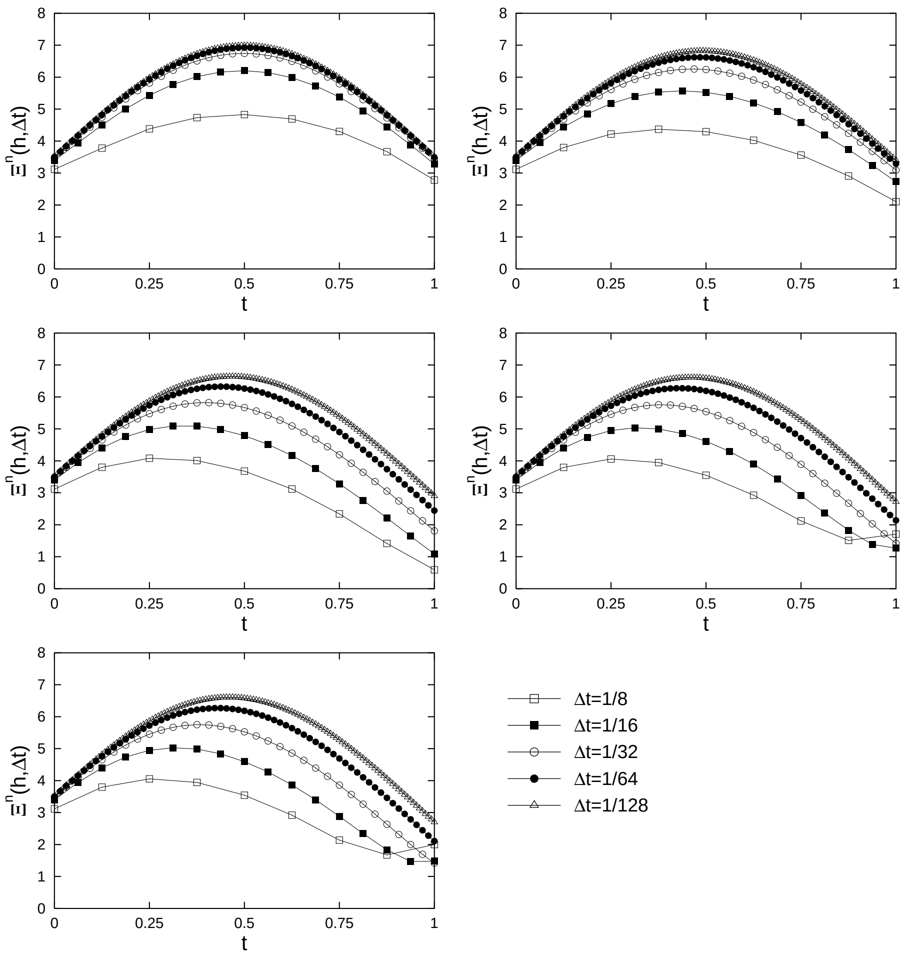

Figure 7.2: The values of $\Xi^n(h, \Delta t)$ in Example 7.1, $\nu = 1$ (top left), 10^{-1} (top right), 10^{-2} (middle left), 10^{-3} (middle right), 10^{-4} (bottom left).

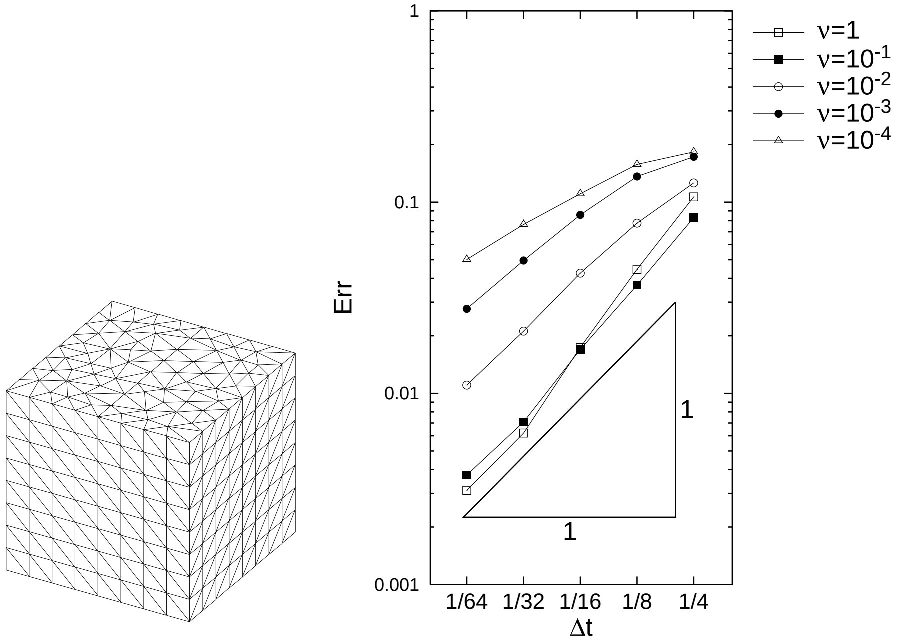

Figure 7.3: A sample mesh ($N_\Omega = 8$) and the graph of $Err_{\mathrm{P1/P1}}$ versus Δt in logarithmic scale, Example 7.2.

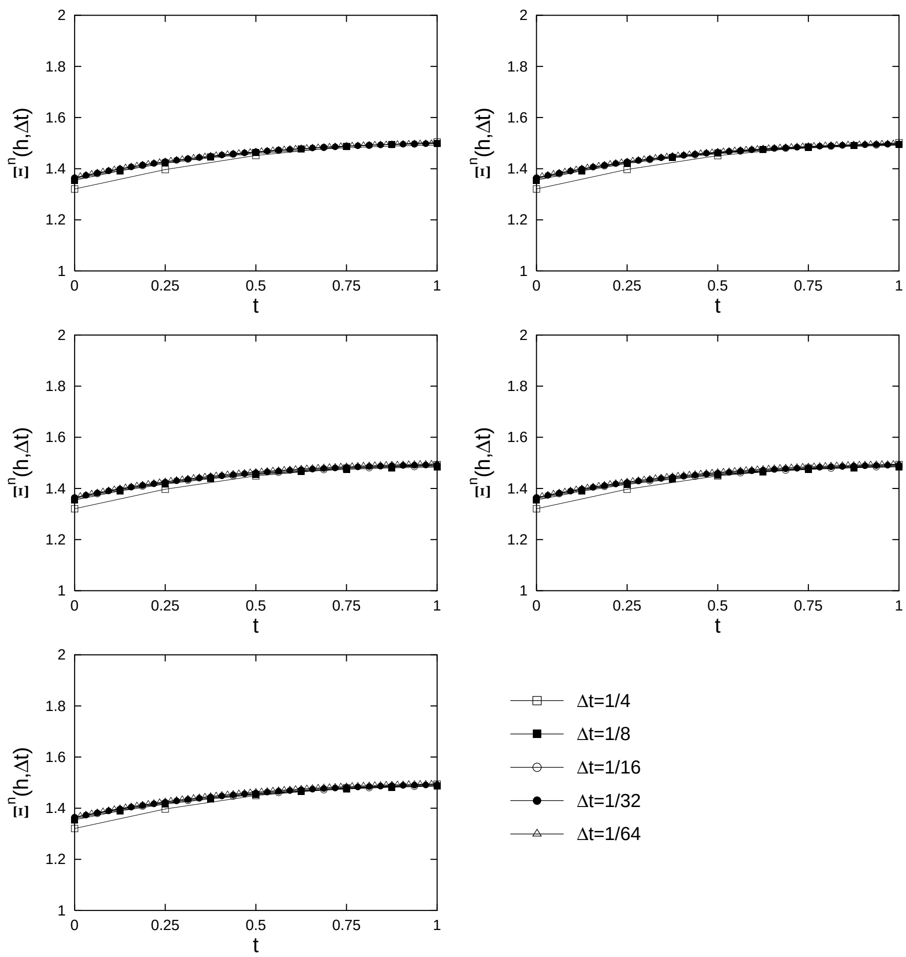

Figure 7.4: The values of $\Xi^n(h,\Delta t)$ in Example 7.2, $\nu = 1$ (top left), 10^{-1} (top right), 10^{-2} (middle left), 10^{-3} (middle right), 10^{-4} (bottom left).

7.3.2 Application to the stationary Navier-Stokes problem

In this section we consider the following stationary Navier-Stokes problem subject to the Dirichlet boundary condition; find $(u,\ p) : \Omega \to \mathbb{R}^d \times \mathbb{R}$ such that

$$\begin{cases} (u\cdot\nabla)u - \dfrac{2}{Re}\nabla D(u) + \nabla p = f & \text{in } \Omega, \\ \nabla\cdot u = 0 & \text{in } \Omega, \\ u = g & \text{on } \Gamma, \end{cases} \tag{7.3}$$

where Re is the Reynolds number corresponding to $1/\nu$. When we apply the scheme (S2) to the problem (7.3), we need to set the functions f, g and u^0 in (2.6). We employ the same given functions f and g in (7.3) for (2.6). For the initial velocity u^0 in (2.6) we use the solution of the stationary Stokes problem (6.1) with the same functions f and g in (7.3). Then, solving the scheme (S2), we find numerical stationary solution of (2.6) as a solution of (7.3).

Remark 7.3. *Since u^0 is the solution of the stationary Stokes problem which is not given explicitly, we compute the solution $(w_h, r_h) \in V_h(g) \times Q_h$ of the problem;*

$$\tilde{a}_h(w_h, v_h) + b_h(v_h, r_h) + b_h(w_h, q_h) + \mathscr{C}_h(r_h, q_h) = (f_h, v_h), \qquad \forall (v_h, q_h) \in V_h \times Q_h, \tag{7.4}$$

where $\tilde{a}_h$ is a_h with $\nu = 1$, and set $u_h^0 \equiv w_h$.

We set two-dimensional cavity flow problems with four Dirichlet boundary conditions.

Problem 7.1 (2D)**.** *In* (7.3) *we take* $f = 0$, $Re = 100,\ 1{,}000$ *and* $5{,}000$, *and consider four boundary conditions as follows (see Figure 7.5).*

$$g_1(x) = \begin{cases} 1 & (x_1 \neq 0, 1,\ x_2 = 1) \\ 0 & (otherwise) \end{cases}, \qquad g_2 = 0, \tag{DC0}$$

$$g_1(x) = \begin{cases} 1 & (x_2 = 1) \\ 0 & (otherwise) \end{cases}, \qquad g_2 = 0, \tag{DC1}$$

$$g_1(x) = \begin{cases} 4x_1(1-x_1) & (x_2 = 1) \\ 0 & (otherwise) \end{cases}, \qquad g_2 = 0, \tag{C0}$$

$$g_1(x) = \begin{cases} \left\{4x_1(1-x_1)\right\}^2 & (x_2 = 1) \\ 0 & (otherwise) \end{cases}, \qquad g_2 = 0. \tag{C1}$$

The problem with the boundary condition (DC0) or (DC1) is known as a benchmark one. The difference between the boundary conditions (DC0) and (DC1) is the values of g_1 at only two corners $(x_1, x_2) = (0,1)$ and $(1,1)$. In the cases of the boundary conditions (DC0) and (DC1), there does not exist a weak solution, i.e., $(u, p) \notin H^1(\Omega)^2 \times L^2(\Omega)$. But we set these problems to compare with the preceding results by Ghia et al.[16] and see the the difference of values of g_1 at the two corners. We can regularize these problems by considering the boundary conditions (C0) or (C1).

Below is three-dimensional cavity flow problems with C^0 and C^1 continuous Dirichlet boundary conditions.

Problem 7.2 (3D)**.** *In* (7.3) *we take* $f = 0$, $Re = 100,\ 400$ *and* $1{,}000$, *and consider two boundary conditions as follows (see Figure 7.6).*

$$g_1(x) = \begin{cases} 16x_1(1-x_1)x_2(1-x_2) & (x_3 = 1) \\ 0 & (otherwise) \end{cases}, \qquad g_2 = g_3 = 0, \tag{C0-3D}$$

$$g_1(x) = \begin{cases} \left\{16x_1(1-x_1)x_2(1-x_2)\right\}^2 & (x_3 = 1) \\ 0 & (otherwise) \end{cases}, \qquad g_2 = g_3 = 0. \tag{C1-3D}$$

Let $n_t \equiv [t/\Delta t]$ be the step number for $t \in \mathbb{N}$. Setting a norm

$$\|(v,\ q)\|_{H^1\times L^2} \equiv \frac{1}{\sqrt{Re}}\|v\|_{H^1} + \|q\|$$

in the product space $H^1(\Omega)^d \times L^2(\Omega)$, for $t \in \mathbb{N} \setminus \{1\}$ we define $Diff_t$ by

$$Diff_t \equiv \frac{\|(u_h^{n_t}, p_h^{n_t}) - (u_h^{n_{t-1}}, p_h^{n_{t-1}})\|_{H^1\times L^2}}{\|(u_h^{n_{t-1}}, p_h^{n_{t-1}})\|_{H^1\times L^2}},$$

which represents a difference of the solutions at times t and $t-1$.

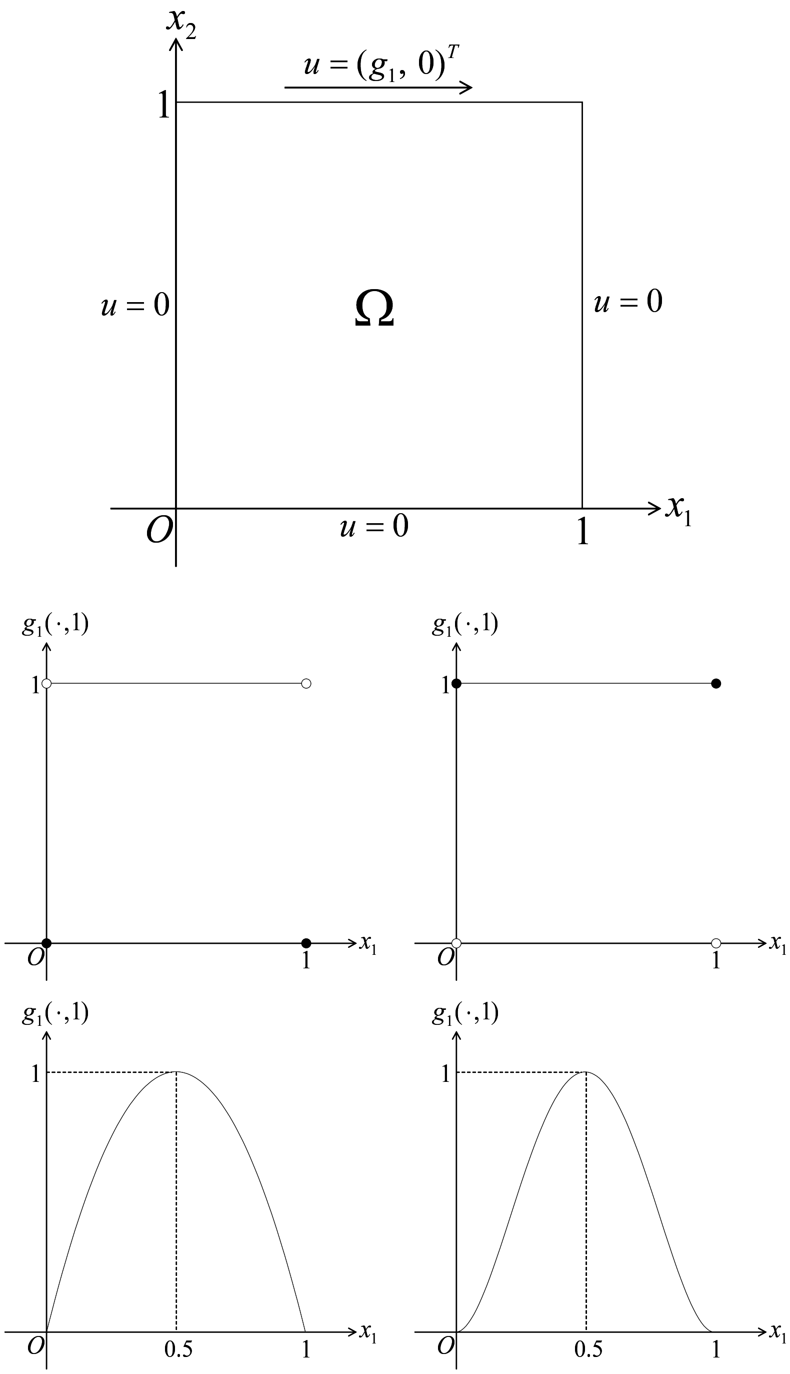

Figure 7.5: The statement of cavity flow problems in 2D (top) and graphs of $g_1(\cdot, 1)$ for the boundary conditions (DC0) (middle left), (DC1) (middle right), (C0) (bottom left) and (C1) (bottom right).

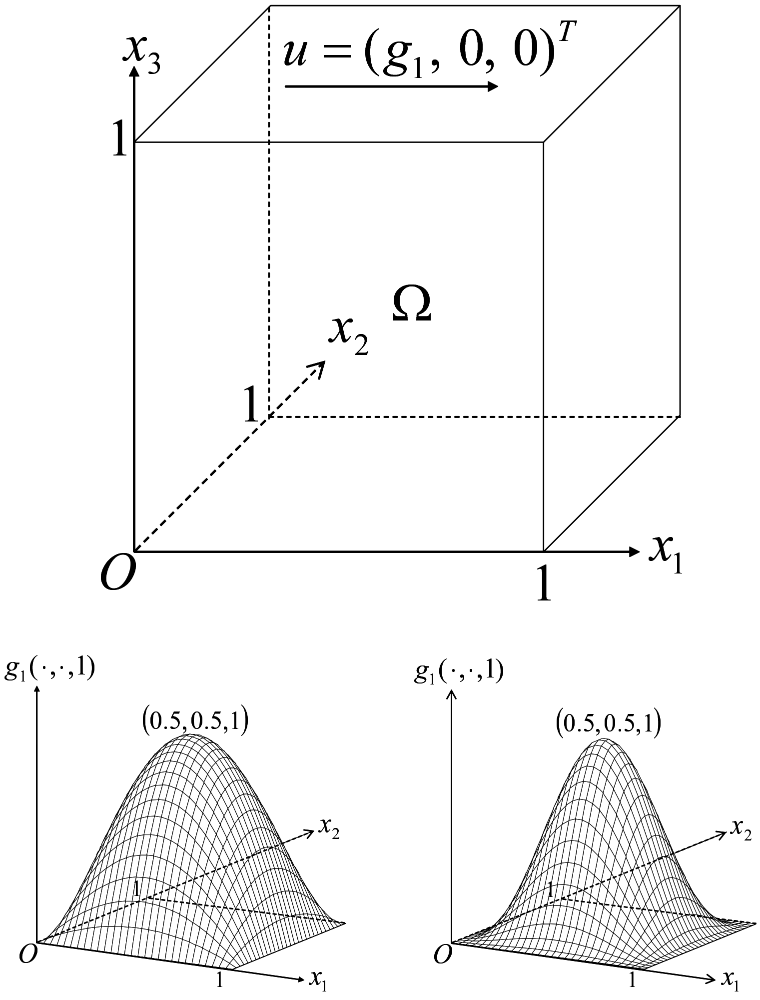

Figure 7.6: The statement of cavity flow problems in 3D (top) and graphs of $g_1(\cdot,\cdot,1)$ for the boundary conditions (C0-3D) (bottom left) and (C1-3D) (bottom right).

7.3.3 Two-dimensional cavity flow problems

In this subsection we show numerical results for Problem 7.1. Considering the boundary layers, we used nonuniform meshes refined near the boundary. Figure 7.7 shows the meshes, and we call the meshes Fine and Coarse meshes, respectively. These two meshes are similar around the center of the domain. The discretization parameters for the meshes are shown in Table 7.2, where $h_{\min}$ is a minimum element size. Table 7.3 shows values of Δt used for Problem 7.1. For high Reynolds number problems an approximation of the nonlinear convection term is important. In the scheme, the approximation depends on not only h but also Δt. This is the reason why we change the values of Δt according to the Reynolds numbers.

Table 7.2: Discretization parameters for meshes in Fig 7.7.

Mesh	$\sharp$ of nodes	$\sharp$ of elements	$h_{\min}$
Fine	$11,470$	$21,914$	2.76×10^{-3}
Coarse	$5,403$	$10,282$	5.52×10^{-3}

Table 7.3: Values of Δt used for Problem 7.1.

	Δt	
Re	Fine mesh	Coarse mesh
100	$1/100$	$1/50$
$1,000$	$1/200$	$1/100$
$5,000$	$1/800$	$1/400$

The numerical solutions converged to stationary solutions in the sense of satisfying the inequality

$$Diff_t < 10^{-5}. \tag{7.5}$$

The times of convergence are listed in Table 7.4. Since we have defined $Diff_t$ for only $t \in \mathbb{N}\setminus\{1\}$, the times in the table are integers. For each *Re*, Figures 7.8, 7.12

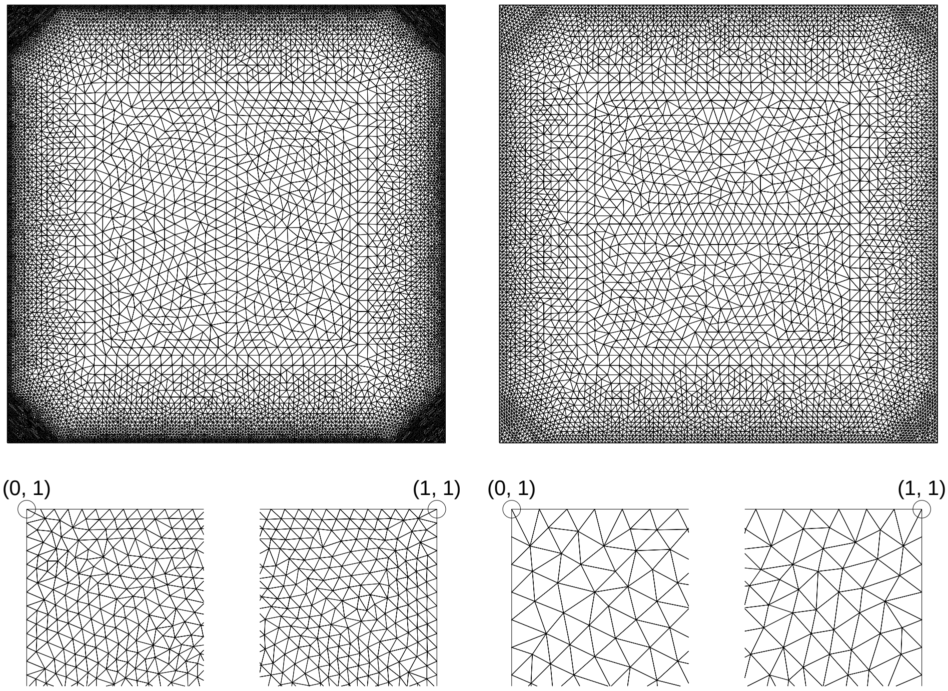

Figure 7.7: Meshes used for Problem 7.1, Fine mesh $(N_\Omega = 256)$ (left top), the mesh magnified around the corners $(x_1, x_2) = (0, 1)$ and $(1, 1)$ (left bottom), Coarse mesh $(N_\Omega = 128)$ (right top) and the mesh magnified around the corners (right bottom).

and 7.16, Figures 7.9, 7.13 and 7.17 show the graphs of $u_{h1}(0.5,\cdot)$ and $u_{h2}(\cdot,0.5)$ of the two stationary solutions on Fine and Coarse meshes, and the streamlines on Fine mesh, respectively. Figures 7.10, 7.14 and 7.18 and Figures 7.11, 7.15 and 7.19 exhibit the pressure contour lines of stationary solutions on Fine and Coarse meshes, respectively. For the boundary conditions (DC0) and (DC1), we plot the results by Ghia et al. [16] in the graphs. In the cases of the boundary conditions (C0) and (C1), the graphs by the two stationary solutions are almost same, and the streamlines exhibit the flow patterns well.

In the cases of the boundary conditions (DC0) and (DC1), although there does not exist a weak solution, the numerical solution exists. For $Re = 100$ and $1,000$ of (DC0) and $Re = 100$ of (DC1), the graphs by the two stationary solutions are almost same and are similar to the results by Ghia et al. For $Re = 5,000$ of (DC0) and $Re = 1,000$ and $5,000$ of (DC1), there are differences in the graphs by the two stationary solutions, and the solutions on Fine mesh are more close to the results by Ghia et al. than ones on Coarse mesh. The difference between the boundary conditions is the values of g_1 at only two corners $(x_1,x_2) = (0,1)$ and $(1,1)$. However, there are evident differences of the streamlines by the two boundary conditions in the three Figures 7.9, 7.13 and 7.17. The similar results have been reported by Cruchaga and Oñate [9]. They have shown the comparison of graphs of $u_{h1}(0.5,\cdot)$ and $u_{h2}(\cdot,0.5)$ for (DC0) and (DC1) with $Re = 1,000,\ 5,000$ and $10,000$.

In the Figures 7.10, 7.14 and 7.18, we can see meaningful pressure contour lines for each flow pattern, although there are oscillations. We think that these oscillations of the pressure become small as Δt and h tend to 0, because the numerical convergence of the scheme to the exact solution by means of a norm using $H^1(\Omega)^d$-norm for the velocity and $L^2(\Omega)$-norm for the pressure has been observed in Subsection 7.3.1. In fact, comparing Figures 7.10, 7.14 and 7.18 with Figures 7.11, 7.15 and 7.19, respectively, we can observe that the oscillations of the pressure on Fine mesh are smaller than ones on Coarse mesh.

Let us study the difference of solutions by the boundary conditions on Fine mesh. Figure 7.20 shows graphs of $u_{h1}(0.5,\cdot)$ and $u_{h2}(\cdot,0.5)$ for the four boundary conditions with the results by Ghia et al., which exhibit the size of boundary layers. Now, we focus on the difference of solutions especially by the boundary conditions (DC0) and (DC1). The difference of the graphs for $Re = 5,000$ is the biggest in Figure 7.20. Detailed graphs for the Reynolds number are presented in Figure 7.21, where (DC1/4), (DC1/2) and (DC3/4) are additional boundary conditions to the Problem 7.1,

$$g_1(x) = \begin{cases} 1 & (x_1 \neq 0,1,\ x_2 = 1) \\ 1/4 & (x_1 = 0,1,\ x_2 = 1) \\ 0 & (otherwise) \end{cases}, \quad g_2 = 0, \tag{DC1/4}$$

$$g_1(x) = \begin{cases} 1 & (x_1 \neq 0,1,\ x_2 = 1) \\ 1/2 & (x_1 = 0,1,\ x_2 = 1) \\ 0 & (otherwise) \end{cases}, \quad g_2 = 0, \tag{DC1/2}$$

and

$$g_1(x) = \begin{cases} 1 & (x_1 \neq 0,1,\ x_2 = 1) \\ 3/4 & (x_1 = 0,1,\ x_2 = 1) \\ 0 & (otherwise) \end{cases}, \quad g_2 = 0, \tag{DC3/4}$$

respectively, and its graphs are by stationary solutions on Fine mesh by the scheme (S2) with the same parameters, whose initial value is the stationary solution for (DC0) to save computational time. We can see the effect of the values of g_1 at two corners, $(x_1,x_2) = (0,1)$ and $(1,1)$.

Table 7.4: Convergence times.

		t $(\in \mathbb{N})$	
	Re	Fine mesh	Coarse mesh
(DC0):	100	15	15
	1,000	85	92
	5,000	370	358
(DC1):	100	15	15
	1,000	87	87
	5,000	390	399
(C0):	100	16	16
	1,000	92	91
	5,000	372	373
(C1):	100	17	17
	1,000	91	90
	5,000	356	360

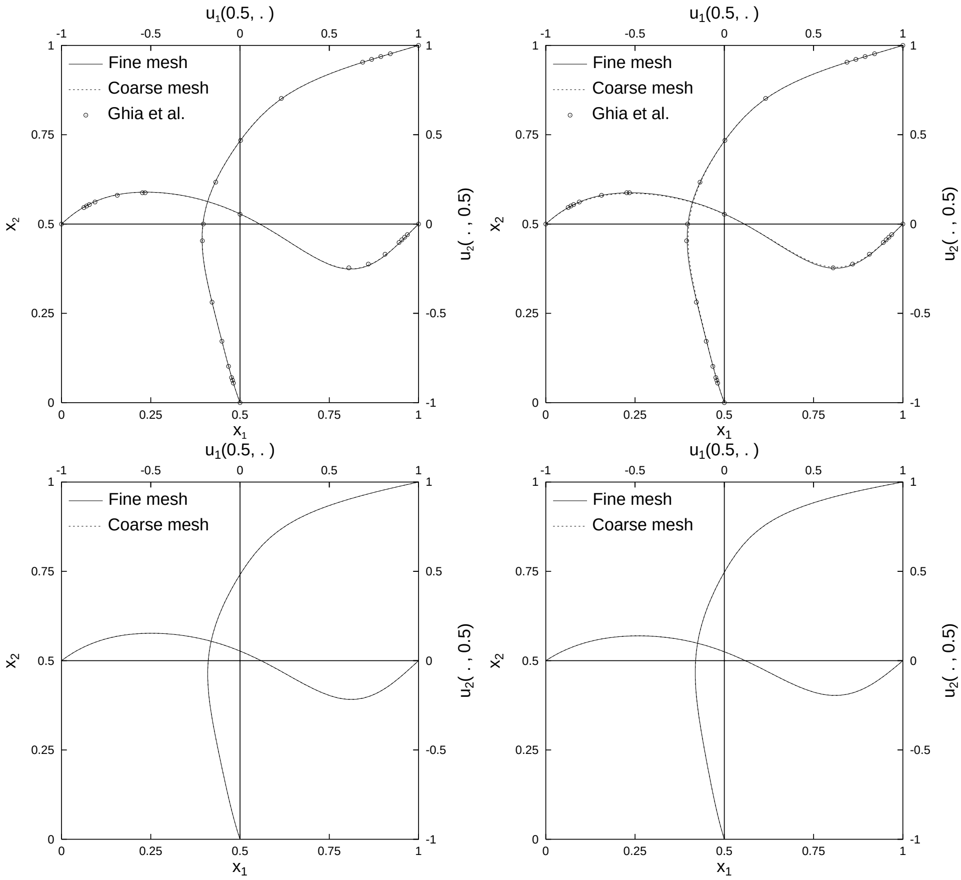

Figure 7.8: Graphs of $u_{h1}(0.5,\cdot)$ and $u_{h2}(\cdot,0.5)$, $Re = 100$, (DC0) (top left), (DC1) (top right), (C0) (bottom left) and (C1) (bottom right).

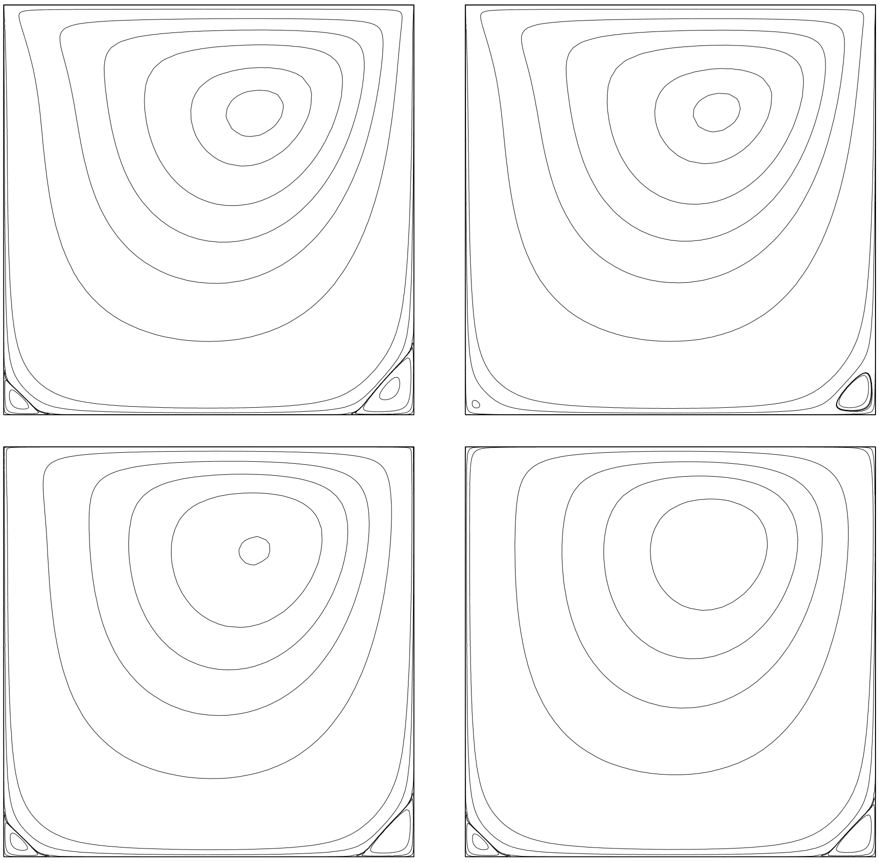

Figure 7.9: Streamlines, $Re = 100$, (DC0) (top left), (DC1) (top right), (C0) (bottom left) and (C1) (bottom right).

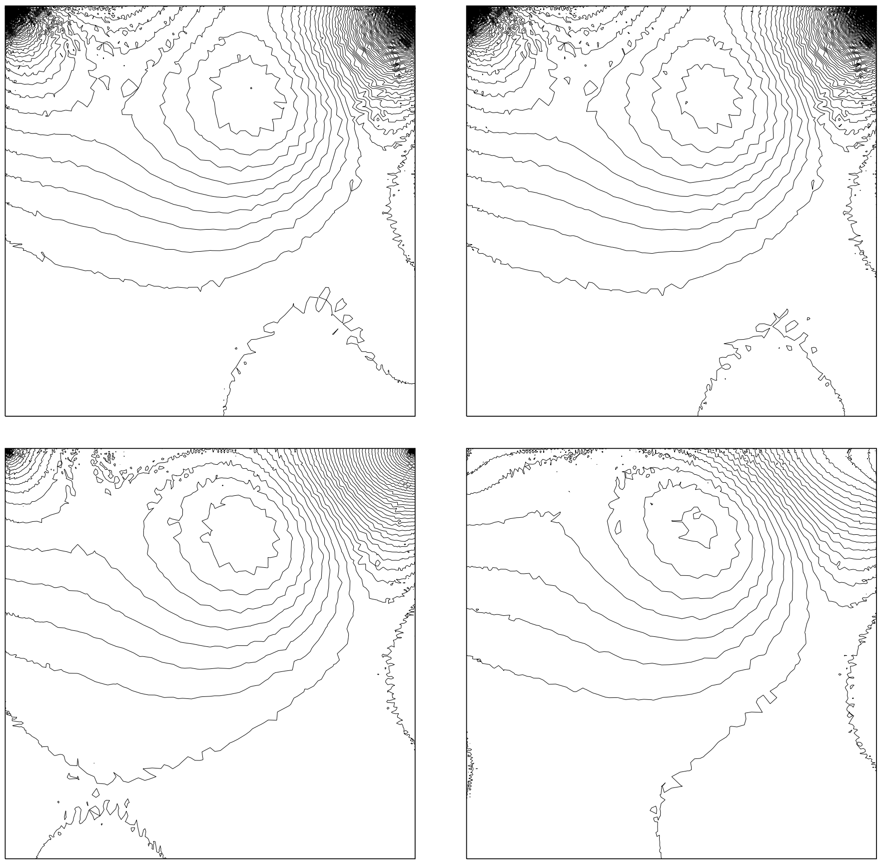

Figure 7.10: Pressure contour lines on Fine mesh, $Re = 100$, $\Delta p = 0.01$, (DC0) (top left), (DC1) (top right), (C0) (bottom left) and (C1) (bottom right).

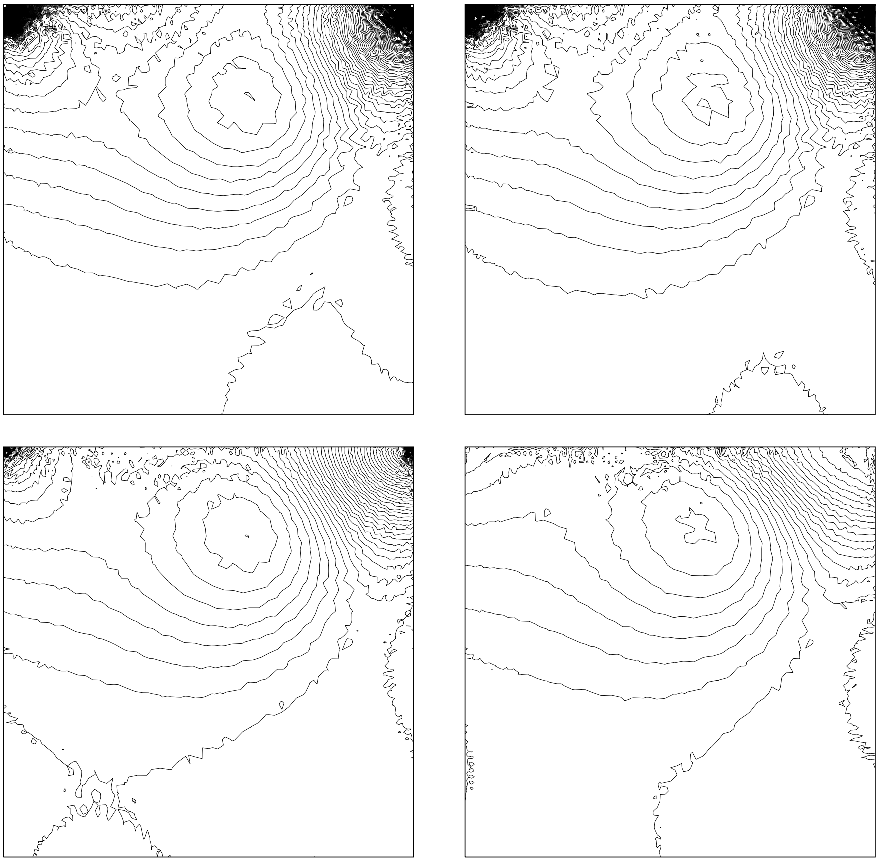

Figure 7.11: Pressure contour lines on Coarse mesh, $Re = 100$, $\Delta p = 0.01$, (DC0) (top left), (DC1) (top right), (C0) (bottom left) and (C1) (bottom right).

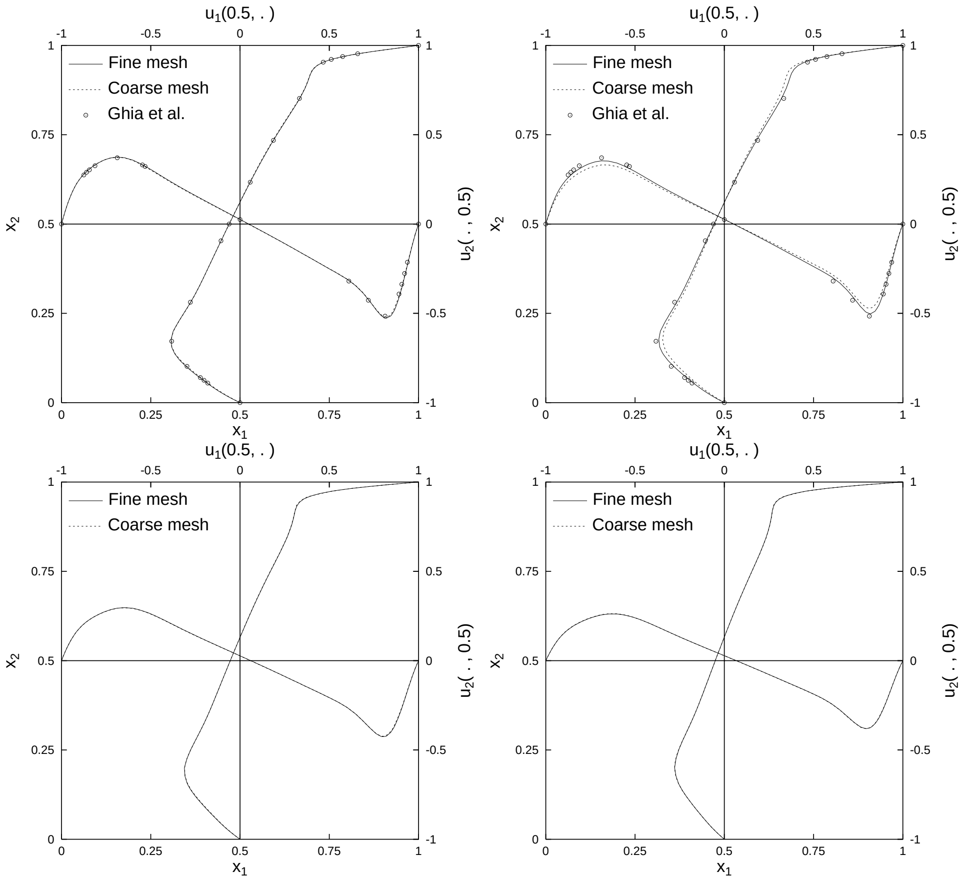

Figure 7.12: Graphs of $u_{h1}(0.5,\cdot)$ and $u_{h2}(\cdot,0.5)$, $Re = 1,000$, (DC0) (top left), (DC1) (top right), (C0) (bottom left) and (C1) (bottom right).

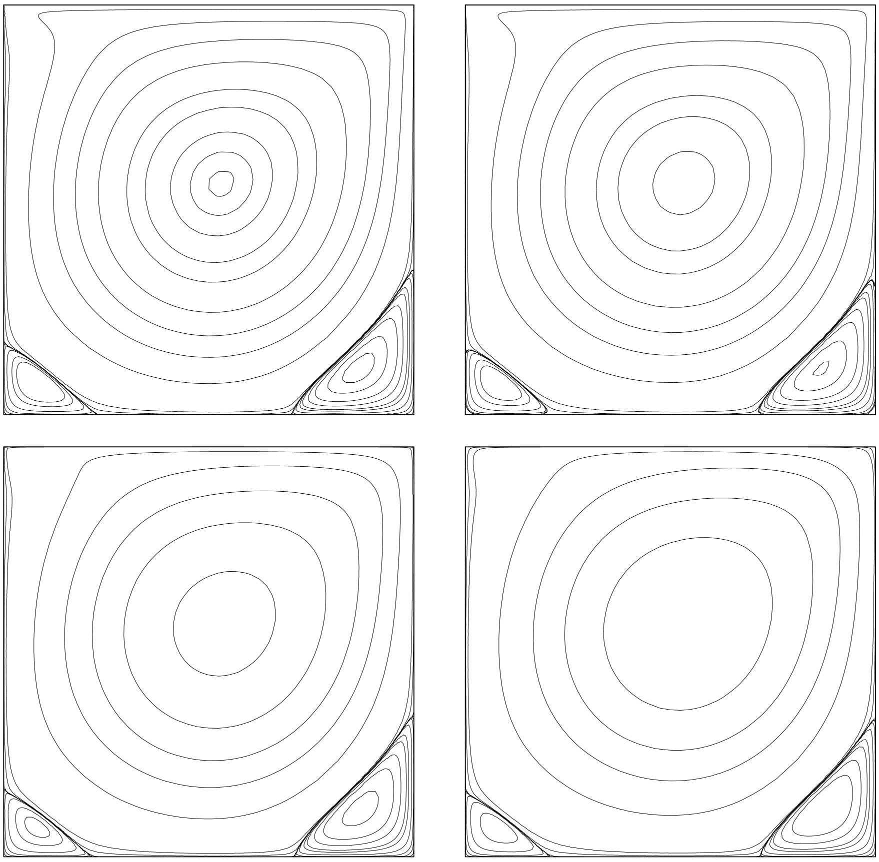

Figure 7.13: Streamlines, $Re = 1{,}000$, (DC0) (top left), (DC1) (top right), (C0) (bottom left) and (C1) (bottom right).

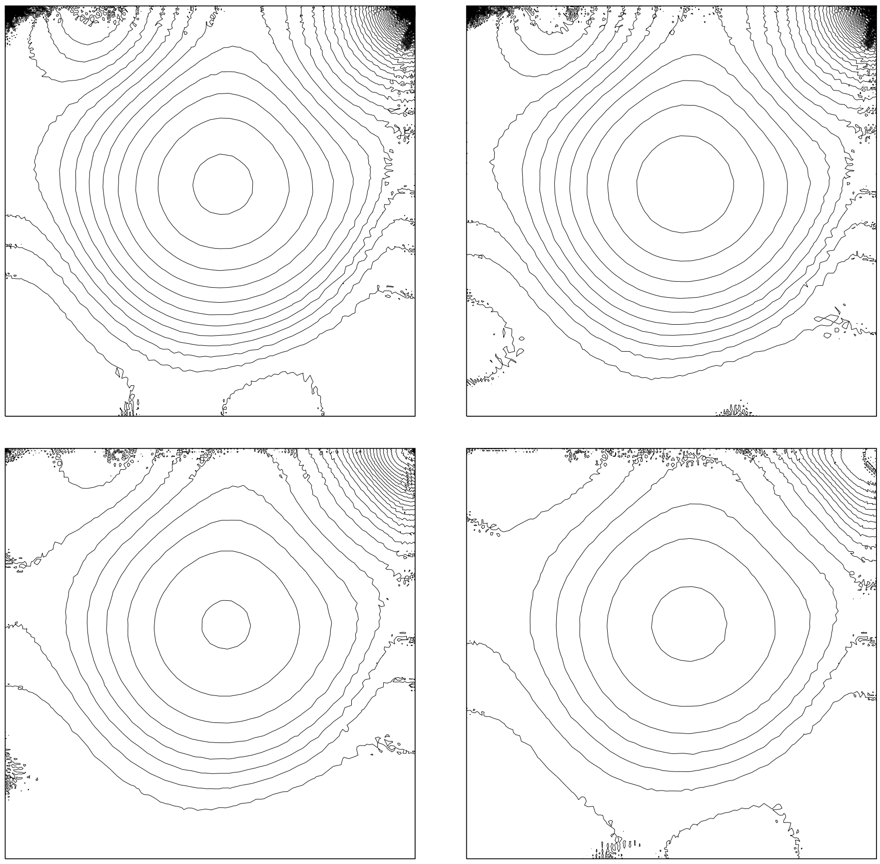

Figure 7.14: Pressure contour lines on Fine mesh, $Re = 1,000$, $\Delta p = 0.01$, (DC0) (top left), (DC1) (top right), (C0) (bottom left) and (C1) (bottom right).

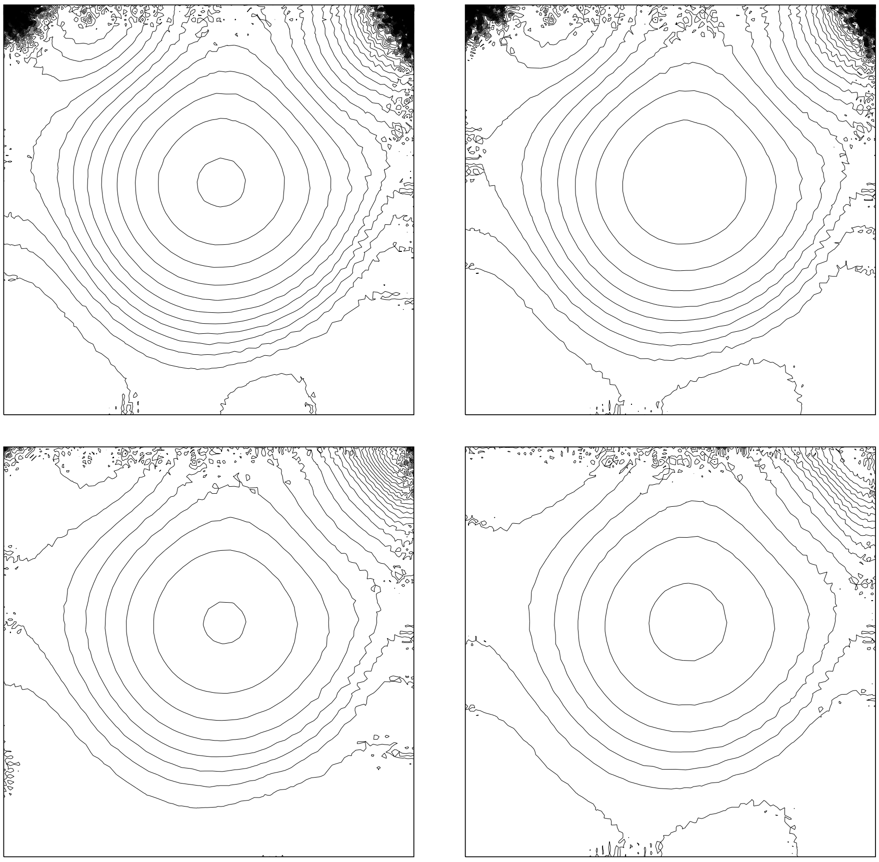

Figure 7.15: Pressure contour lines on Coarse mesh, $Re = 1{,}000$, $\Delta p = 0.01$, (DC0) (top left), (DC1) (top right), (C0) (bottom left) and (C1) (bottom right).

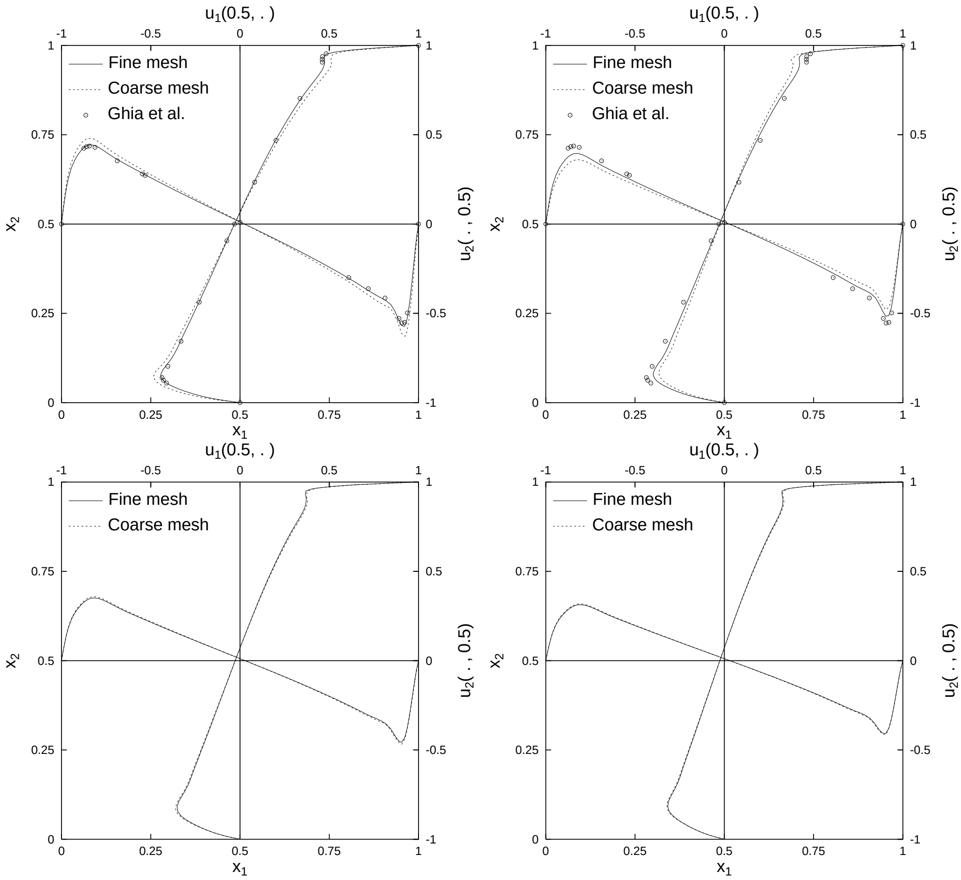

Figure 7.16: Graphs of $u_{h1}(0.5,\cdot)$ and $u_{h2}(\cdot,0.5)$, $Re = 5{,}000$, (DC0) (top left), (DC1) (top right), (C0) (bottom left) and (C1) (bottom right).

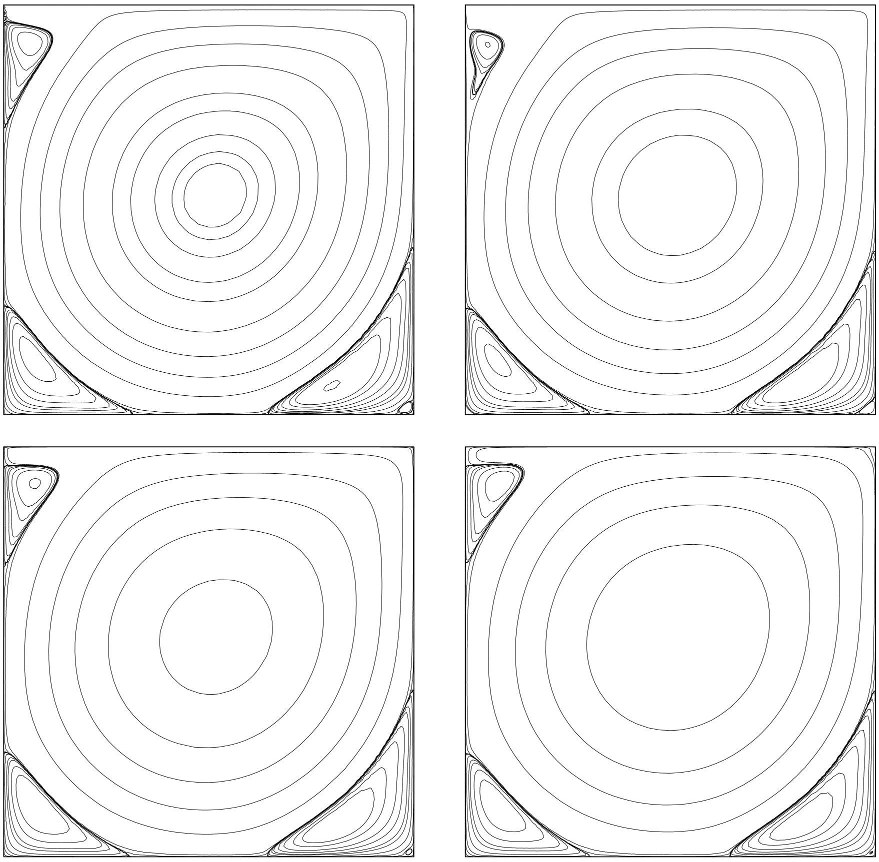

Figure 7.17: Streamlines, $Re = 5,000$, (DC0) (top left), (DC1) (top right), (C0) (bottom left) and (C1) (bottom right).

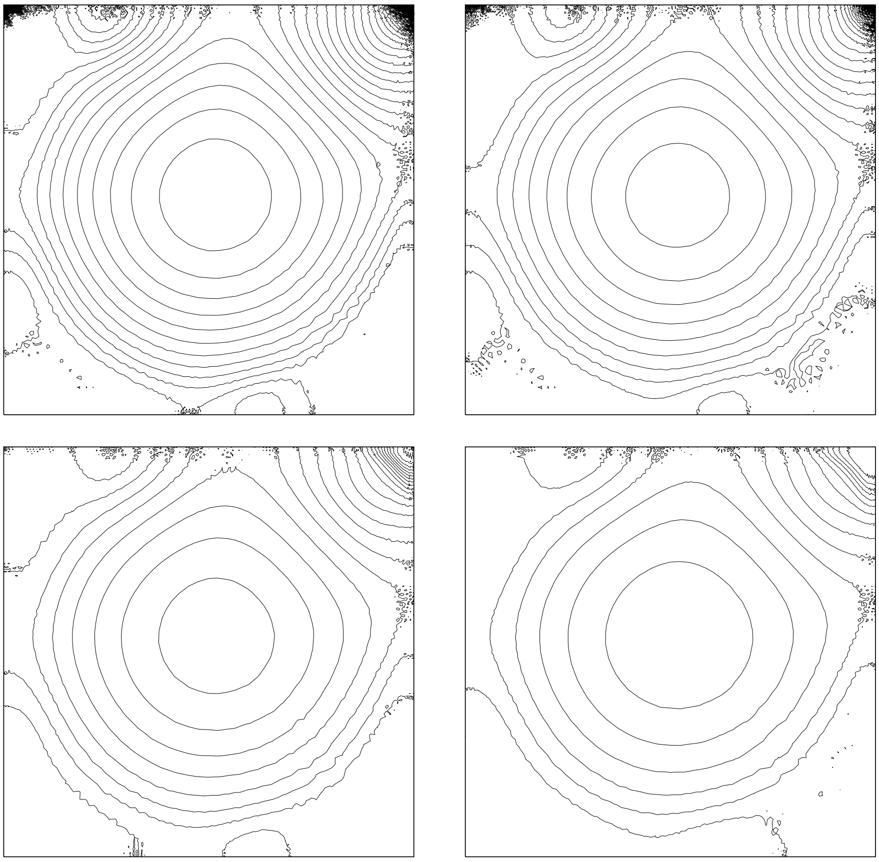

Figure 7.18: Pressure contour lines on Fine mesh, $Re = 5,000$, $\Delta p = 0.01$, (DC0) (top left), (DC1) (top right), (C0) (bottom left) and (C1) (bottom right).

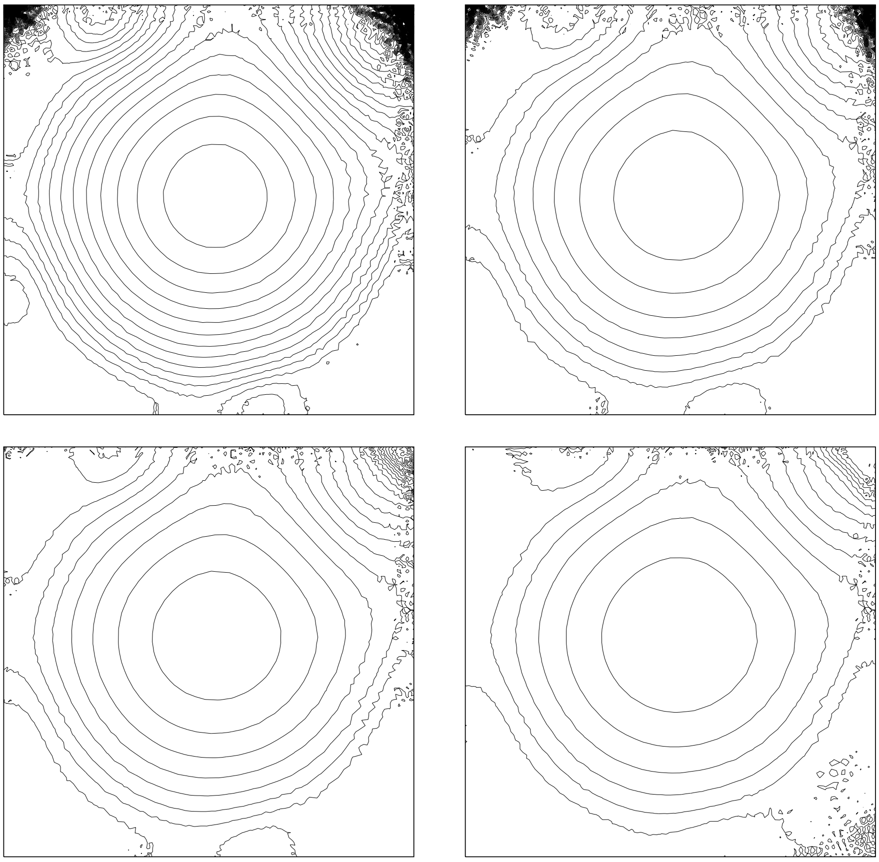

Figure 7.19: Pressure contour lines on Coarse mesh, $Re = 5,000$, $\Delta p = 0.01$, (DC0) (top left), (DC1) (top right), (C0) (bottom left) and (C1) (bottom right).

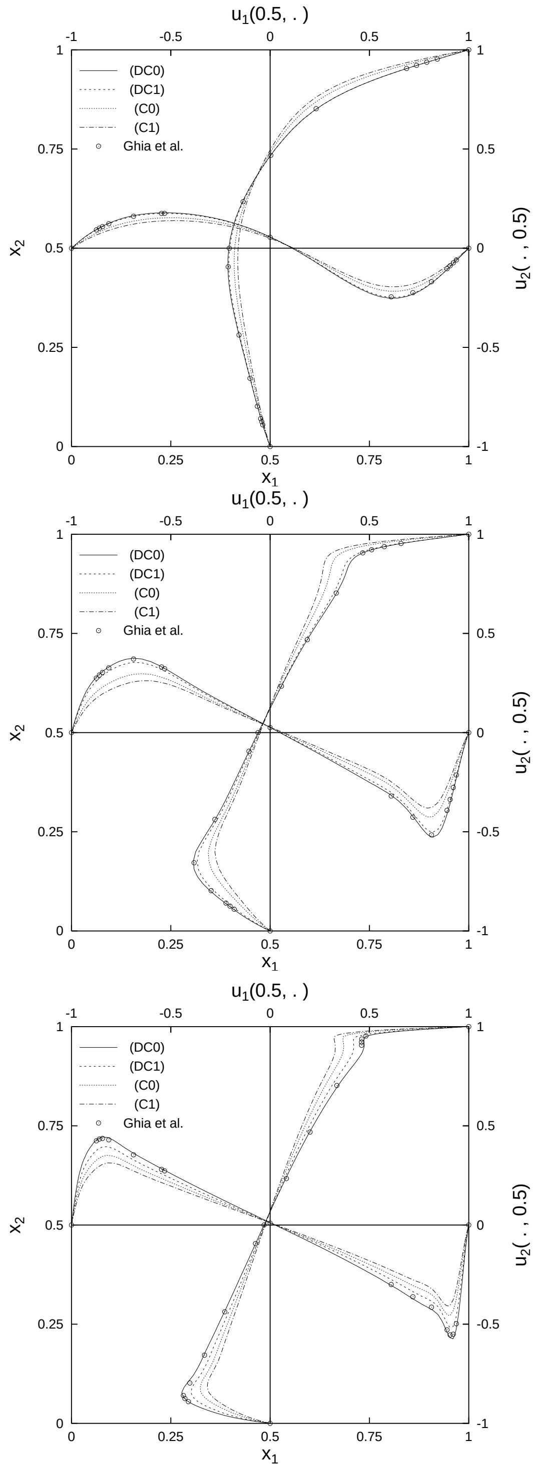

Figure 7.20: Graphs of $u_{h1}(0.5,\cdot)$ and $u_{h2}(\cdot,0.5)$ for the four boundary conditions, (DC0), (DC1), (C0) and (C1), $Re = 100$ (top), $1,000$ (middle) and $5,000$ (bottom).

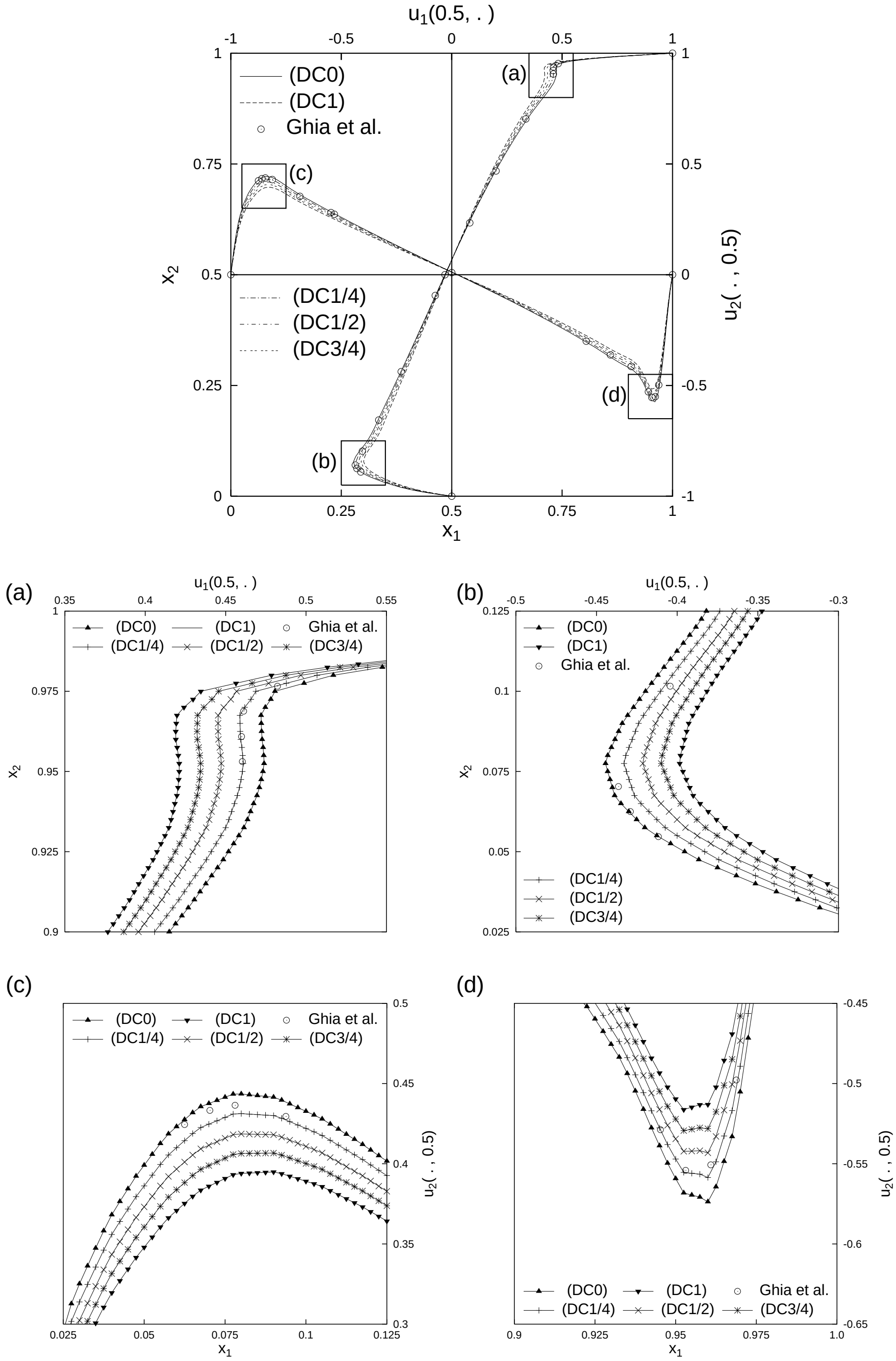

Figure 7.21: Graphs of $u_{h1}(0.5,\cdot)$ and $u_{h2}(\cdot,0.5)$ for the five boundary conditions, (DC0), (DC1/4), (DC1/2), (DC3/4) and (DC1), and its magnified ones (top to bottom), $Re = 5,000$.

7.3.4 Three-dimensional cavity flow problems

In this subsection we show numerical results for Problem 7.2. Considering the boundary layers, we used nonuniform two meshes in Figure 7.22. We call the meshes Fine and Coarse meshes, respectively, whose discretization parameters are shown in Table 7.5. In three-dimensional case, for all the Reynolds numbers we set $\Delta t = 1/32$ for Fine mesh and $\Delta t = 1/24$ for Coarse mesh.

The numerical solutions converged to stationary solutions in the sense of satisfying the inequality (7.5). The times of convergence are listed in Table 7.6. Figure 7.23 shows the graphs of $u_{h1}(0.5, 0.5, \cdot)$ and $u_{h3}(\cdot, 0.5, 0.5)$ of the two stationary solutions on Fine and Coarse meshes for the two boundary conditions (C0-3D) and (C1-3D) for each *Re*. The graphs of the two stationary solutions are almost same. Figures 7.24, 7.27 and 7.30 are projections of velocity vectors on each plane for each *Re*, which exhibit the flow patterns well of these problems. Pressure contour lines on Fine and Coarse meshes are shown in Figures 7.25, 7.28 and 7.31 and Figures 7.26, 7.29 and 7.32, respectively. Comparing Figures 7.25, 7.28 and 7.31 with Figures 7.26, 7.29 and 7.32, respectively, we can see that the oscillations of the pressure on Fine mesh are a little smaller than ones on Coarse mesh. An improvement for the pressure oscillations by the scheme in both 2D and 3D is a future work.

The effect of the two boundary conditions are presented in Figure 7.33.

Table 7.5: Discretization parameters for meshes in Figure 7.22.

Mesh	♯ of nodes	♯ of elements	$h_{\min}$
Fine	$172,965$	$972,288$	5.16×10^{-3}
Coarse	$74,627$	$410,688$	7.09×10^{-3}

Table 7.6: Convergence times.

		t $(\in \mathbb{N})$	
	Re	Fine mesh	Coarse mesh
(C0-3D):	100	12	12
	400	32	32
	$1,000$	58	58
(C1-3D):	100	11	11
	400	33	33
	$1,000$	53	53

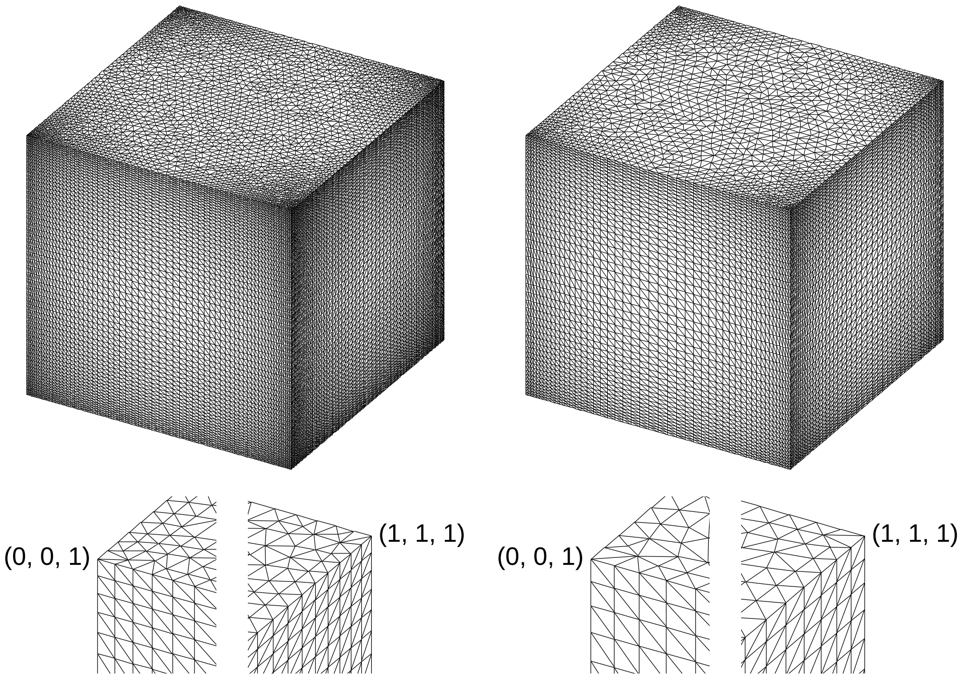

Figure 7.22: Meshes used for Problem 7.2, Fine mesh $(N_\Omega = 64)$, the mesh magnified around the points $(x_1, x_2, x_3) = (0,0,1)$ and $(1,1,1)$, Coarse mesh $(N_\Omega = 48)$ and the mesh magnified around the points (top to bottom).

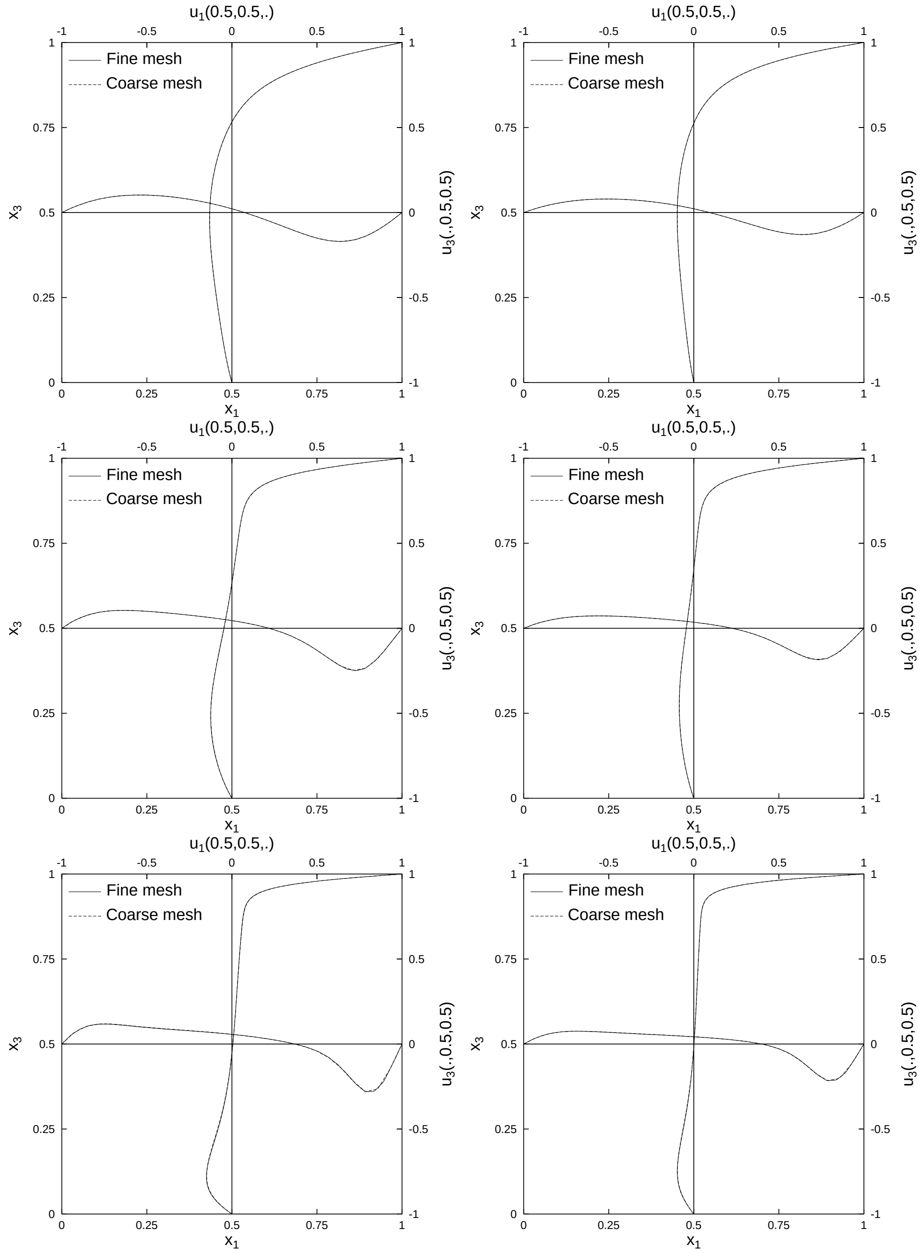

Figure 7.23: Graphs of $u_{h1}(0.5, 0.5, \cdot)$ and $u_{h3}(\cdot, 0.5, 0.5)$ for the Reynolds numbers, $Re = 100,\ 400$ and $1,000$ (top to bottom), (C0-3D) (left) and (C1-3D) (right).

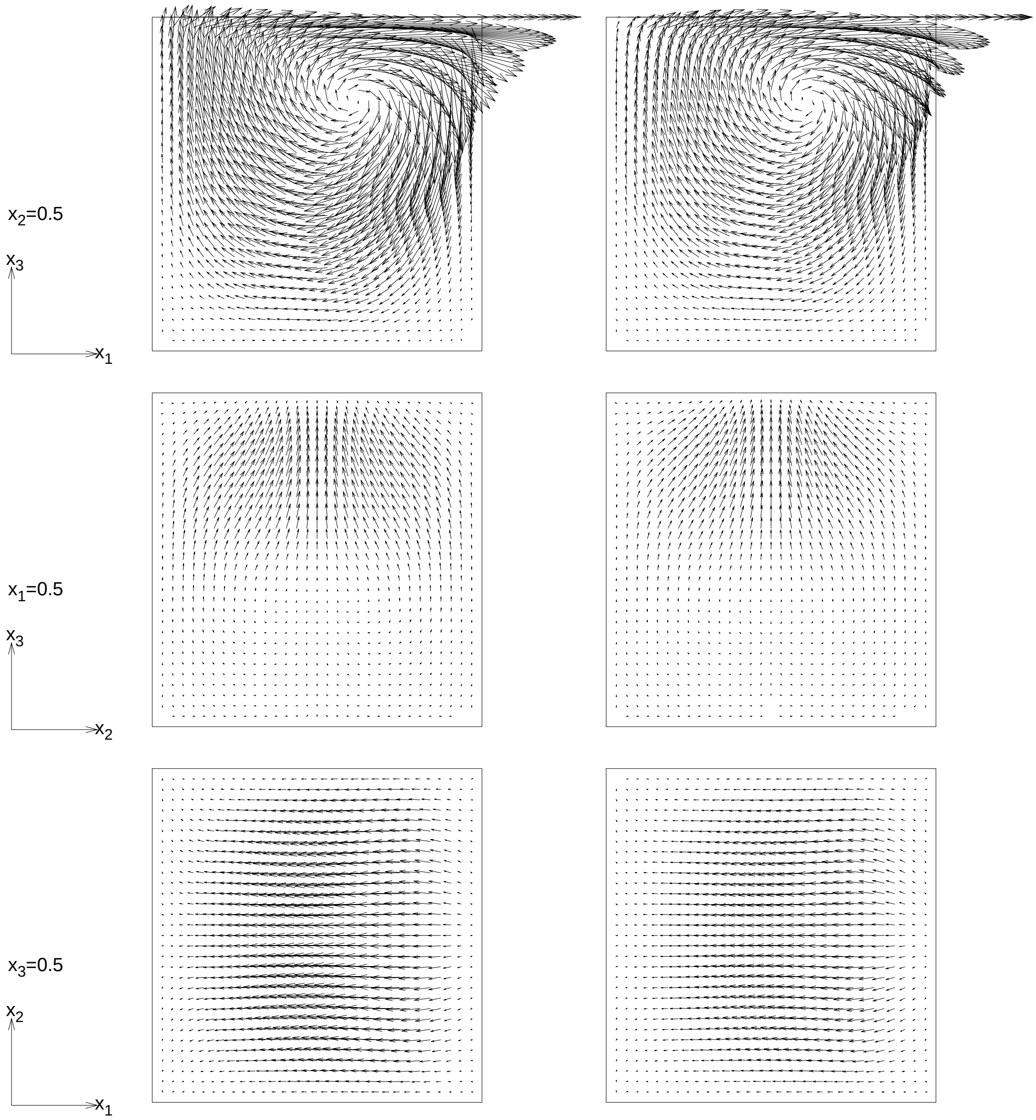

Figure 7.24: Projections of velocity vectors on each plane, $Re = 100$, (C0-3D) (left) and (C1-3D) (right).

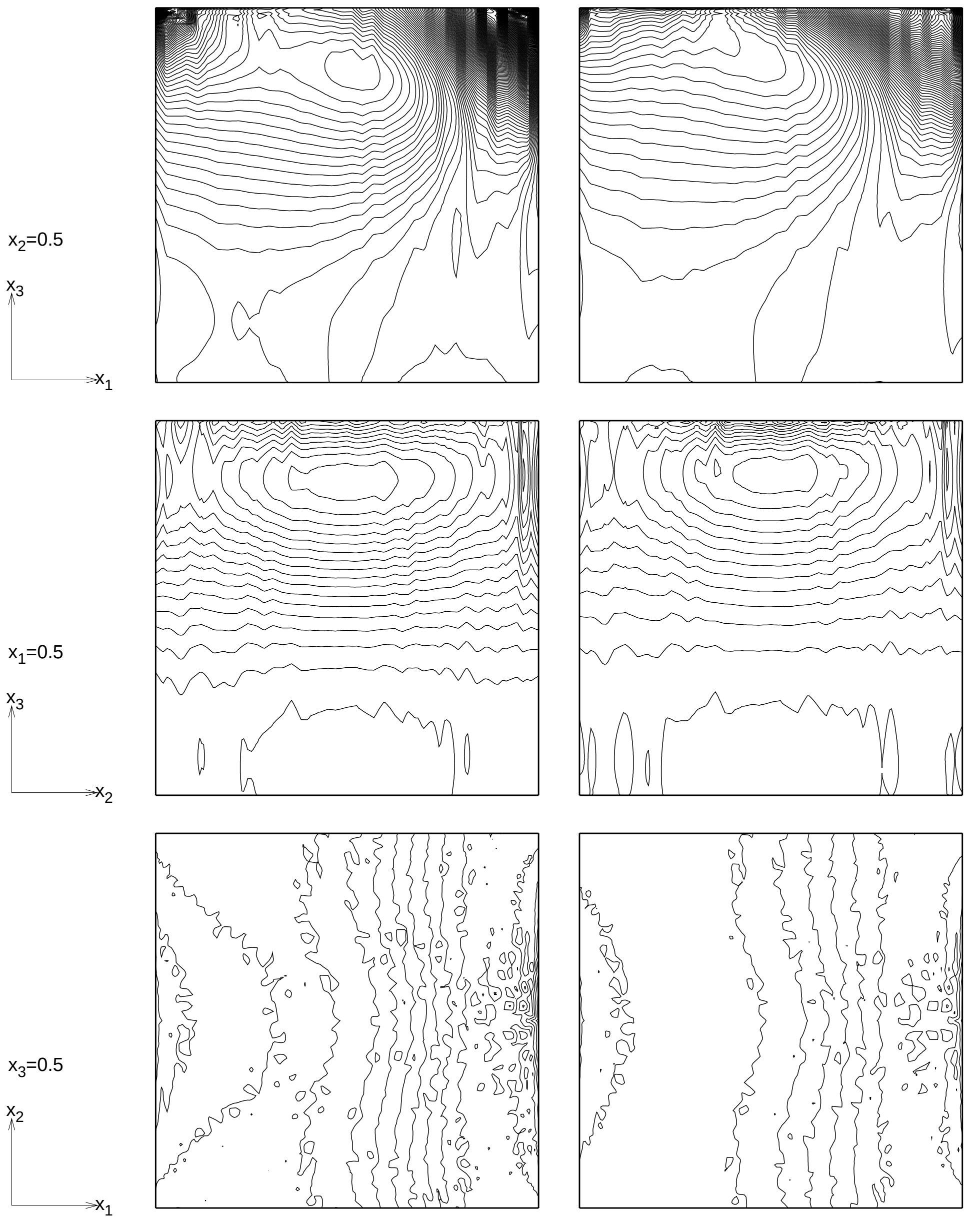

Figure 7.25: Pressure contour lines on each plane by Fine mesh, $Re = 100$, $\Delta p = 0.0025$, (C0-3D) (left) and (C1-3D) (right).

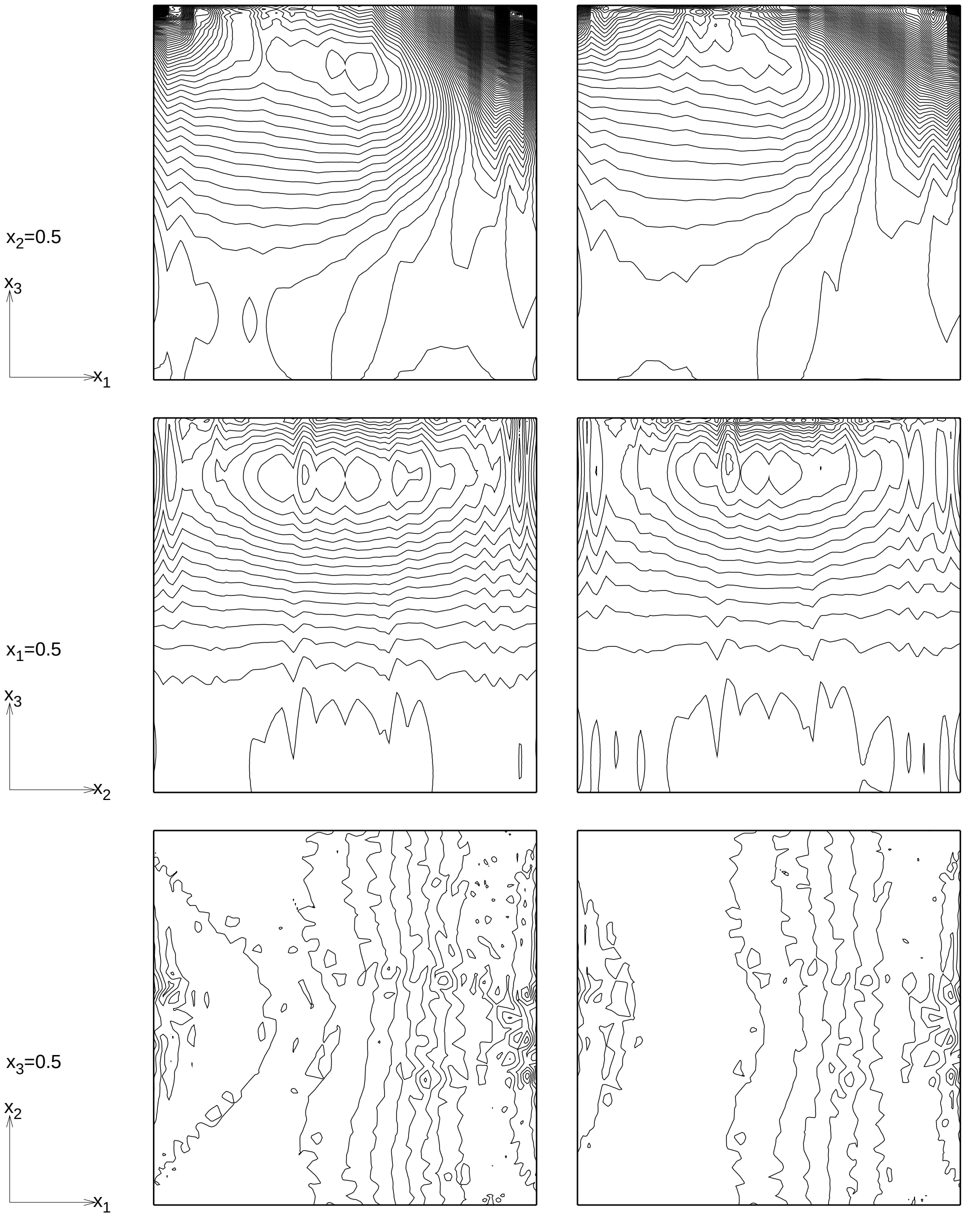

Figure 7.26: Pressure contour lines on each plane by Coarse mesh, $Re = 100$, $\Delta p = 0.0025$, (C0-3D) (left) and (C1-3D) (right).

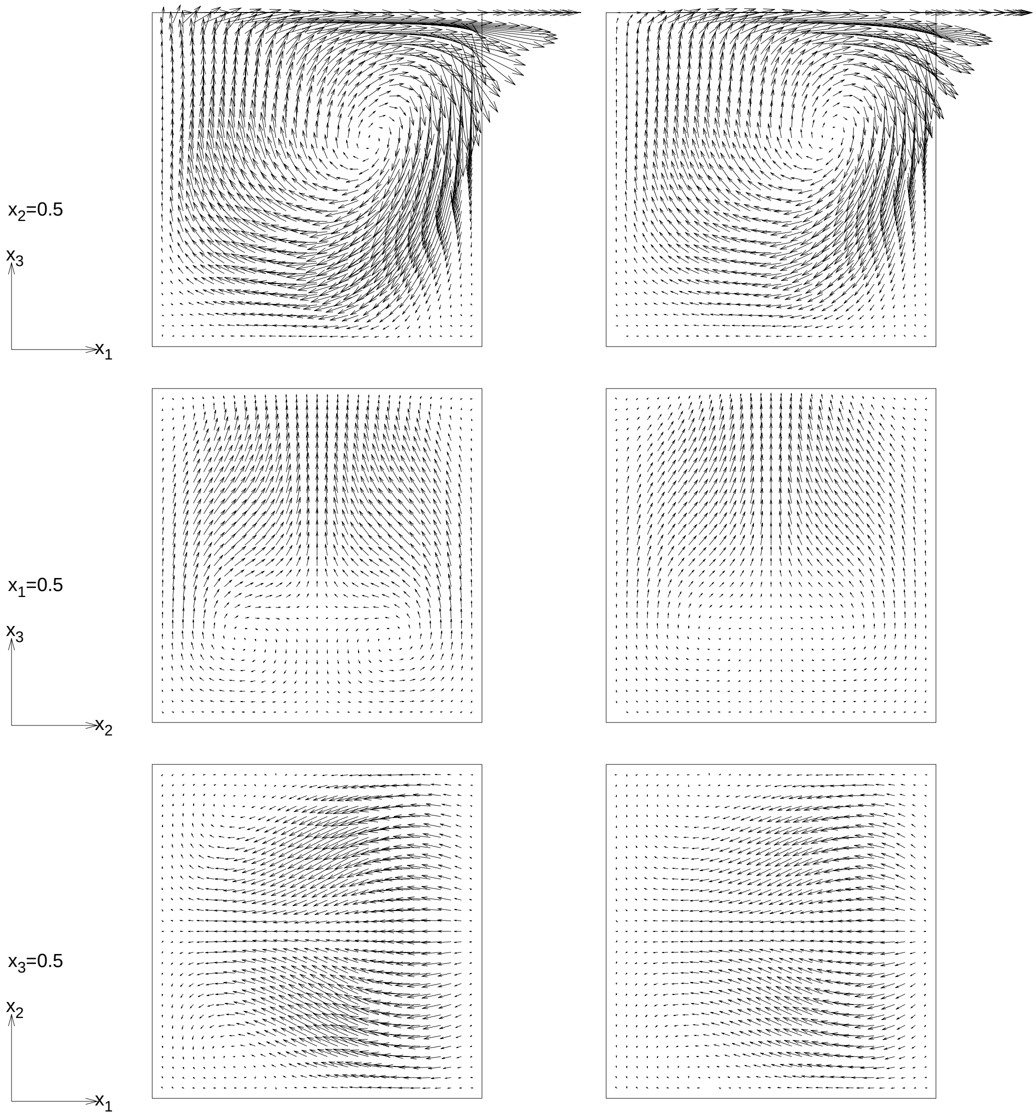

Figure 7.27: Projections of velocity vectors on each plane, $Re = 400$, (C0-3D) (left) and (C1-3D) (right).

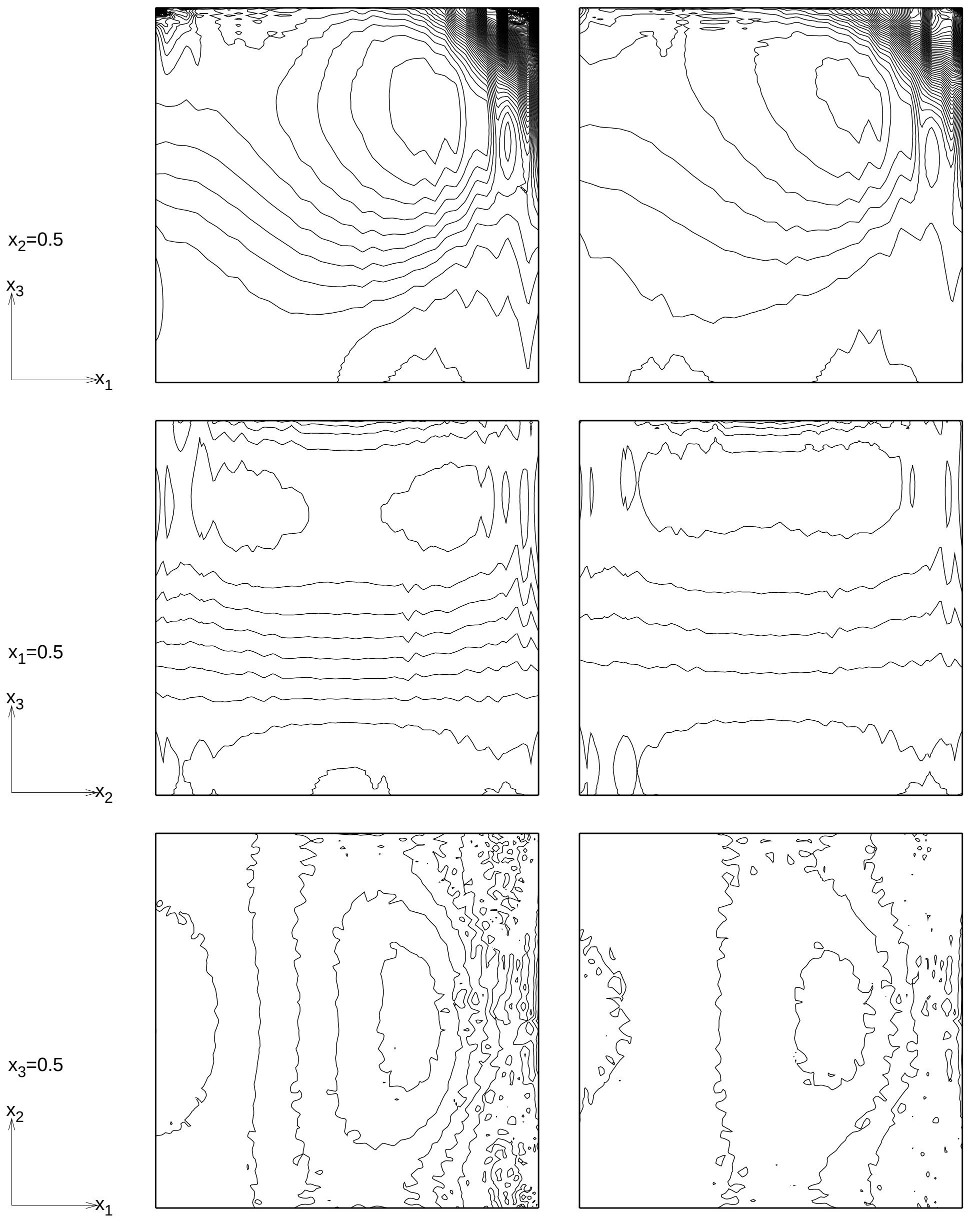

Figure 7.28: Pressure contour lines on each plane by Fine mesh, $Re = 400$, $\Delta p = 0.0025$, (C0-3D) (left) and (C1-3D) (right).

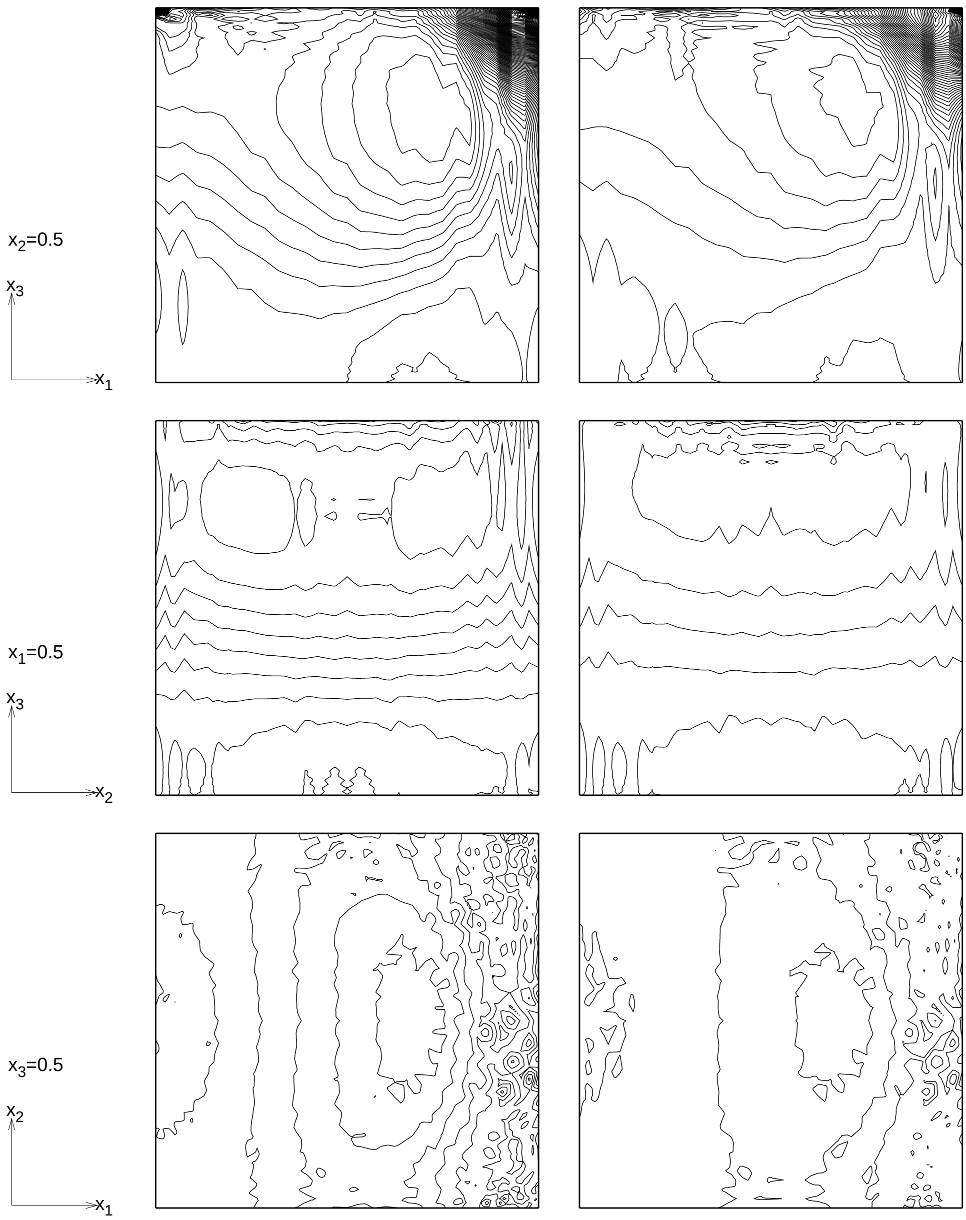

Figure 7.29: Pressure contour lines on each plane by Coarse mesh, $Re = 400$, $\Delta p = 0.0025$, (C0-3D) (left) and (C1-3D) (right).

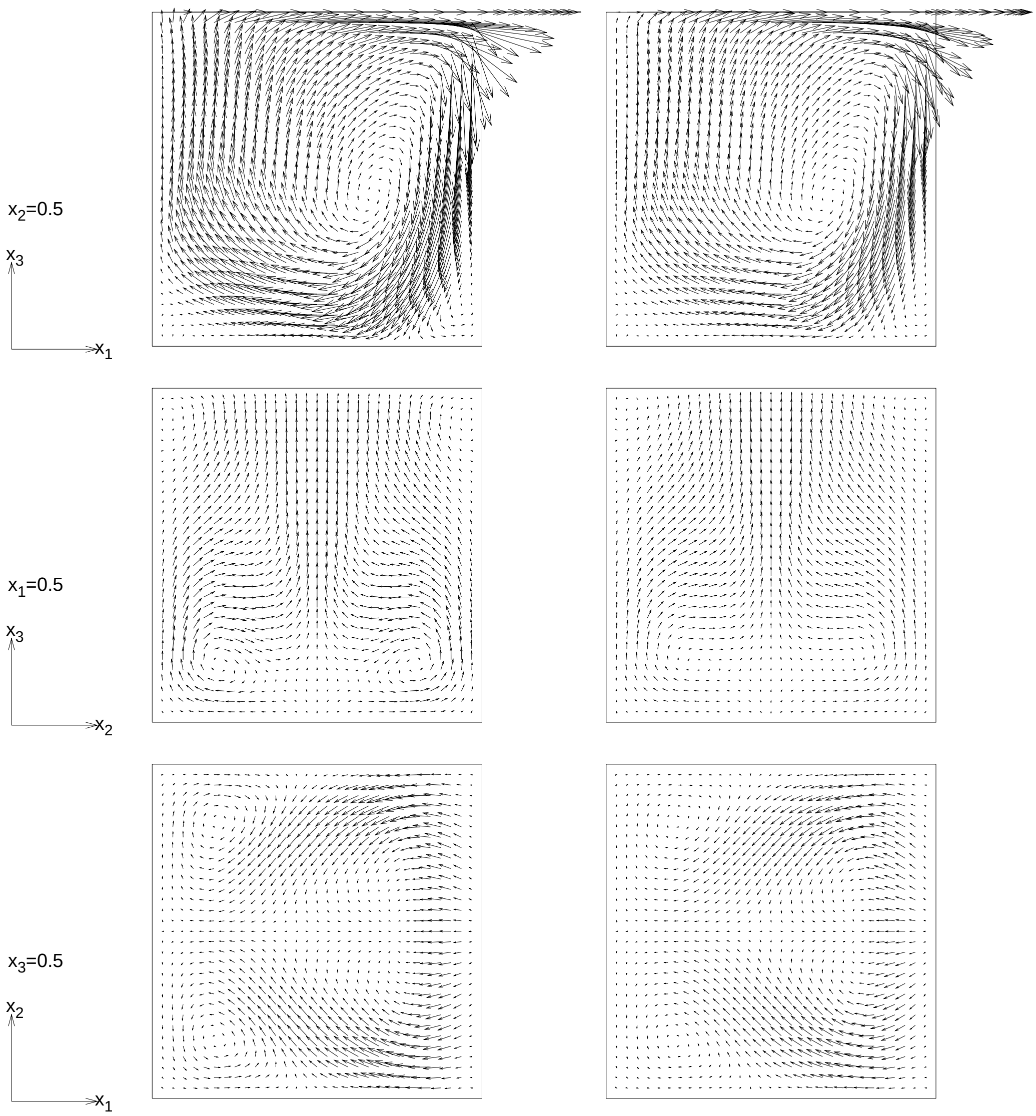

Figure 7.30: Projections of velocity vectors on each plane, $Re = 1,000$, (C0-3D) (left) and (C1-3D) (right).

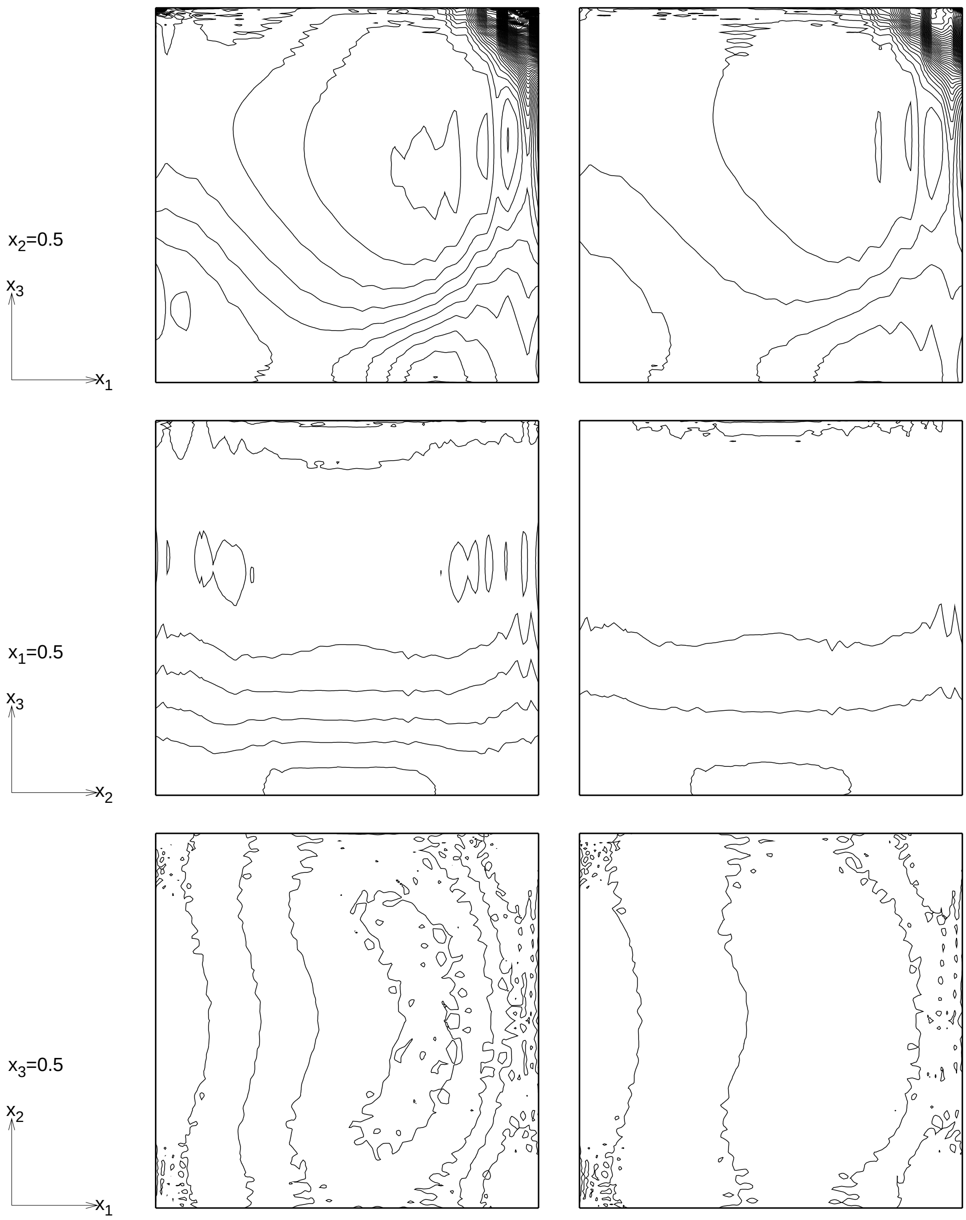

Figure 7.31: Pressure contour lines on each plane by Fine mesh, $Re = 1,000$, $\Delta p = 0.0025$, (C0-3D) (left) and (C1-3D) (right).

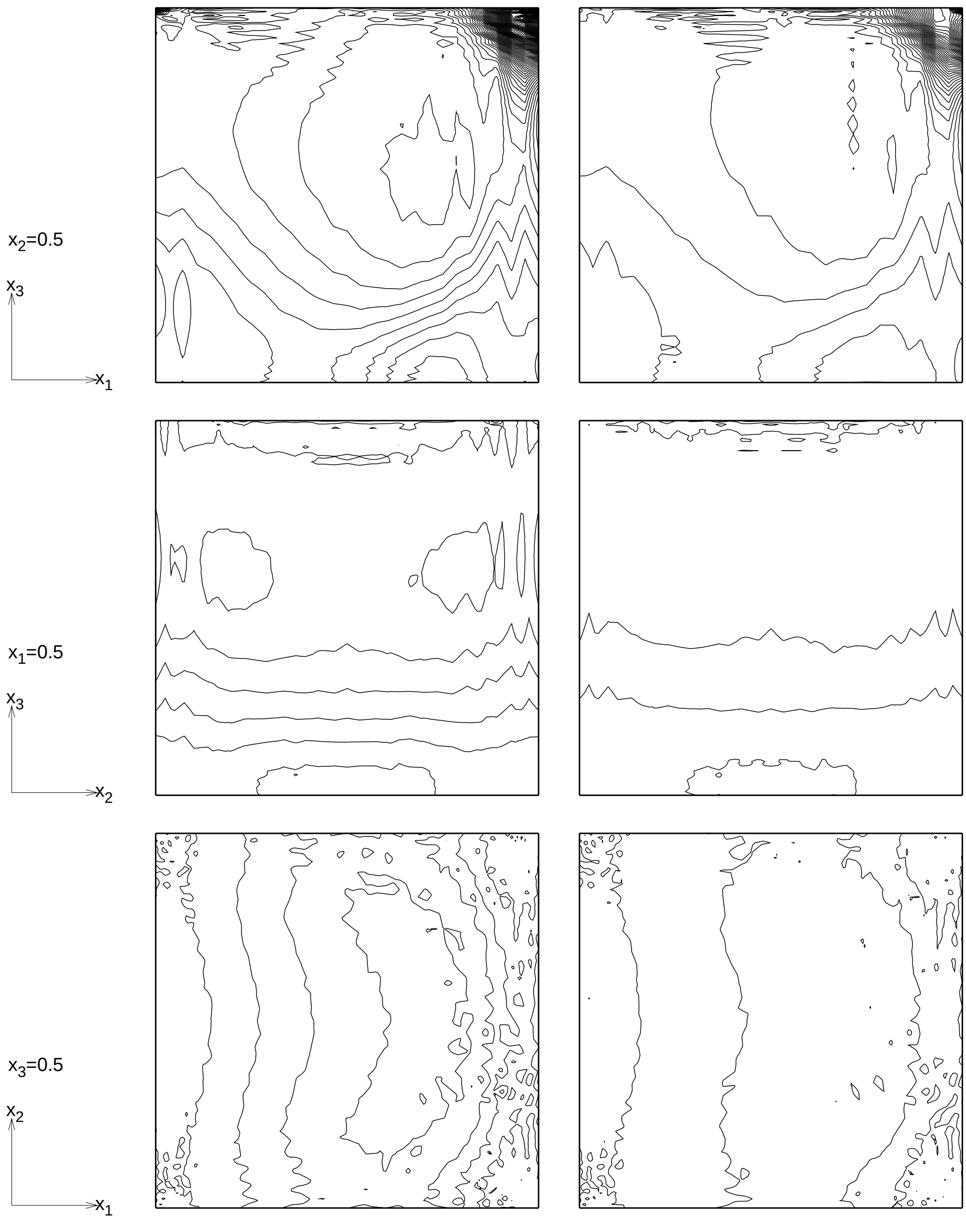

Figure 7.32: Pressure contour lines on each plane by Coarse mesh, $Re = 1,000$, $\Delta p = 0.0025$, (C0-3D) (left) and (C1-3D) (right).

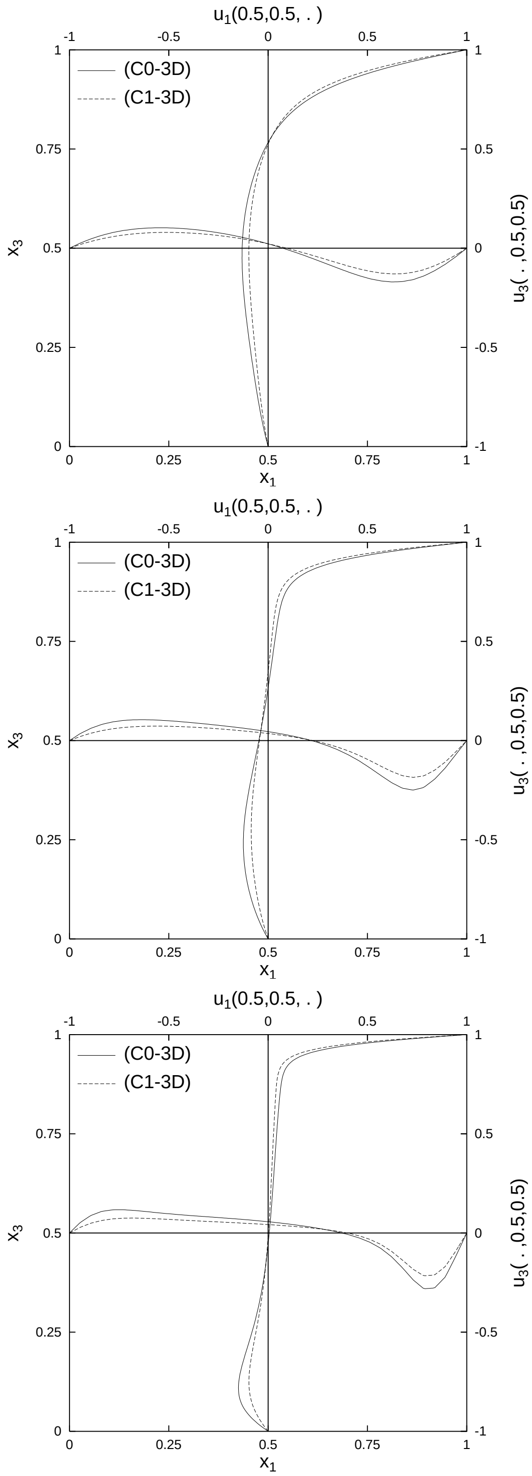

Figure 7.33: Graphs of $u_{h1}(0.5,0.5,\cdot)$ and $u_{h3}(\cdot,0.5,0.5)$ for the two boundary conditions, (C0-3D) and (C1-3D), $Re = 100$ (top), 400 (middle) and $1,000$ (bottom).

Chapter 8

Conclusions

We have presented two characteristic-curve finite element schemes for the non-stationary incompressible Navier-Stokes equations, and given two- and three-dimensional numerical results in order to see the advantages of the schemes.

First, we have proposed a single-step characteristic-curve finite element scheme of second order in time. The scheme uses the second order approximation of the material derivative term by the single step method described in Subsection 3.1.2. We have given an additional correction term for the scheme in order to realize a second order accuracy in time. Our approximation is based on the Crank-Nicolson method on the trajectory of the fluid particle, which is the reason why the additional correction term is required. Since the scheme is nonlinear, we have presented an internal iteration procedure. In each internal iteration the matrix is symmetric and identical. From this, we can use symmetric linear solvers. We have also given numerical results which confirm the second order accuracy in time and the importance of the additional correction term.

Next, we have presented a pressure-stabilized characteristic-curve finite element scheme. The scheme employs a cheap element P1/P1 with the penalty pressure-stabilized method reviewed in Subsection 6.2.2. The matrix of resulting linear system is symmetric and identical. Therefore, the scheme enables us to use symmetric linear solvers and leads to easy large scale computations. A proposition on the stability of the scheme has been given. We have solved two- and three-dimensional test problems and cavity flow problems. The Reynolds numbers are up to 10,000 in the test problems, and up to 5,000 (2D) and 1,000 (3D) in the cavity flow problems. In the test problems, we have observed the first order accuracy in both time and space. For the cavity problems in 2D and 3D, the obtained streamlines, velocity vectors and pressure contour lines have shown the flow patterns well. These results imply that the scheme is a reliable and can be applied for practical problems.

The computations in this thesis were carried out on IBM eServer p5 595 (power 5, 1.9GHz) with IBM XL C/C++ Enterprise Edition V7.0 at Research Institute for Information Technology of Kyushu University.

Bibliography

[1] Baba, K. and Tabata, M., On a conservative upwind finite element scheme for convective diffusion equations, *R.A.I.R.O. Analyse nuérique/Numerical Analysis*, **15**, 1981, 3–25.

[2] Barrett, R., Berry, M., Chan, T. F., Demmel, J., Donato, J., Dongarra, J., Eijkhout, V., Pozo, R., Romine, C. and van der Vorst, H., *Templates for the Solution of Linear Systems: Building Blocks for Iterative Methods*, SIAM, Philadelphia, 1994.

[3] Boukir, K., Maday, Y., Métivet, B. and Razafindrakoto, E., A high-order characteristics/finite element method for the incompressible Navier-Stokes equations, *International Journal for Numerical Methods in Fluids*, **25**, 1997, 1421–1454.

[4] Brenner, S. C. and Scott, L. R., *The Mathematical Theory of Finite Element Methods*, Springer, New York, 2002.

[5] Brooks, A. N. and Hughes, T. J. R., Streamline upwind/Petrov-Galerkin formulations for convection dominated flows with particular emphasis on the incompressible Navier-Stokes equations, *Computer Methods in Applied Mechanics and Engineering*, **32**, 1982, 199–259.

[6] Brezzi, F. and Douglas Jr., J., Stabilized mixed methods for the Stokes problem, *Numerische Mathematik*, **53**, 1988, 225–235.

[7] Brezzi, F. and Fortin, M., *Mixed and Hybrid Finite Element Methods,* Springer, New York, 1991.

[8] Ciarlet, P. G., *The Finite Element Method for Elliptic Problems,* SIAM, Philadelphia, 2002.

[9] Cruchaga, M. A. and Oñate, E., A finite element formulation for incompressible flow problems using a generalized streamline operator, *Computer Methods in Applied Mechanics and Engineering*, **143**, 1997, 49–67.

[10] Douglas Jr., J. and Russell, T. F., Numerical methods for convection-dominated diffusion problems based on combining the method of characteristics with finite element or finite difference procedures, *SIAM Journal on Numerical Analysis*, **19**, 1982, 871–885.

[11] Franca, L. P. and Frey, S. L., Stabilized finite element methods: II. The incompressible Navier-Stokes equations, *Computer Methods in Applied Mechanics and Engineering*, **99**, 1992, 209–233.

[12] Franca, L. P. and Stenberg, R., Error analysis of some Galerkin least squares methods for the elasticity equations, *SIAM Journal on Numerical Analysis*, **28**, 1991, 1680–1697.

[13] FreeFem++, http://www.freefem.org/.

[14] Fujima, S., Tabata, M. and Fukasawa, Y., Extension to three-dimensional problems of the upwind finite element scheme based on the choice of up- and downwind points, *Computer Methods in Applied Mechanics and Engineering*, **112**, 1994, 109–131.

[15] Gresho, P. M., Chan, S. T., Lee, R. L. and Upson, C. D., A modified finite element method for solving the time-dependent, incompressible Navier-Stokes equations. Part 1: Theory, *International Journal for Numerical Methods in Fluids*, **4**, 1984, 557–598.

[16] Ghia, U., Ghia, K. N. and Shin, C. T., High-Re solutions for incompressible flow using the Navier-Stokes equations and a multigrid method, *Journal of Computational Physics*, **48**, 1982, 387–411.

[17] Girault, V. and Raviart, P.-A., *Finite Element Methods for Navier-Stokes Equations, Theory and Algorithms*, Springer, Berlin, 1986.

[18] Hansbo, P. and Johnson, C., Adaptive streamline diffusion methods for compressible flow using conservation variables, *Computer Methods in Applied Mechanics and Engineering*, **87**, 1991, 267–280.

[19] Hughes, T. J. R., Franca, L. P. and Balestra, M., A new finite element formulation for computational fluid dynamics: V. Circumventing the Babuška-Brezzi condition: a stable Petrov-Galerkin formulation of the Stokes problem accommodating equal-order interpolations, *Computer Methods in Applied Mechanics and Engineering*, **59**, 1986, 85–99.

[20] Hughes, T. J. R., Franca, L. P. and Hulbert, G. M., A new finite element formulation for computational fluid dynamics: VIII. The Galerkin/least-squares method for advective-diffusive equations, *Computer Methods in Applied Mechanics and Engineering*, **73**, 1989, 173–189.

[21] Hughes, T. J. R. and Tezduyar, T. E., Finite element methods for first-order hyperbolic systems with particular emphasis on the compressible Euler equations, *Computer Methods in Applied Mechanics and Engineering*, **45**, 1984, 217–284.

[22] Johnson, C., *Numerical Solution of Partial Differential Equations by the Finite Element Method*, Cambridge Univ. Press, Cambridge, 1987.

[23] Le Beau, G. J., Ray, S. E., Aliabadi, S. K. and Tezduyar, T. E., SUPG finite element computation of compressible flows with the entropy and conserva-

tion variables formulations. *Computer Methods in Applied Mechanics and Engineering*, **104**, 1993, 397–422.

[24] Iwatsu, R., Hyun, J. M. and Kuwahara, K., Analyses of three-dimensional flow calculations in a driven cavity, *Fluid Dynamics Research*, **6**, 1990, 91–102.

[25] Jiang, B., Lin, T. L. and Povinelli, L. A., Large-scale computation of incompressible viscous flow by least-squares finite element method, *Computer Methods in Applied Mechanics and Engineering*, **114**, 1994, 213–231.

[26] Kondo, N., Tosaka, N. and Nishimura, T., Third-order upwind finite element formulations for incompressible viscous flow problems, *Computer Methods in Applied Mechanics and Engineering*, **93**, 1991, 169–187.

[27] Ku, H. C., Hirsh, R. S. and Taylor, T. D., A pseudospectral method for solution of the three-dimensional incompressible Navier-Stokes equations, *Journal of Computational Physics*, **70**, 1987, 439–462.

[28] Mori, M., Sugihara, M. and Murota, K., *Matrix Computations*, Iwanami, Tokyo, 1994 (in Japanese).

[29] Nallasamy, M. and Prasad, K. K., On cavity flow at high Reynolds numbers, *Journal of Fluid Mechanics*, **79**, 1977, 391–414.

[30] Notsu, H., Numerical computations of cavity flow problems by a pressure stabilized characteristic-curve finite element scheme, *Transactions of Japan Society for Computational Engineering and Science*, **2008**, 2008, No.20080032, available at http://www.jstage.jst.go.jp/article/jsces/2008/0/20080032/_pdf.

[31] Notsu, H. and Tabata, M., A combined finite element scheme with a pressure stabilization and a characteristic-curve method for the Navier-Stokes equa-

tions, *Transactions of the Japan Society for Industrial and Applied Mathematics*, **18**, No.3, 2008, 427–445 (in Japanese).

[32] Notsu, H. and Tabata, M., A single-step characteristic-curve finite element scheme of second order in time for the incompressible Navier-Stokes equations, *Journal of Scientific Computing*, **38**, No.1, 2009, 1–14.

[33] Pironneau, O., On the transport-diffusion algorithm and its applications to the Navier-Stokes equations. *Numerische Mathematik*, **38**, 1982, 309–332.

[34] Pironneau, O., *Finite Element Methods for Fluids*, John Wiley & Sons, Chichester, 1989.

[35] Pironneau, O., Liou, J. and Tezduyar, T. E., Characteristic-Galerkin and Galerkin/least-squares space-time formulations for the advection-diffusion equation with time-dependent domains, *Computer Methods in Applied Mechanics and Engineering*, **100**, 1992, 117–141.

[36] Rui, H. and Tabata, M., A second order characteristic finite element scheme for convection-diffusion problems, *Numerische Mathematik*, **92**, 2002, 161–177.

[37] Stroud, A. H., *Approximate calculation of multiple integrals*, Prentice-Hall, Englewood Cliffs, New Jersey, 1971.

[38] Süli, E., Convergence and nonlinear stability of the Lagrange-Galerkin method for the Navier-Stokes equations, *Numerische Mathematik*, **53**, 1988, 459–483.

[39] Tabata, M., A finite element approximation corresponding to the upwind finite differencing, *Memoirs of Numerical Mathematics*, **4**, 1977, 47–63.

[40] Tabata, M., *Numerical Solution of Differential Equations II*, Iwanami, Tokyo, 1994 (in Japanese).

[41] Tabata, M., Discrepancy between theory and real computation on the stability of some finite element schemes, *Journal of Computational and Applied Mathematics*, **199**, 2007, 424–431.

[42] Tabata, M. and Fujima, S., An upwind finite element scheme for high-Reynolds-number flows, *International Journal for Numerical Methods in Fluids*, **12**, 1991, 305–322.

[43] Tabata, M. and Fujima, S., Finite-element analysis of high Reynolds number flows past a circular cylinder, *Journal of Computational and Applied Mathematics*, **38**, 1991, 411–424.

[44] Tabata, M. and Fujima, S., Robustness of a characteristic finite element scheme of second order in time increment, in *Computational Fluid Dynamics 2004*, editors Groth, C. and Zingg, D. W., Springer, Berlin, 2006, 177–182.

[45] Tabata, M. and Suzuki, A., A stabilized finite element method for the Rayleigh-Bénard equations with infinite Prandtl number in a spherical shell, *Computer Methods in Applied Mechanics and Engineering*, **190**, 2000, 387–402.

[46] Tabata, M., and Tagami, D., Error estimates for finite element approximations of drag and lift in nonstationary Navier-Stokes flows. *Japan Journal of Industrial and Applied Mathematics*, **17**, 2000, 371–389.

[47] Tezduyar, T. E., Stabilized finite element formulations for incompressible flow computations, *Advances in Applied Mechanics*, **28**, 1992, 1–44.